STATE UNIVERSITY OF MARINGÁ
CHEMICAL ENGINEERING DEPARTMENT
CHEMICAL ENGINEERING GRADUATE PROGRAM

Willian Dimas Pompeo Siqueira

Process Intensification in Biodiesel Production: A Multi-Objective Optimization Approach

Maringá
2025

STATE UNIVERSITY OF MARINGÁ
CHEMICAL ENGINEERING DEPARTMENT
CHEMICAL ENGINEERING GRADUATE PROGRAM

Process Intensification in Biodiesel Production: A Multi-Objective Optimization Approach

Willian Dimas Pompeo Siqueira

Advisor: Prof. Dr. Leandro Vitor Pavão, PhD.

Master's Dissertation submitted to the Graduate Program in Chemical Engineering at the State University of Maringá, as part of the requirements for obtaining the Master's Degree in Chemical Engineering.

Maringá – PR – Brazil

August 2025

Dados Internacionais de Catalogação-na-Publicação (CIP)
(Biblioteca Central - UEM, Maringá - PR, Brasil)

S618p

Siqueira, Willian Dimas Pompeo

Process intensification in biodiesel production : a multi-objective optimization approach / Willian Dimas Pompeo Siqueira. -- Maringá, PR, 2025.

160 f. : il. color., figs., tabs.

Orientador: Prof. Dr. Leandro Vitor Pavão.

Dissertação (mestrado) - Universidade Estadual de Maringá, Centro de Tecnologia, Departamento de Engenharia Química, Programa de Pós-Graduação em Engenharia Química, 2025.

1. Biodiesel - Produção - Intensificação de processos. 2. Biodiesel - Destilação reativa. 3. Otimização multiobjetivo. 4. Bomba de calor. I. Pavão, Leandro Vitor, orient. II. Universidade Estadual de Maringá. Centro de Tecnologia. Departamento de Engenharia Química. Programa de Pós-Graduação em Engenharia Química. III. Título.

CDD 23.ed. 665.3

Marinalva Aparecida Spolon Almeida - 9/1094

UNIVERSIDADE ESTADUAL DE MARINGÁ
CENTRO DE TECNOLOGIA
DEPARTAMENTO DE ENGENHARIA QUÍMICA
PROGRAMA DE PÓS-GRADUAÇÃO EM ENGENHARIA QUÍMICA

Esta é a versão final da Dissertação de Mestrado apresentada por **Willian Dimas Pompeo Siqueira** perante a Comissão Julgadora do Programa de Pós-graduação em Engenharia Química em 21 de agosto de 2025.

COMISSÃO JULGADORA

Documento assinado digitalmente
gov.br
LEANDRO VITOR PAVAO
Data: 21/08/2025 19:22:05-0300
Verifique em https://validar.iti.gov.br

Prof. Dr. Leandro Vitor Pavão
Presidente/Orientador - PEQ/UEM

Documento assinado digitalmente
gov.br
SARA REGINA OSIPI
Data: 21/08/2025 22:10:51-0300
Verifique em https://validar.iti.gov.br

Profª. Drª. Sara Regina Osipi
Membro - PEQ/UEM

Documento assinado digitalmente
gov.br
LILIAN RAQUEL HICKERT
Data: 25/08/2025 13:16:40-0300
Verifique em https://validar.iti.gov.br

Profª. Drª. Lilian Raquel Hickert
Membro – Departamento de Engenharia/UERGS

I dedicate this work to my mother, Ivoni Olanda Pompeo Siqueira, my father, José Dimas de Siqueira, and in memory of my grandmother Ana G. Olanda Pompeo for their unwavering support, which has been the foundation of my academic aspirations and perseverance throughout this journey.

Acknowledgements

To God and the Virgin Mary for guiding me spiritually throughout my personal and academic journey and blessing my life with protection.

To the financial support provided by CAPES (Finance Code 001), which was essential for the development of this work, as well as for providing access to scientific literature through the CAPES Journals Portal (*Portal de Periódicos*), which greatly facilitated the bibliographic research.

To my friends and my family, especially my mother, Ivoni Olanda Pompeo Siqueira, and my father, José Dimas de Siqueira, for their unwavering love, support, and dedication throughout every academic task. I also extend my gratitude to my grandparents, Osvaldo Constantino Pompeo, Joaquim Maciel de Siqueira, Leonides do Nascimento Siqueira, José Pedro Freitas, Sinvaldo, and Maria das Graças dos Reis Freitas, and especially to my grandmother Ana G. Olanda Pompeo, with whom I had the honor of sharing her final months of life alongside my mother.

To my advisor, Dr. Leandro Vitor Pavão, for his guidance and for providing the best conditions for the development of this research and members of the LSCP/UEM research group (in special, Diego Rafael) for their valuable feedback and discussions during our meetings, which significantly contributed to the progress of this work.

"What makes the desert beautiful", said the little prince, "is that somewhere hides a well…"

Antoine de Saint-Exupéry in *The Little Prince* (1943)

List of Figures

List of Tables

List of Symbols

Abbreviations

AI	Artificial Intelligence
ANP	National Agency of Petroleum, Natural Gas and Biofuels
APS	Announced Pledges Scenario
CEPCI	Chemical Engineering Plant Cost Index
CNPE	National Energy Policy Council
CO_2e	Carbon Dioxide Emissions
CPO	Crude Palm Oil
CS-1	Case Study 1
CS-2	Case Study 2
CS-3	Case Study 3
CSO	Cottonseed Oil
CU	Cold Utility
DWC	Dividing Wall Column
ele	Electricity
FAEE	Fatty Acid Ethyl Ester
FAME	Fatty Acid Methyl Ester
GA	Genetic Algorithm
GC	Glycerol Carbonate
GLC	Glycidol
HIDiC	Heat Integrated Distillation Column
HIRDiC	Heat Integrated Reactive Distillation Column
HU	Hot Utility
IEA	International Energy Agency
LHS	Latin Hypercube Sampling
MEOH	Methanol
ML	Machine Learning
MOO	Multi-Objective Optimization
NSGA	Non-dominated Sorting Genetic Algorithm
NZE	Net Zero Emissions
ORC	Organic Rankine Cycle
OOO	Triolein

PBP	Payback Period
PI	Process Intensification
PSO	Particle Swarm Optimization
RD	Reactive Distillation
RDC	Reactive Distillation Column
RDWC	Reactive Distillation Dividing Wall Column
SA	Simulated Annealing
SAW	Simple Additive Weighting
SBO	Soybean Oil
SRC	Side Reactor Column
SRD	Separated Reactor and Distillation Process
STEPS	Stated Policies Scenario
SVRRD	Side Vapor Recompression Reactive Distillation
TAC	Total Annualized Cost
TCDS	Thermally Coupled Distillation Sequences
TCRD	Thermal Coupling Reactive Distillation
TIC	Total Installed Cost
TOC	Total Operating Cost
TOPSIS	Technique for Order of Preference by Similarity to Ideal Solution
USP	United States Pharmacopeia
VC	Vapor Compression
VCC	Vapor Compression Column
VR	Vapor Recompression
VRC	Vapor Recompression Column
WCO	Waste Cooking Oil
WVO	Waste Vegetable Oil
YGP	Yearly Gross Profit

Parameters and Variables

α	Conversion factor representing the molar ratio of CO_2 to C (-)
ΔI_{ij}	Difference between the maximum normalized value and each normalized solution (depend on the variable)
η_{Carnot}	Carnot Efficiency (-)
Δ_i	Deviation from the constraint limit for constraint *i* (depend on the variable)
λ_{proc}	Latent heat of process steam delivered to the process (kJ/kg)
$C\%$	Percentage of carbon present in the fuel composition (%)
C_i	Closeness to the ideal solution (depend on the variable)
$CEPCI$	Chemical Engineering Plant Cost Index (-)
CO_2e	Carbon Dioxide Emissions (kg/s)
$\widehat{CO_2e_{,ele}}$	Specific emissions for electricity generation (kg/GJ)
COP	Coefficient of performance (-)
D_{col}	Column diameter (m)
DF^d	Molar distillate to feed ratio of column *d* (-)
f_{holdup}^{RDC-1}	Reactive holdup factor in RDC-1 (-)
f_{ij}^{norm}	Normalized objective function (depend on the variable)
F_{lang}	Lang Factor (-)
FS^d	Feed Stage of column *d* (-)
GRC	Grey Relational Coefficient (-)
H_{proc}	Enthalpy of steam delivered to the process (kJ/kg)
H_{water}	Enthalpy of boiler feedwater (kJ/kg)
h_{weir}	Weir height (cm)
IC_c^d	Installed Cost of device *d* in case study *c* (USD)
k_0	Penalty scaling factor (-)
L_{DS}	Available length for downcomer liquid (cm)
$\dot{m}$	Mass flowrate of stream *i* (kg/h)
$M\&S$	Marshall and Swift index (-)
$\dot{n}_i$	Molar flowrate of stream *i* (kmol/h)

n_{prod}	Number of products (-)
N_R^d	Number of rectifying stages in column *d*
N_T^d	Number of stages in column *d*
N_S^d	Number of stripping stages in column *d*
n_{rea}	Number of reactants (-)
NHV	Net Heating Value (kJ/kg)
$OC_{u,cs}^d$	Operating Cost of utility, catalyst or electricity (*u*) in case study *cs* for device *d* (USD/h)
P^d	Pressure of device *d* (atm)
$P_{i/u}$	Unit price of stream *i* or utility, catalyst or electricity (*u*) (USD/kg)
PBP	Payback Period (year)
Pen_i	Penalty associated with constraint *i* (depend on the variable)
$\dot{q}$	Volumetric flow rate (L/h)
Q_{fuel}	Thermal Energy provided by the fuel for steam generation (kW)
Q_{proc}	Heat duty of the process (kW)
r	Correlation coefficient (-)
$R_{in}^{process/RDC-1}$	Molar process inlet metanol-to-oil ratio in process or RDC-1 (-)
RC	Raw materials cost (USD/year)
RF^{RDC-1}	Reflux split to enter in RDC-1 (-)
RR^d	Molar Reflux Ratio in column *d* (-)
S_{i-}	Positive ideal solution (depend on the variable)
S_{i+}	Negative ideal solution (depend on the variable)
T_{cond}	Condenser temperature (°C)
T_{FTB}	Flame temperature of the boiler flue gases (°C)
T_o	Ambient Temperature (°C)
t_{op}	Operational time (h/year)
T_{reb}^d	Reboiler temperature of device *d* (°C)
T_{stack}	Stack temperature (°C)

TC	Total Costs (USD/year)
TIC	Total Installed Costs (USD)
TOC	Total Operating Costs (USD/year)
tol_i	Tolerance of constraint *i* (depend on the variable)
TR	Total Revenue (USD/year)
VF^{RDC-1}	Vapor fraction in RDC-1 Reboiler (-)
x_i^j	Mass fraction of component *i* in stream *j* (-)
W_c^d	Workload of device *d* in case study *c* (kW)
wn_{ij}	Weighted normalized value (depend on the variable)
YGP	Yearly Gross Profit (USD/year)

Abstract

The pursuit of sustainable and energy-efficient processes has intensified due to the worsening of the greenhouse effect and its environmental consequences. Conventional biodiesel production is characterized by multiple reaction and separation steps, leading to high energy consumption and CO_2 emissions (CO_2e). In this context, this work proposed the application of process intensification strategies for the continuous industrial-scale production of biodiesel, through the full integration of reactive distillation (RD) and a heat pump, eliminating the need for external utilities, an aspect still scarcely explored in the literature. Three case studies were defined to investigate different glycerol purification levels and biodiesel quality requirements. These scenarios were analyzed using a multi-objective optimization approach implemented through Aspen Plus–Python integration, aiming to maximize the Yearly Gross Profit (YGP), minimize CO_2e, and, in the most restrictive case, maximize biodiesel purity (FAME). Operational and quality constraints were addressed using an exponential penalty function, and the non-dominated solutions obtained were evaluated using multicriteria decision-making techniques. The results showed that the Heat Pump Reactive Distillation (HPRD) outperformed conventional RD in reducing CO_2e (up to 93%) and operational costs (up to 74%), despite its higher capital cost. Glycerol purification to pharmaceutical grade (CS-2) increased the YGP to approximately from 80 to 120 million USD/year, albeit with a rise in CO_2e. Even under the strict quality standards set by the Brazilian National Agency for Petroleum (ANP) (CS-3), the HPRD configuration remained economically viable (above 100 million USD/year) and environmentally superior to conventional RD. Compared to technologies reported in the literature, HPRD stood out by operating without external utilities, establishing itself as a more sustainable alternative for biodiesel production.

Keywords: Biodiesel, Reactive Distillation, Heat Pump, Process Intensification, Optimization.

Resumo

A busca por processos sustentáveis e energeticamente eficientes tem se intensificado devido ao agravamento do efeito estufa e de suas consequências ambientais. A produção convencional de biodiesel é caracterizada por múltiplas etapas de reação e separação, resultando em elevado consumo de energia e emissões de CO_2 (CO_2e). Nesse contexto, este trabalho propôs a aplicação de estratégias de intensificação de processos para a produção contínua de biodiesel em escala industrial, por meio da integração total entre destilação reativa (RD) e bomba de calor, eliminando a necessidade de utilidades externas, um aspecto ainda pouco explorado na literatura. Três estudos de caso foram definidos para investigar diferentes níveis de purificação do glicerol e requisitos de qualidade do biodiesel. Esses cenários foram analisados utilizando uma abordagem de otimização multiobjetivo implementada por meio da integração entre Aspen Plus e Python, com o objetivo de maximizar o Lucro Bruto Anual (YGP), minimizar as emissões de CO_2e e, no caso mais restritivo, maximizar a pureza do biodiesel (FAME). Restrições operacionais e de qualidade foram tratadas por meio de uma função de penalização exponencial, e as soluções não dominadas obtidas foram avaliadas por técnicas de decisão multicritério. Os resultados demonstraram que a destilação reativa assistida por bomba de calor (HPRD) superou a RD convencional na redução de CO_2e (até 93%) e dos custos operacionais (até 74%), apesar do maior custo de capital. A purificação do glicerol para grau farmacêutico (CS-2) elevou o YGP de, aproximadamente, 80 para 120 milhões de dólares/ano, embora com aumento em CO_2e. Mesmo sob os rigorosos padrões de qualidade estabelecidos pela Agência Nacional do Petróleo (ANP) (CS-3), a configuração HPRD manteve-se economicamente viável (acima de 100 milhões de dólares/ano) e ambientalmente superior à RD convencional. Em comparação com tecnologias descritas na literatura, a HPRD destacou-se por operar sem utilidades externas, consolidando-se como uma alternativa mais sustentável para a produção de biodiesel.

Palavras-chave: Biodiesel, Destilação Reativa, Bomba de Calor, Intensificação de Processos, Otimização.

Table of Contents

1 Introduction

The intensification of the greenhouse effect has led to many social and environmental consequences, including rising sea levels (Tebaldi *et al*., 2021), more severe and frequent extreme weather phenomena (Mann; Emanuel, 2006), significant biodiversity loss (Nunez *et al*., 2019), a surge of respiratory diseases due to air pollution and drastic changes in rainfall patterns (Knapp *et al*., 2015).

According to the International Energy Agency (IEA), there are three global carbon dioxide emissions (CO_2e) scenarios: Net Zero Emissions (NZE), Announced Pledges Scenario (APS), and Stated Policies Scenario (STEPS). NZE is the most ambitious, predicting a sharp reduction in CO_2e to achieve carbon neutrality by 2050, limiting the global temperature rise to 1.5 °C above pre-industrial levels, as outlined in the Paris Agreement. To meet these targets, strict mitigation policies must be implemented under NZE. Conversely, APS and STEPS are less optimistic; while APS accounts for all climate policies and commitments announced by governments, STEPS includes only those already in effect. Both scenarios foresee a continued increase in global average temperature, exceeding 1.7 °C by the end of the century (IEA, 2023). Figures 1 and 2 illustrate the projected CO_2e by 2050 and the associated temperature rise by the end of the century under these projections.

Figure 1 – CO_2e by 2050 (gigatons) in each IEA scenario.

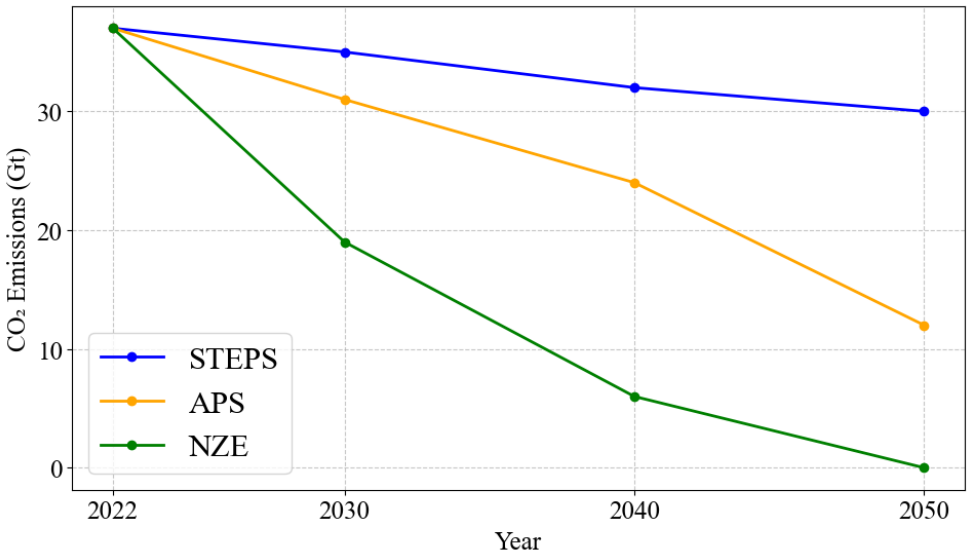

Source: Adapted from IEA (2023).

Figure 2 – Projected temperature rise by 2100 in each IEA scenario.

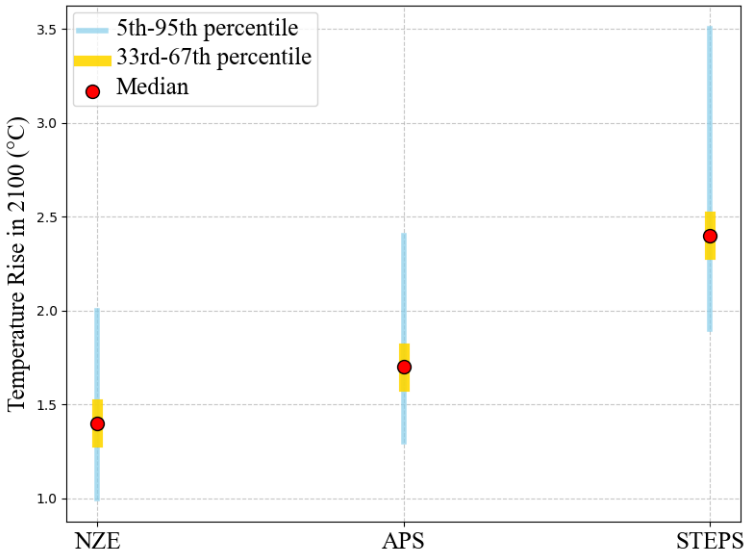

Source: Adapted from IEA (2023).

As illustrated in Figures 1 and 2, achieving NZE by 2050 demands a more rapid deployment of low-carbon technologies, especially in the energy sector. In this context, biofuels appear as renewable alternatives to fossil fuels and as practical solutions for reducing lifecycle emissions, particularly in the transportation sector. Reflecting the global movement, the Brazilian government, through the National Energy Policy Council (*Conselho Nacional de Política Energética* – CNPE, in Portuguese), has mandated an increase in the biodiesel blend in fossil diesel from 10% in 2023 to 15% by 2025. As a result, national production is projected to surpass 10 billion liters by 2026, up from 6.3 billion liters in 2023 (Brasil, 2023; Brasil, 2024a).

Biodiesel consists of fatty acid esters produced from vegetable sources via esterification and transesterification reactions, depending on the free fatty acid content of the feedstock. In conventional production, the reaction occurs in a reactor, followed by a distillation column, which is termed as separated reactor and distillation column system (SRD) in this document (Myint; El-Halwagi, 2009). However, SRD presents economic and environmental drawbacks due to high energy consumption and substantial CO_2e.

Process intensification (PI) emerges as a promising strategy to overcome these limitations and process efficiency. According to Harmsen and Verkerk (2020), “PI is a set of radically innovative process-design principles which can bring significant benefits in terms of efficiency, cost, product quality, safety and health over conventional process-design based on unit operations”. Among the various PI approaches, Reactive Distillation (RD) is an

extensively researched technique in literature. This method combines reaction and separation within a single unit, allowing simultaneous transesterification reaction and methanol recovery in biodiesel production. Beyond simplifying the process, RD addresses conversion limitations through the continuous removal of products (Qiu; Zhao; Weatherley, 2010).

Another PI technique commonly applied in distillation processes is Vapor Recompression (VR). In VR, vapor from the distillation column is compressed and reheated, enabling it to be used as the heat source for the reboiler. The compressed vapor is then expanded through a valve and partially refluxed back into the column. When VR is integrated into a Reactive Distillation Column (RDC), the process is referred to as a Heat Pump for RD (HPRD), which combines energy integration with reaction and separation efficiency (Steffen; Oliveira; Silva, 2024).

Although RD and VR have been extensively studied individually in biodiesel production, their full integration into a single intensified configuration, as proposed in this work, remains unexplored.

1.1 General Objective

Propose a novel intensified process configuration for biodiesel production on an industrial scale, combining PI, energy integration, and product purification strategies to meet technical, economic, and environmental targets with the assistance of commercial software (Aspen Plus).

1.2 Specific Objectives

- Develop and simulate biodiesel production processes that integrate different PI strategies (RD and HPRD) under multiple scenarios related to glycerol purification and biodiesel quality, in accordance with Brazilian and International standards.
- Analyze the technical, economic, and environmental impacts of adopting glycerol purification via vacuum distillation for pharmaceutical use.
- Implement multi-objective optimization (MOO) in Python language to identify the optimal trade-offs between Yearly Gross Profit (YGP) and CO_2e.
- Apply decision-making strategies to select representative optimal solutions and compare the results with those of other proposed intensified configurations in the literature.

2 Theoretical Background

This chapter aims to provide a theoretical foundation on biodiesel production, PI technologies applied to distillation, methods for solving MOO problems and selecting solutions from the Pareto Front, as well as previous studies on simulation-based biodiesel production.

2.1 Biodiesel Production: Overview and Challenges

Biodiesel is an alternative fuel originated from biological sources, composed of fatty acid methyl esters (FAMEs) and fatty acid ethyl esters (FAEEs), which are produced through transesterification and esterification reactions. In the transesterification process (Figure 3), the triglycerides of animal fats and vegetable oils react with short-chain alcohols, typically methanol or ethanol, producing FAME when methanol is used or FAEE when ethanol is employed. Glycerol is generated as a by-product of this reaction (Antczak *et al*., 2009; Talebian-Kiakalaieh; Amin; Mazaheri, 2013). Alternatively, in the esterification process (Figure 4), the free fatty acids and alcohol produce water, besides the fatty acid alkyl ester (Khan *et al*., 2021).

Figure 3 – Schematic representation of simplified transesterification reaction.

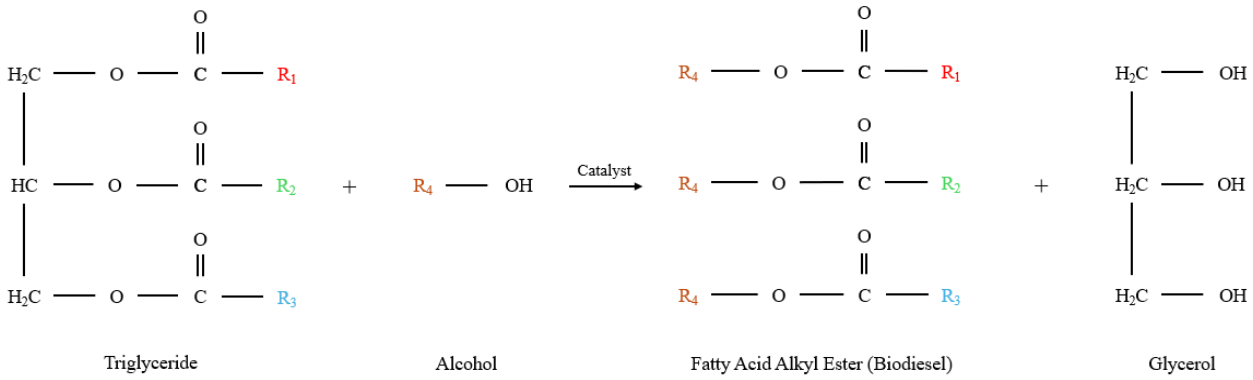

Source: Adapted from Camino Feltes *et al*. (2011).

Figure 4 – Schematic representation of simplified esterification reaction.

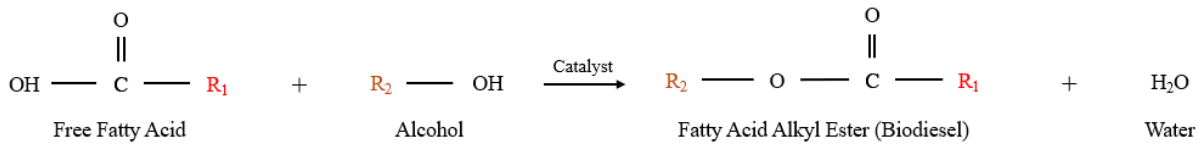

Source: Adapted from Haigh *et al*. (2012).

Biodiesel is a renewable, biodegradable, and non-toxic fuel that achieves an 78% reduction in CO_2e over its life cycle compared to petroleum diesel, while also requiring less production time by eliminating drilling and refining steps (Decarpigny *et al*., 2022; Mishra; Goswami, 2018). The higher cetane number contributes to shorter ignition delay, whereas superior lubricity enhances the durability of injector systems and fuel pumps (Alptekin; Canakci, 2008; Shahid; Jamal, 2011). However, the energy content is lower than of conventional diesel (Saxena; Jawale; Joshipura, 2013), and reduced volatility may lead to incomplete combustion, resulting in deposit formation in engines (Hoang; Le, 2019). Furthermore, large scale production using edible oils may disrupt the food supply-demand equilibrium (Sing; Mahali; Roy, 2024).

Soybean oil constitutes the dominant source in the Brazilian biodiesel production market, accounting for 69.8% of the total, followed by "Other Fatty Materials" with 16.1%. Figure 5 shows the feedstocks used in Brazil, where the category “Others” encompasses chicken fat, pork fat, cottonseed oil, rapeseed/canola oil, corn oil, palm oil, and waste cooked oil.

Figure 5 – Distribution of feedstocks for biodiesel production in Brazil (September 2024).

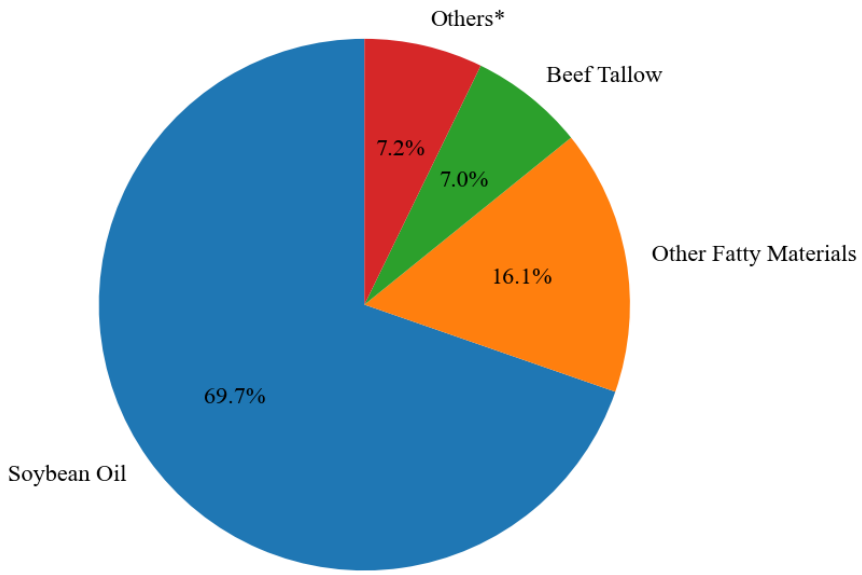

Source: Adapted from ANP (2024c).

To stimulate the production and integration of biodiesel into the energy matrix, the Brazilian government has implemented policies mandating a minimum blend in petroleum diesel. The required content has been gradually increasing over time, starting at 2% in 2008 and projected to attain 15% by March 2025, with annual increment of 1% thereafter, reaching 20%

in 2030 (ANP, 2024b; Brasil, 2024b; Craide, 2023). Figure 6 depicts the country commitment to renewable energy development.

Figure 6 – Evolution of required biodiesel content in fossil diesel in Brazil.

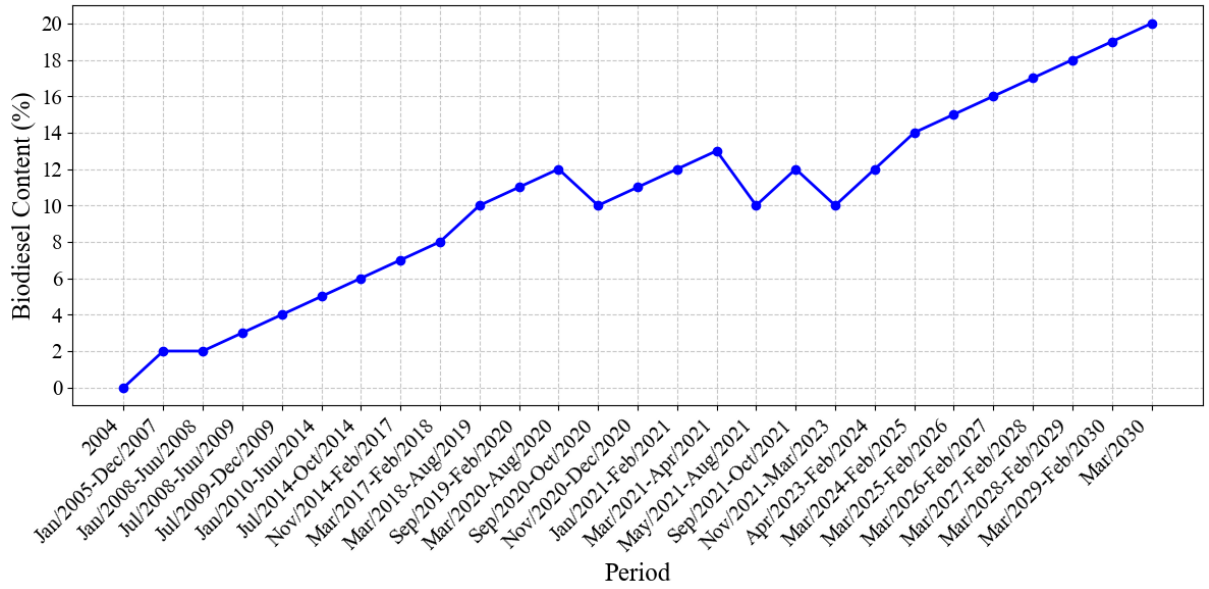

Source: Adapted from ANP (2024b), Brasil (2024b) and Craide (2023).

In Brazil, the National Agency of Petroleum, Natural Gas and Biofuels (*Agência Nacional do Petróleo, Gás Natural e Biocombustíveis* – ANP, in Portuguese) regulates the technical requirements to ensure biodiesel quality and compatibility with engines. A comparison of specifications in Brazil, Europe, and the United States is presented in Table 1.

Conventional heterogeneous-catalyzed production typically involves several key steps. If only the transesterification reaction is desired, pre-treatment of oils or fats may be necessary, depending on the free fatty acid content. Oil and alcohol are subsequently combined in a catalytic reactor to initiate the transesterification reaction. After the reaction, a distillation column is employed to recover unreacted methanol. The organic phase, biodiesel, is then separated from glycerol and excess alcohol. The degree of product purity achieved determines the need for additional purification steps. Figure 7 summarizes the process for heterogeneous-catalyzed biodiesel production (Faruque; Razzak; Hossain, 2020; Leung; Wu; Leung, 2010).

Table 1 – Required biodiesel specifications according to Brazil, Europe and the US Regulations.

Property	Brazilian Regulation (ANP 920)	European Regulation (EN 14214)	American Regulation (ASTM D6751)
Density (at 20 ºC for Brazil and at 15 ºC for Europe and the US) (kg/m^3)	850 to 900	880	860 to 900
Kinematic viscosity at 40 ºC (mm^2/s)	3.0 to 5.0	3.5 to 5.0	1.9 to 6.0
Minimum flash Point (ºC)	100	101	130
Minimum ester content (wt.%)	96.5	96.5	96.5
Maximum sulfated ash content (wt.%)	0.020	0.020	0.002
Maximum phosphorus content	3.0	1.0	1.0
Minimum cetane number	--	51	47
Maximum acid number (mg KOH/g)	0.50	0.50	0.50
Maximum total glycerol (wt.%)	0.20	0.25	0.24
Maximum monoglycerides content (wt.%)	0.50	0.80	--
Maximum diglycerides content (wt.%)	0.20	0.20	--
Maximum triglycerides content (wt.%)	0.20	0.20	--
Maximum methanol and/or ethanol content (wt.%)	0.20	--	--
Maximum total contamination (mg/kg)	24	24	24
Minimum oxidation stability (h)	13	3	--

Source: ANP (2023); Sakthivel *et al*. (2018).

Figure 7 – Simplified representation of heterogeneous catalyzed biodiesel production.

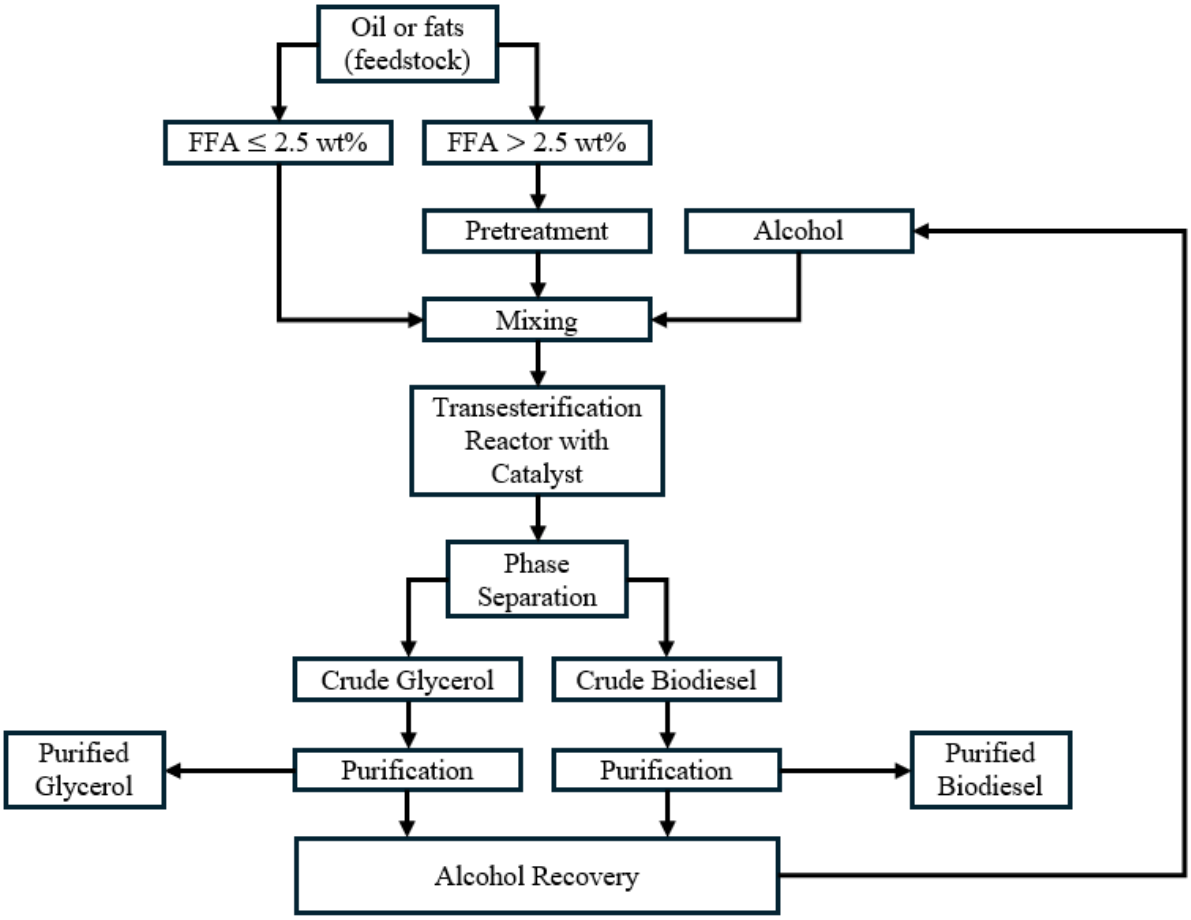

Source: Adapted from Faruque, Razzak and Hossain (2020); Leung, Wu and Leung (2010).

2.2 Process-Intensified Distillation Systems

Although the conventional biodiesel route and traditional distillation processes remain consolidated in the chemical industry, both are constrained by high energy consumption and the use of multiple unit operations. As a result, several PI strategies have been proposed for distillation systems, aiming to improve separation efficiency, reduce utility demands, and enhance process integration. This subsection presents the main PI strategies applied to distillation, emphasizing their operational principle and potential benefits.

2.2.1 Reactive Distillation (RD)

RD is a PI technology that combines chemical reaction and product separation within a single unit. By continuously removing reaction products, RD promotes equilibrium-limited reactions to proceed more efficiently, increasing conversion rates according to Le Chatelier`s principle (Rodriguez-Robles *et al*., 2019).

RD offers substantial advantages over traditional processes (Chuah *et al*., 2022):

- Reduces reaction time.
- Eliminates the need for excess reactant.
- Lowers capital costs by eliminating additional separation units.
- Enhances conversion rates and selectivity by continuously removing reactants and products.
- Avoids reheating requirements, as the heat of vaporization fulfills the energy demands of exothermic reactions.

The choice of catalysts is essential in RD. Two types of catalysts can be used: homogeneous and heterogeneous. Homogeneous catalysts allow uniform contact between reactants but depend on mixing patterns and require additional steps such as neutralization and separation. Heterogeneous catalysts, in contrast, are insoluble solids that simplify purification and enable reuse, making them attractive for industrial RD applications. However, they require structured packing or fixed beds (Mittelbach, 2012).

Additionally, the placement of the reaction zone is important; in some cases, the reaction occurs throughout the column, while in others, only specific sections are active. Meanwhile, the non-reactive zones improve the purification and can break azeotropes using an entrainer (Coker, 2010). Inadequate design results in inefficient performance or even infeasibility; therefore, it is essential to carefully consider design parameters to ensure the effectiveness of RD (Muthia; Jobson; Kiss, 2020).

In this context, reactive holdup is a relevant variable. It directly impacts reaction performance by affecting temperature, composition, and residence time (Kroeze *et al*., 2021). The total reactive holdup depends on geometric and operational factors. It is influenced by column diameter (D_{col}), weir height (h_{weir}), available length for downcomer liquid (L_{DS}), and number of reactive stages (Lee; Hsiao, 2017; Yu, 2020). Common heuristics are adopted in the literature to estimate the reactive holdup. Typically, the effective area available for liquid flow is approximately 90% of the tray's cross-sectional area, while liquid heights beyond 15 cm can result in operational challenges, such as higher pressure drops and reduced efficiency.

Reactive holdup influences both operational and fixed costs in RD. Increased holdup improves conversion, yield, and selectivity due to extended residence time. However, it requires column modifications, such as increasing D_{col} or h_{weir}, which leads to higher capital costs for vessel construction and installation. From an operational standpoint, this condition reduces the required reflux ratio and vapor boilup rate, minimizing energy expenses. Nonetheless, it can

introduce hydraulic constraints and controllability issues, potentially offset the benefits (Saleem *et al*., 2023). Figure 8 illustrates the internal configuration of an RDC, assuming a catalyst loading is 50% full in the tray (Tsatse *et al*., 2021).

Figure 8 – Schematic Representation of RDC internals using heterogeneous catalyst.

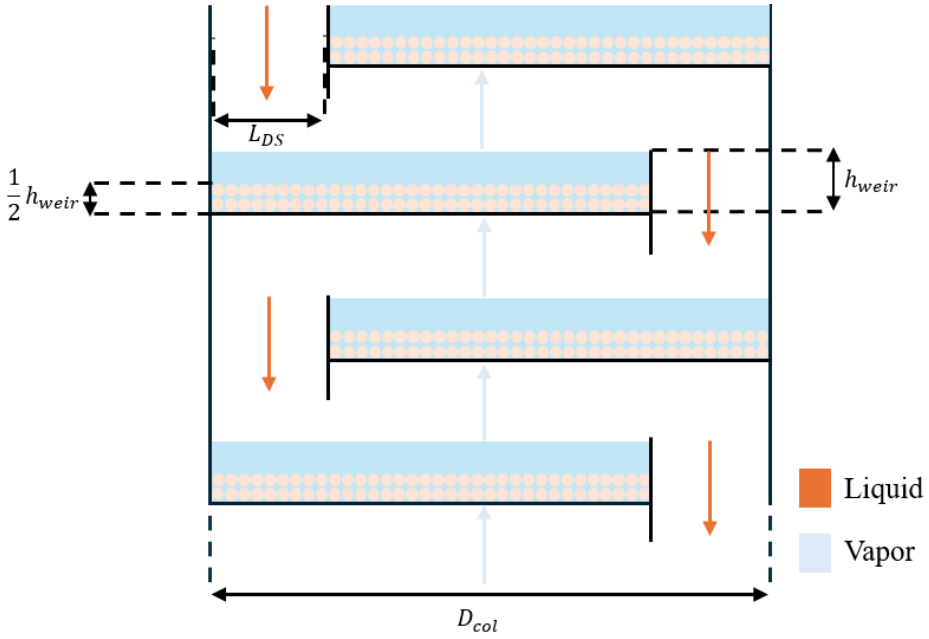

Source: Adapted from Lee and Hsiao (2017).

2.2.2 Heat Pump Distillation

Heat pump distillation is a technology designed to mitigate the energy losses inherent in conventional distillation processes. In a typical distillation column, the reboiler at the bottom requires heat from a hot utility, while the overhead condenser releases heat to a cold utility. Heat pump distillation reduces this energy consumption by integrating a heat pump, which transfers the latent heat from the overhead vapor to the reboiler, thereby minimizing external utility demands (Jana, 2014).

There are two main types of heat pump-assisted distillation systems: vapor compression column (VCC) and vapor recompression column (VRC). In a VRC system, the vapor leaving the top of the column is compressed, increasing both its pressure and temperature. This stream is then used as a heat source for the reboiler, providing the necessary boil-up for the distillation process (Kazemi *et al*., 2016). On the other hand, VCC system uses an external working fluid as the medium for energy transfer. This fluid evaporates by absorbing heat from the condenser, is compressed to increase its thermal energy, and then releases heat to the reboiler (Šulgan *et al*., 2021).

When the VC or VR method is applied to an RDC, the system is referred to as a Heat Pump for RD (HPRD). Figure 9 illustrates a schematic representation with VCC, VRC, and HPRD.

Figure 9 – Schematic Representation of (a) VCC, (b) VRC and (c) HPRD.

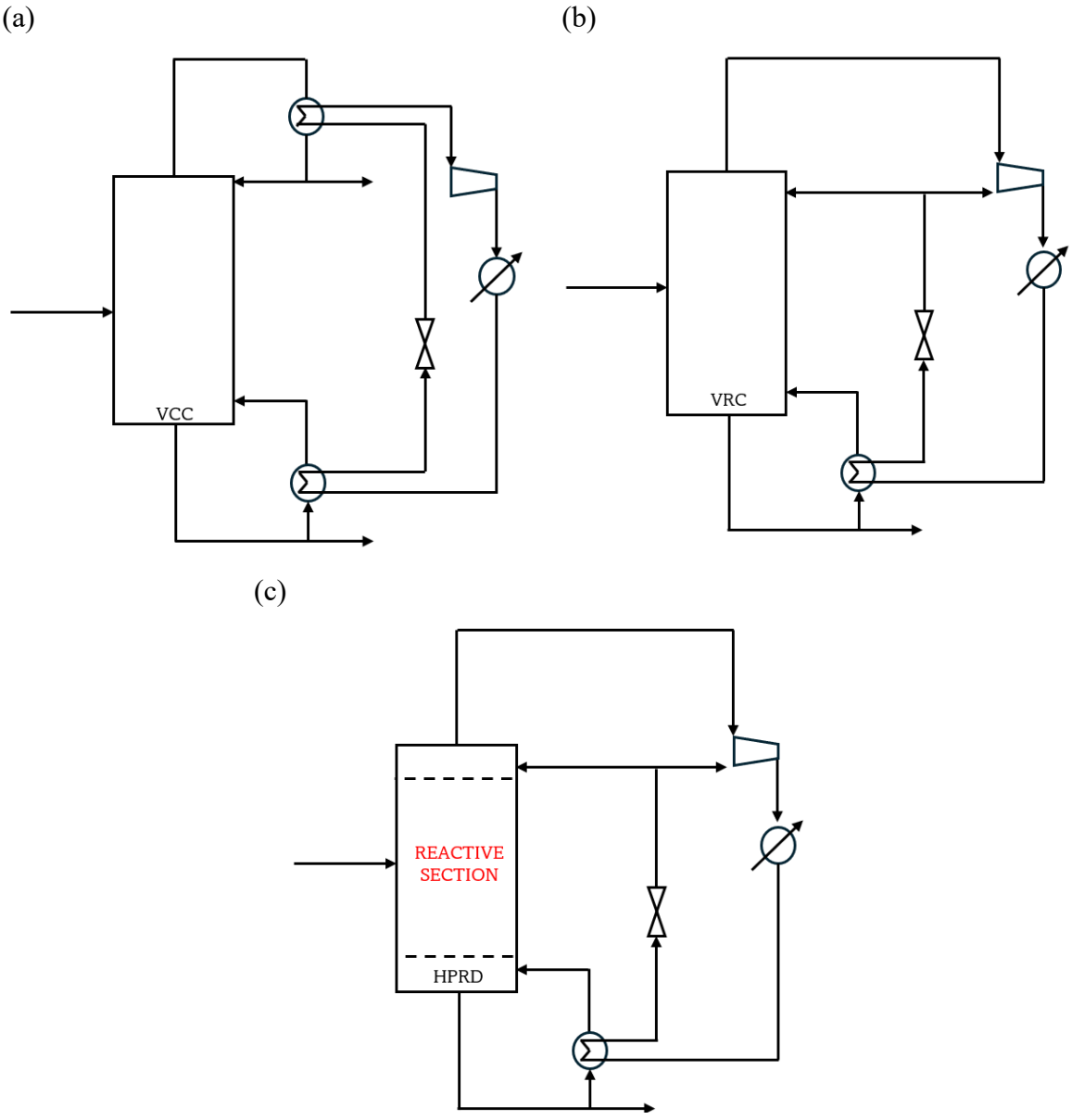

Source: Adapted from Kazemi *et al*. (2016); Šulgan *et al*. (2021).

The feasibility of integrating heat pump technology in a distillation column depends on the temperature difference between the condenser and the reboiler. To evaluate this feasibility, Pleşu *et al*. (2014) proposed the use the Coefficient of Performance (COP), which is defined as:

$$COP = \frac{1}{\eta_{Carnot}} = \frac{T_{cond}}{T_{reb} - T_{cond}} \quad (1)$$

Where η_{Carnot} is the Carnot efficiency, T_{cond}, condenser temperature, and T_{reb}, reboiler temperature.

According to Zhang *et al*. (2025), COP determines whether a heat pump should be implemented:

- If $COP > 10$, using a heat pump is highly recommended.
- If $10 \geq COP \geq 5$, further economic and operational analysis is required to assess feasibility.
- If $COP < 5$, using a heat pump is not beneficial.

2.2.3 Other PI technologies

One of the most notable PI configurations is the Side Reactor Column (SRC) (Figure 10), which integrates at least one side reactor with a conventional distillation column through an external loop. In this system, liquid streams from specific column trays are pumped to external reactors that operate either isothermally or adiabatically (Baur; Krishna, 2004; Hussain *et al*., 2019; Kaymak; Luyben, 2004). SRC is recommended when reaction and separation processes require distinct operating conditions, such as high-pressure reactors and vacuum distillation columns. Additionally, it addresses challenges such as unfavorable volatility differences, slow reaction kinetics, and hydraulic limitations (Krishna, 2002). The flexibility in SRC design enables variation in the number and type of reactors, as well as the linked column stages.

Figure 10 – Schematic Representation of SRC.

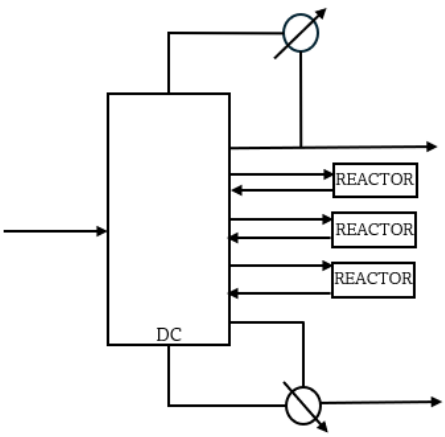

Source: Adapted from Baur and Krishna (2004).

For multicomponent distillation, the Dividing Wall Column (DWC) is an efficient PI configuration capable of separating three or more compounds within a single unit, eliminating the need for multiple conventional distillation columns using a partial vertical partition integrated into the shell. The column separates the species with the highest and lowest volatilities on the feed side of the wall, while those with intermediate volatility are distributed to both the top and bottom of the partition. On the product side, the components with intermediate volatility are further separated from the light and heavy fractions and withdrawn as a side stream (Weinfeld; Owens; Eldridge, 2018). When chemical reactions are incorporated into a DWC, the system is referred to as a Reactive Distillation Dividing Wall Column (RDWC) (Egger; Fieg, 2019).

On the other hand, Thermally Coupled Distillation Sequences (TCDS) and Heat Integrated Distillation Columns (HIDiC) provide substantial energy savings in processes with high energy requirements by optimizing heat recovery and minimizing dependency on external utilities. Fundamentally, thermal coupling involves the transfer of liquid and vapor streams between interconnected distillation columns, allowing efficient redistribution of energy throughout the system (Jiang; Agrawal, 2019).

A classic example of TCDS configuration is the Petlyuk Column, which uses a prefractionator to split the feed into light and heavy fractions, while distributing the component with medium volatility between the top and bottom streams. Then, they are introduced into specific trays of the main column, where the final separation is completed (Carranza-Abaíd; González-García, 2020).

Alternatively, HIDiC combines VR with internal heat integration. In diabatic stages, HIDiC distributes heat rejection along the rectifying section and heat absorption along the stripping section (Jana, 2010; Mah; Nicholas; Wodnik, 1977). The efficiency of HIDiC is further optimized by incorporating a compressor and throttling valve to manipulate the pressure difference between the rectifying and stripping sections, ensuring a favorable temperature driving force (Suphanit, 2010). When HIDiC is applied to an RDC, the system is referred to as Heat Integrated Reactive Distillation Column (HIRDiC) (Vanaki; Eslamloueyan, 2012).

Figure 11 illustrates the schematic representations of all the previous mentioned PI configurations, showing their structural differences.

Figure 11 – Schematic Representation of (a) DWC, (b) RDWC, (c) Petlyuk Column, (d) HIDiC and (e) HIRDiC,

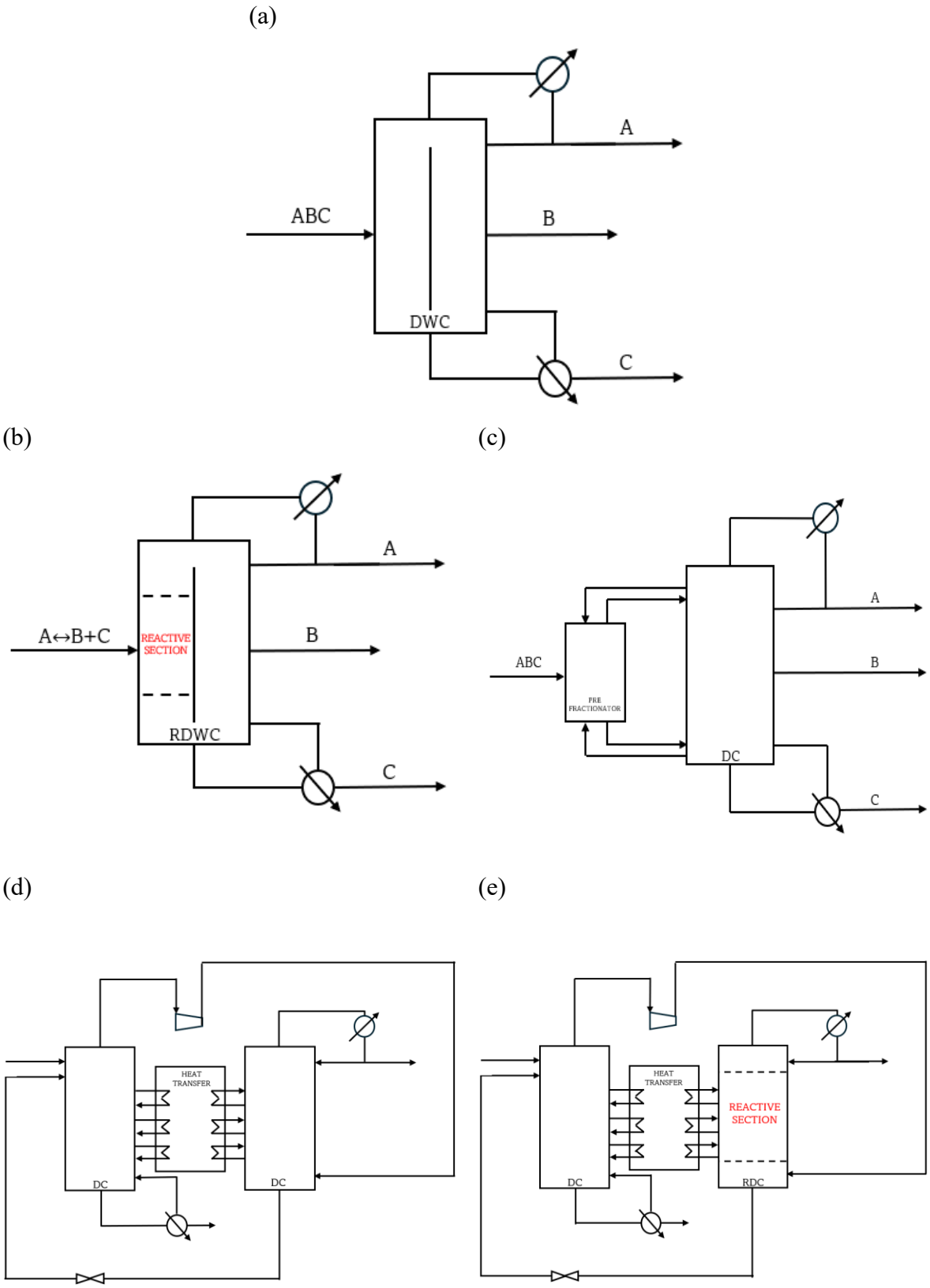

Source: Adapted from Carranza-Abaid and Gonzalez-García (2020); Jana (2010); Vanaki and Eslamloueyan (2012); Weinfeld, Owen and Eldridge (2018).

2.3 Multi-Objective Optimization (MOO)

Multi-objective optimization (MOO) is a typical methodology used to optimize multiple conflicting objectives simultaneously. Unlike single-objective optimization, which identifies a single best solution, MOO generates a set of non-dominated solutions, known as the Pareto Front, where improving one objective compromise at least one other (Li *et al*., 2021). The Pareto Front allows decision-makers to evaluate trade-offs and select the solution that best satisfies specific process requirements.

Over the past decades, interest in MOO has grown exponentially, driven by the development of advanced computational techniques (Cerda-Flores; Rojas-Punzo; Nápoles-Rivera, 2022). Integrating artificial intelligence (AI) and machine learning (ML), particularly through evolutionary algorithms, has further expanded its industrial applicability. These innovations have led to more efficient exploration of complex solution spaces, enhancing the identification of optimal Pareto Fronts while reducing computational cost (Zapotecas-Martínez; García-Nájera; Menchaca-Méndez, 2023).

2.3.1 Metaheuristic methods

Metaheuristic algorithms generate a population of candidate solutions and iteratively improve them using exploration and exploitation strategies. Their effectiveness is derived from the ability to balance randomness, which enables them to explore the global search space and avoid premature convergence, with local search techniques that refine solutions in promising regions of the solution space. Although these algorithms are flexible and capable of identifying excellent solutions across diverse applications, they are unable to guarantee convergence to the global optimum. Nonetheless, they often yield satisfactory results when the algorithm parameters are appropriately tuned (Halim; Ismail; Das, 2021).

Metaheuristics are particularly valuable in process systems engineering (PSE), where optimization problems tend to be complex and nonlinear. Applications include process design, scheduling, and control. Algorithms such as the Genetic Algorithm (GA) (Holland, 1975), Particle Swarm Optimization (PSO) (Kennedy; Eberhart, 1995), and Simulated Annealing (SA) (Kirkpatrick; Gelatt; Vecchi, 1983) have demonstrated efficiency in optimizing energy-intensive operations, including the design of heat exchanger networks and distillation column configurations (Shelokar *et al*., 2014).

2.3.2 Genetic Algorithm (GA)

Among the various metaheuristic methods proposed in the literature, GA stands out as one of the most popular optimization algorithms. It iteratively refines a population of candidate solutions through mechanisms inspired by natural selection and heredity (Lambora; Gupta; Chopra, 2019). Unlike traditional gradient-based optimization techniques, GA employs a probabilistic search strategy to explore highly constrained and multimodal spaces while reducing the risk of premature convergence to local optima (Mirjalili, 2019).

The main GA operators are selection, crossover, and mutation. The selection operators prioritize better candidate solutions (chromosomes), allowing them to pass their "genes" to the next generation while maintaining population diversity (Katoch; Chauhan; Kumar, 2021). In the crossover phase, an exchange of genetic information between the selected parent chromosomes is conducted, generating new offspring that inherit characteristics from both parents (Hussain *et al*., 2017). Then, in the mutation, random modifications are introduced into offspring chromosomes to maintain genetic diversity, prevent premature convergence, and enhance exploration of the solution space (Alhijawi; Awajan, 2024).

In this context, the Non-dominated Sorting Genetic Algorithm (NSGA) extends the standard GA framework to handle MOO problems. Rather than converting multiple objectives into a single weighted objective function, NSGA applies non-dominated sorting and ranking solutions based on Pareto dominance to maintain a diverse set of trade-off solutions (Srinivas; Deb, 1994). While the NSGA has been widely adopted for solving MOO problems, it presents certain limitations when applied to complex systems, including high computational cost in sorting procedures, lack of elitism, and the necessity to define a sharing parameter to maintain diversity in the population. Deb *et al.* (2002) proposed an improved version named as NSGA-II to overcome these drawbacks. This enhanced algorithm reduces the number of dominance comparisons (introducing a more efficient sorting approach), incorporates elitism, and introduces a crowding distance mechanism (encouraging the selection of solutions in less populated regions of the Pareto Front).

Several recent studies have applied the NSGA-II algorithm for biodiesel production optimization (Ahmed *et al*., 2022; Deshpande *et al*., 2022a; Mondal *et al*., 2021; Mondal; Rangaiah; Jana, 2022; Patle *et al*., 2014; Tóth *et al*., 2016). Figure 12 illustrates the principles of the NSGA-II algorithm, and Table 2 provides a comparative overview of the objective functions employed in each of the referenced studies.

Figure 12 – Schematic Representation of NSGA-II functioning.

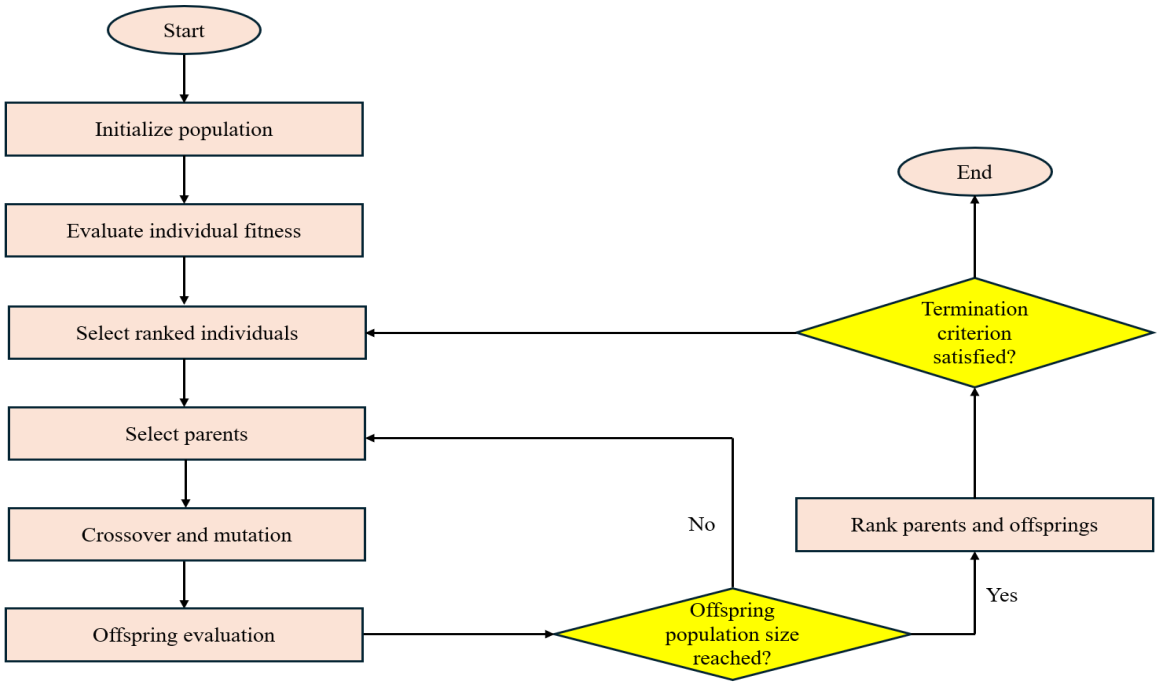

Source: Adapted from Chang, Bouzarkouna and Devegowda (2015).

Table 2 – Objective Functions in MOO Studies on Biodiesel Production Using the NSGA-II Algorithm.

Work	Metric		
	Economic	Environmental	Product Quality / Process
Ahmed *et al*. (2022)	TAC	Organic waste and CO_2e	None
Deshpande *et al*. (2022a)	TAC	Organic waste and CO_2e	Individual risk
Mondal *et al*. (2021)	TAC	CO_2e	Biodiesel purity
Mondal; Rangaiah; Jana (2022)	TAC	CO_2e	Biodiesel purity
Patle *et al*. (2014)	TAC	Organic waste	Heat duty
Tóth *et al*. (2016)	TAC	None	Energy usage, productivity and purity

TAC: Total Annualized Cost

Source: Author.

2.3.3 Decision-Making Strategies in Pareto-Front Optimum Selection

A pivotal step in MOO is selection of a single non-dominated solution from the Pareto front. Despite its importance, this phase often receives limited attention, even though the chosen solution defines the operational conditions in a chemical plant system. Choosing an appropriate solution in practical applications ensures that optimization results are effectively implemented into real-world operational process operations.

Among the various available selection methods, Wang and Rangaiah (2017) identified three techniques as the most suitable for optimal solution selection in PSE, considering their simplicity and applicability: Technique for Order of Preference by Similarity to Ideal Solution (TOPSIS), Grey Relational Analysis (GRA), and Simple Additive Weighting (SAW). These methods provide structured decision-making frameworks for selecting a solution that best aligns with process requirements and performance criteria.

2.3.3.1 TOPSIS

The TOPSIS selects the optimal solution based on its Euclidean distance from the positive and negative ideal solutions. The ideal solution represents the best possible values for all criteria, while the negative ideal solution represents the worst. The selected solution should be as close as possible to the positive ideal and as far as positive from the negative ideal (Hwang; Yoon, 1981). Figure 13 represents the steps of selecting the best solution using the TOPSIS method.

Figure 13 – Schematic Representation of TOPSIS.

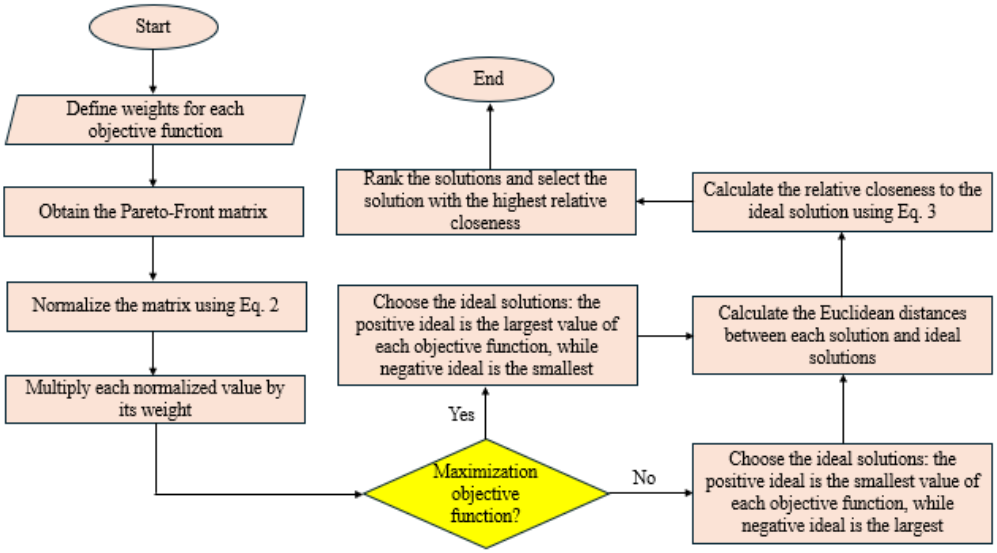

Source: Adapted from Hwang and Yoon (1981).

The objective function normalized value (f_{ij}^{norm}) and closeness to the ideal solution (C_i) are given by:

$$f_{ij}^{norm} = \frac{f_{ij}}{\sqrt{\sum_{i=1}^{m} f_{ij}^2}} \tag{2}$$

$$C_i = \frac{S_{i-}}{S_{i-} + S_{i+}} \tag{3}$$

Where f_{ij} is the objective function value, S_{i-} is the negative ideal and S_{i+} the positive ideal.

2.3.3.2 GRA

The GRA method is a decision-making approach that selects the highest Grey Relational coefficient (GRC). This coefficient quantifies the similarity between each solution and the maximum normalized value. An advantage of this method is that it does not require any prior input (Martinez-Morales; Pineda-Rico; Stevens-Navarro, 2010). Figure 14 illustrates the process for selecting the optimal solution using the GRA.

Figure 14 – Schematic Representation of GRA.

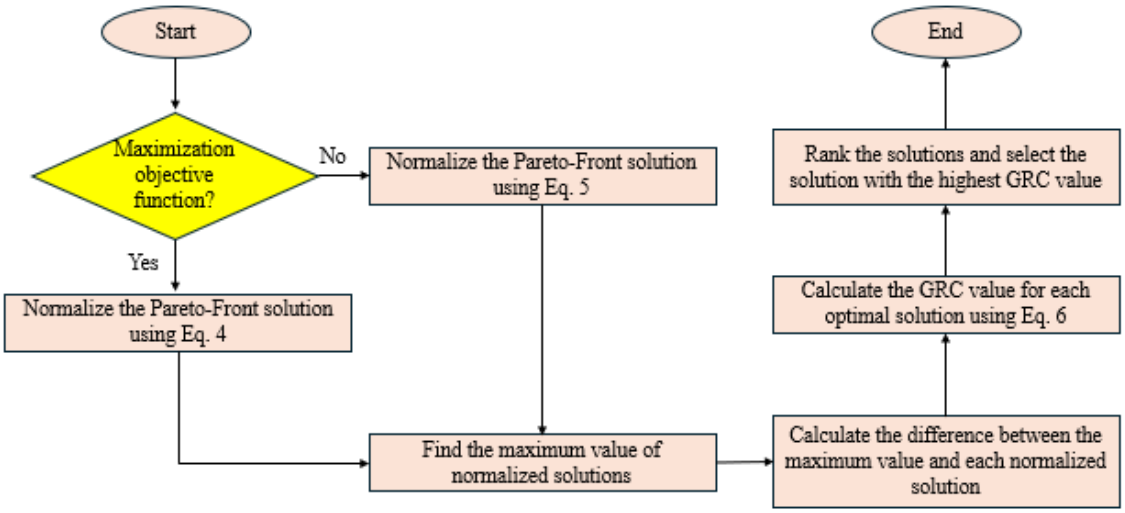

Source: Adapted from Martinez-Morales, Pineda-Rico and Stevens-Navarro (2010).

The GRC value and f_{ij}^{norm} and are computed using the following equations:

$$f_{ij}^{norm} = \frac{f_{ij} - \min_i f_{ij}}{\max_i f_{ij} - \min_i f_{ij}} \tag{4}$$

$$f_{ij}^{norm} = \frac{\max_i f_{ij} - f_{ij}}{\max_i f_{ij} - \min_i f_{ij}} \tag{5}$$

$$GRC_i = \frac{1}{m}\sum_{j=1}^{m}\frac{\min_{i,j}(\Delta I_{ij}) + \max_{i,j}(\Delta I_{ij})}{\Delta I_{ij} + \max_{i,j}(\Delta I_{ij})} \quad (6)$$

Where ΔI_{ij} is the difference between the maximum normalized value and each normalized solution.

2.3.3.3 SAW

The SAW is a simple method that considers each criterion independent and their additive contributions to the final decision. In this approach, each objective is assigned a weight reflecting its relative importance, and the performance of each alternative is evaluated by computing the weighted sum of its normalized values across all criteria (Martinez-Morales; Pineda-Rico; Stevens-Navarro, 2010). Figure 15 details the SAW methodology.

Figure 15 – Schematic Representation of SAW method.

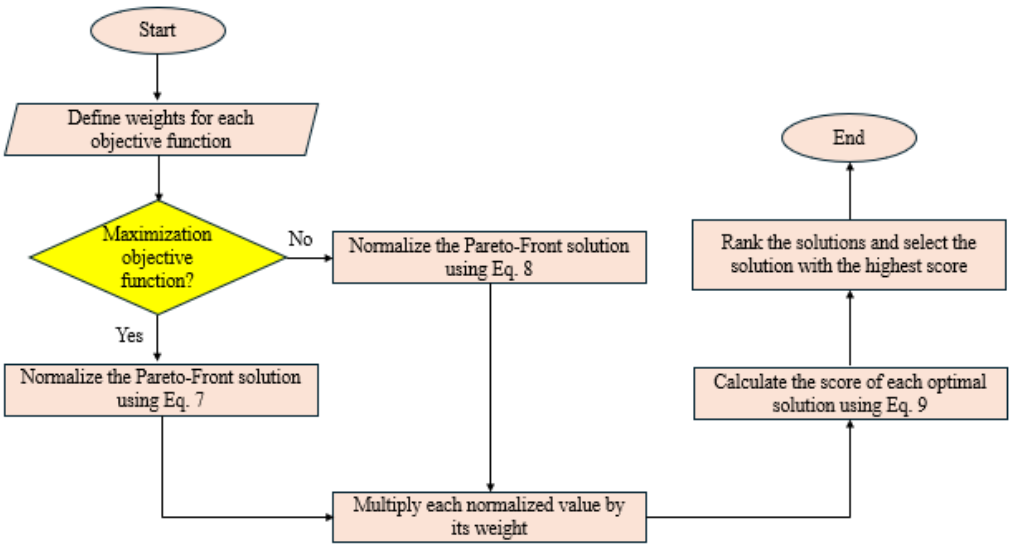

Source: Adapted from Martinez-Morales, Pineda-Rico and Stevens-Navarro (2010).

The SAW score (S_i) and f_{ij}^{norm} and are calculated using Equation x-y:

$$f_{ij}^{norm} = \frac{f_{ij}}{\max_i f_{ij}} \quad (7)$$

$$f_{ij}^{norm} = \frac{\min_i f_{ij}}{f_{ij}} \quad (8)$$

$$S_i = \sum_{j=1}^{n} wn_{ij} \quad (9)$$

Where wn_{ij} is the weighted normalized values.

2.3.4 Correlation Analysis

In MOO studies, correlation analysis is a commonly adopted approach for analyzing the impact of each decision variable on the objective function. The correlation coefficient (r) measures the monotonic or linear dependencies between input and output variables, with positive values representing direct correlations and negative values reflecting inverse correlations, as illustrated in Table 3.

Pearson and Spearman correlations are the two prevalent statistical analysis methods. The Pearson correlation coefficient measures how strongly and in which direction two continuous variables are linearly related assuming that the data are normally distributed and free from significant outliers (Benesty *et al*., 2009).

Table 3 – Classification of correlation strength based on coefficient value.

r	Strength of relationship
-1.0 to -0.5 or 0.5 to 1.0	Strong
-0.5 to -0.3 or 0.3 to 0.5	Moderate
-0.3 to -0.1 or 0.1 to 0.3	Weak
-0.1 to 0.1	None or very weak

Source: Xiao *et al*. (2016).

In contrast, the Spearman correlation assesses the strength of a monotonic relationship (independent of linearity) by ranking the data before calculating the correlation (Puth; Neuhäuser; Ruxton, 2015). Consequently, Spearman correlation is more robust to outliers and does not require the assumption that of normality (Schober; Boer; Schwarte, 2018), making it suitable for analyzing complex or nonlinear behaviors, as frequently observed in process engineering.

2.4 Literature Review in Simulation-Based Biodiesel Production

Many simulation studies have been conducted in recent years to explore different technological routes and catalytic systems for biodiesel production. Table 4 summarizes the relevant literature, detailing their focus, feedstock, technology, and catalyst used. Furthermore, Table 5 represents the main results in terms of economic performance, environmental aspect, and product quality.

Table 4 – Overview of studies in Simulation-Based Biodiesel Production.

Study	Study approach	Feedstock*	Technology	Catalyst(s) Type
Simasatitkul *et al*. (2011)	Simulation	SBO	RD	Homogeneous
Souza *et al*. (2014)	Simulation	CSO	SRD (batch) and RD	Homogeneous
Patle et al. (2014)	Simulation and optimization	WCO	SRD	Homogeneous
Karacan and Karacan (2015)	Optimization	Canola Oil	RD	Homogeneous
Boon-Anuwat *et al*. (2015)	Simulation	SBO	SRD and RD	Homogeneous and heterogeneous
Pérez-Cisneros *et al*. (2016)	Simulation	WVO	RD	Heterogeneous
Giwa and Ogunware (2017)	Modelling, simulation and control	Triolein	RD	Homogeneous
Treeyawetchakul (2020)	Simulation and PI	CPO	SRD and RD + Steam Reformer	Heterogeneous
Mondal *et al*. (2021)	Optimization and PI	Algal Oil	RD and SVRRD	Heterogeneous
Ahmed *et al*. (2022)	Optimization	Microalgae	SRD	Homogeneous
Deshpande *et al*. (2022b)	Optimization and PI	Microalgae	SRD-DWC + VR	Homogeneous
Aworanti *et al.* (2022)	Simulation and control	Triolein	RD	Heterogeneous
Mondal; Rangaiah; Jana (2022)	Optimization and PI	Algal Oil	RD and TCRD	Heterogeneous
Nascimento *et al*. (2023)	Simulation and PI	WCO	SRD and SRD+VR	Homogeneous
Sun *et al*. (2023)	Simulation and PI	WVO	SRD, SRD+VR and SRD+VR+ORC	Heterogeneous
Bose *et al*. (2024)	Optimization and PI	WVO	RD	None (supercritical conditions)

*All studies used methanol as reagent.

Source: Author

Table 5 – Main results of studies in Simulation-Based Biodiesel Production.

(continuate)

Source	Biodiesel Production (kmol/h)	Normalized Economic indicator (USD/$kmol_{biodiesel}$)	CO_2e from Steam generation (kg/ $kmol_{biodiesel}$)	Mass Biodiesel purity
Simasatitkul *et al*. (2011)	142.5	Not discussed	Not discussed	0.975
Souza *et al*. (2014)	0.93	TIC/PBP: 2.133 (batch SRD) and 1.526 (RD)	Not discussed	0.997
Patle *et al*. (2014)	57.26	Profit: 120.07	Not discussed	> 0.990
Karacan and Karacan (2015)	Low capacity	Not discussed	Not discussed	0.989
Boon-Anuwat *et al*. (2015)	3.25	Not discussed	Not discussed	0.973 (homogeneous RD) and 0.970 (heterogeneous RD)
Pérez-Cisneros *et al*. (2016)	268.60	Not discussed	Not discussed	0.999
Giwa and Ogunware (2017)	50.4	Not discussed	Not discussed	0.597
Treeyawetchakul (2020)	3.77	Cost ($/L): 0.93 (SRD) and 0.68 (with reformer)	Not discussed	≅ 0.990
Mondal *et al*. (2021)	18.60	TIC/PBP: 0.561 (RD) and 0.628 (SVRRD), TOC: 0.217 (RD) and 0.144 (SVRRD), TIC/PBP+TOC: 0.778 (RD) and 0.772 (SVRRD)	1.53 (RD) and 1.00 (SVRRD)	0.953 (RD), 0.934 (SVRRD)
Deshpande *et al*. (2022b)	8.45	BEC ($/kg): 1.85	EI99 (not normalized): $2.11x10^6$	> 0.965 (MOO constraint)

(conclusion)

Source	Biodiesel Production (kmol/h)	Normalized Economic indicator (USD/$kmol_{biodiesel}$)	CO_2e from Steam generation (kg/ $kmol_{biodiesel}$)	Mass Biodiesel purity
Aworanti *et al*. (2022)	2.97	Not discussed	Not discussed	0.983
Mondal; Rangaiah; Jana (2022)	18.11	Only for RD Column – TIC/PBP: 0.397 (RD) and 0.395 (TCRD), TOC: 0.124 (RD), 0.106 (TCRD), TAC: 0.521 (RD) and 0.502 (TCRD)	0.90 (RD) and 0.77 (TCRD)	After decanter: 0.995 (TCRD)
Nascimento *et al*. (2023)	3.36	TOC: 17.26 (SRD) and 7.50 (SRD+VR)	183.04 (SRD) and 57.74 (SRD+VR)	0.999
Sun *et al*. (2023)	28.14	TAC: 7.24 (SRD), 3.24 (SRD+VR) and 3.40 (SRD+VR+ORC)	50.06 (SRD), 15.33 (SRD+VR) and 11.86 (SRD+VR+ORC)	> 0.990
Bose *et al*. (2024)	299.96	TIC/PBP: 0.187, TOC: 0.472 and TIC/PBP+TOC: 0.659	Not discussed	0.752

Source: Author.

Early studies focused on simulation between conventional (SRD) and RD systems, while more recent works have integrated more PI strategies to enhance process efficiency. Treeyawetchakul (2020) coupled RD with steam reforming to utilize glycerol byproduct for hydrogen production, while Mondal *et al*. (2021) proposed a Side Vapor Recompression RD (SVRRD), which differs from HPRD, as it recompresses a side vapor stream rather than distillate and a total condenser must be used. Other PI techniques include DWC (Deshpande *et al*., 2022b), Thermal Coupling RD (TCRD) (Mondal; Rangaiah; Jana, 2022), VR (Nascimento *et al*., 2023; Sun *et al*., 2023) and Organic Rankine Cycle (ORC) (Sun *et al*., 2023).

The reviewed studies also explore a diverse range of feedstocks. In the literature, vegetable oils such as soybean oil (SBO) and cottonseed oil (CSO) are assumed to have low free fatty acid content, making it suitable for direct transesterification (Boon-anuwat *et al*., 2015; Simasatitkul *et al*., 2011; Souza *et al*., 2014). On the other hand, waste raw materials (waste vegetable oil (WVO) and waste cooking oil (WCO)), crude oils (crude palm oil (CPO) and canola oil) are modeled as a mixture of free fatty acids and triglycerides and require pre-treatment as previously discussed in Figure 7 (Bose *et al*., 2024; Nascimento *et al*., 2023; Pérez-Cisneros *et al*., 2016; Treeyawetchakul, 2020). Additionally, triolein has been employed as a model compound to provide controlled conditions for process evaluation (Aworanti *et al*., 2022; Giwa; Ogunware, 2017). Recently, some studies presented algal biodiesel as a promising alternative with high sustainability potential, through existing challenges in oil extraction (Ali *et al*., 2023; Deshpande *et al*., 2022b; Mondal *et al*., 2021; Mondal; Rangaiah; Jana, 2022).

Homogeneous catalysts are frequently employed in simulation studies due to availability of kinetic data when compared to heterogeneous catalysis. In contrast, as discussed in Boon-anuwat *et al*. (2015), heterogeneous catalysts offer advantages in terms of energy consumption and capital costs due to elimination of neutralization and water washing steps.

Economic viability is another consideration, but direct comparisons between studies are challenging due to differing economic metrics and levels of detail provided for operational and capital costs. To establish a common ground, when sufficient cost data are available, the Total Annualized Cost (TAC) is calculated as the sum of annualized Total Installed Cost (TIC/PBP) and Total Operating Cost (TOC), assuming a payback period (PBP) of 5 years and an operational time of 8000 h/year. Costs are updated using the latest Chemical Engineering Plant Cost Index (CEPCI) of 793.1 for October 2024, with historical CEPCI values obtained from Chemical Engineering Online Magazine (CE Plant Cost Index Report, 2025).

Lower TAC values are often associated with PI strategies. Mondal *et al*. (2021) and Mondal, Rangaiah, and Jana (2022) reported lower TAC for SVRRD (0.77 USD/kmol) and

TCRD (0.50 USD/kmol) compared to conventional RD (0.78 USD/kmol and 0.52 USD/kmol, respectively). Similarly, Sun *et al*. (2023) found that incorporating VR and ORC decreased TAC from 7.24 (SRD) to 3.24 USD/kmol. However, it is important to critically assess these economic benefits, as not all PI strategies necessarily translate into cost reductions or increased profitability. For example, VR requires expensive compressors, which can offset expected savings. Sun et al. (2023) also reported that adding ORC to a system with VR reduced energy consumption from 54.12 to 46.94 kWh/kmol but increased TAC from 3.24 to 3.40 USD/kmol.

Although not consistently reported across all studies, CO_2e from steam generation have been used as a key metric to evaluate the environmental performance of biodiesel production via RD. Studies that incorporated PI strategies generally demonstrated significant reductions in emissions. For example, emissions decreased from 1.53 to 1.00 kg CO_2/kmol in SVRRD (Mondal *et al*., 2021), 0.90 to 0.77 kg CO_2/kmol in TCRD (Mondal; Rangaiah; Jana, 2022), and from 50.06 to 11.86 kg CO_2/kmol in SRD+VR+ORC (Sun *et al*., 2023). Regarding biodiesel purity, most studies achieved high levels of methyl ester content (≥ 0.965), which is essential for compliance with international fuel standards, as result of effective use of catalysts along with optimized operating conditions.

As will be further discussed in the next section, SBO was selected as the feedstock for biodiesel production simulations, as it remains widely used feedstock in industrial-scale production. Therefore, it is essential to identify the most suitable kinetic parameters, specifically the pre-exponential Arrhenius factor and activation energy, from literature to ensure an accurate representation of the studied systems. Table 6 summarizes the experimental conditions employed to determine the kinetic parameters for the transesterification of SBO using different catalysts.

Table 6 – Experimental Studies for Kinetic Parameters Determination in SBO Transesterification.

Work	Catalyst	Catalyst type	Temperature range (°C)
Pasupulety *et al*. (2013)	CaO/Al_2O_3	Heterogeneous	125 – 200
Noureddini and Zhu (1997)	NaOH	Homogeneous	30 – 70
Liu *et al.* (2010)	CaO	Heterogeneous	40 – 65
Onyia, Mbah and Udeh (2015)	KOH	Homogeneous	45 – 65
Huang *et al.* (2009)	$Mg(OCH_3)_2$	Heterogeneous	50 – 65

Source: Author

When analyzing the temperature ranges reported in the studies and comparing them with the typical operating conditions observed in RDCs, the kinetic parameters provided by Pasupulety *et al*. (2013) are the most appropriate for this work. The choice is justified by the fact that their temperature range aligns well with the expected process conditions, minimizing the need for extrapolation. In contrast, the kinetic data from other studies require significant extrapolation, which could introduce inaccuracies in the reaction rate estimations for reactive stages of RDC.

3 Methodology

The simulations and optimization tasks were performed on a laptop equipped with an AMD Ryzen 7 7730U processor with 16 GB of RAM (15.3 GB usable), and Windows 11 Home operating system (Version 23H2 – 64 bit). Aspen Plus v14.0 was utilized for modelling the process, while cost estimations and optimization tasks were implemented in Python using the NSGA-II algorithm available in the *Pymoo* library (Blank; Deb, 2020).

3.1 Simulation Description

A preliminary evaluation of RD system to biodiesel production indicated a COP close to 5, which, according to literature criteria, suggests that the implementation of VR may be justifiable. In addition, although studies have explored RD and VR in biodiesel production, no research to date has integrated these technologies in a single HPRD column without use of external utilities. Based on these observations, the HPRD configuration was selected as the intensified alternative scenario to conventional RDC.

Soybean oil was selected as the feedstock for the simulations because it is the main raw material used for biodiesel production in Brazil, as previously discussed. Its low content of free fatty acid eliminates the need of pre-treatment (Simasatitkul *et al*., 2011). In Aspen simulations, soybean oil was modeled as triolein ($C_{57}H_{104}O_6$), a commonly adopted approach in the literature. This choice was based on studies which indicate that differences in the number of chains between the compounds have a negligible effect on the FAME yield within the same operating temperature range as this work (Soh *et al*., 2018). The selected component list for the simulations is presented in Table 7.

Table 7 - List of components and their representations in the simulations.

Component ID	Component name	CAS number	Representation
OOO	Triolein	122-32-7	Soybean Oil
MEOH	Methanol	67-56-1	Methanol
FAME	Methyl-Oleate	112-62-9	FAME
GLY	Glycerol	56-81-5	Glycerol

Source: Author.

To determine the appropriate thermodynamic package for the simulations, a decisional flow diagram was consulted. According to it, UNIQUAC and NRTL were identified as suitable

candidates, as highlighted in Figure 16 red line. Studies demonstrate that NRTL provides greater accuracy than UNIQUAC in similar systems (Mesquita *et al*., 2011; Mesquita *et al*., 2012; Sun *et al*., 2023). Consequently, the NRTL model was chosen with missing binary interaction parameters estimated using UNIFAC.

Figure 16 – Decisional diagram for thermodynamic package selection.

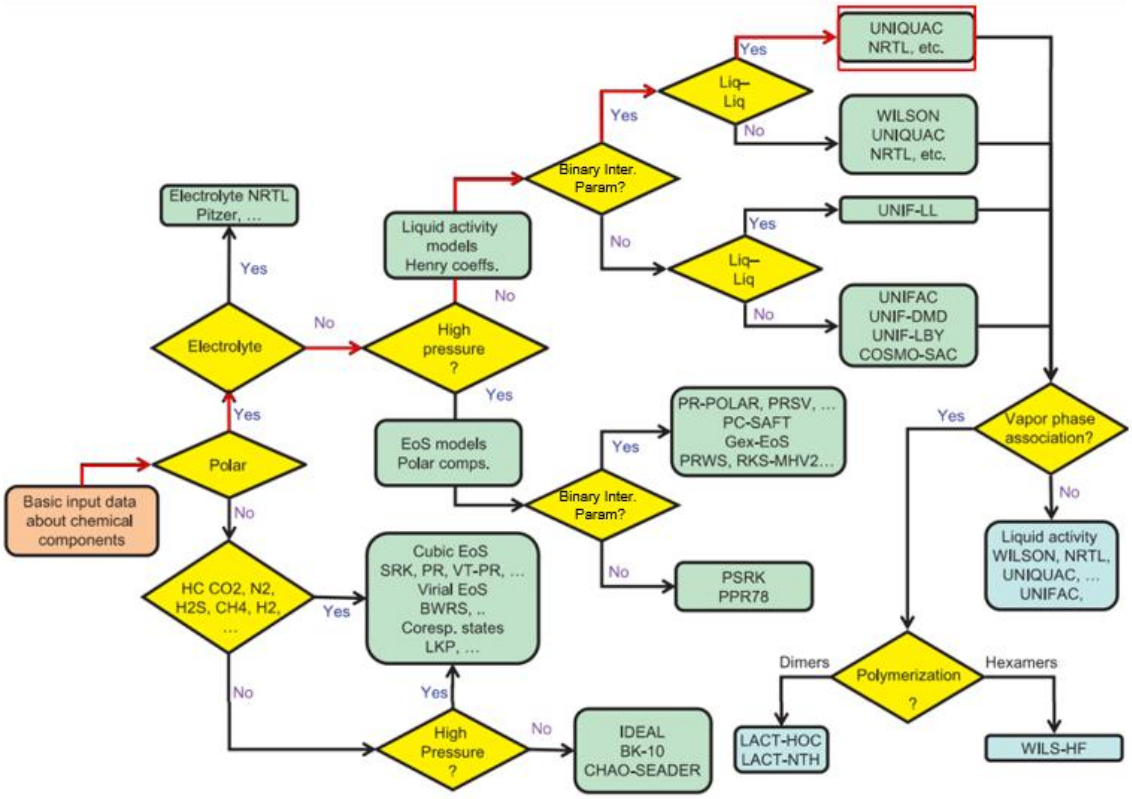

Source: Adapted from De Tommaso *et al*. (2020).

Given the experimental temperature range and use of heterogeneous catalysts, the kinetic model proposed by Pasupulety *et al.* (2013) was adopted to represent the reaction kinetics in the simulation. In their work, the reaction rate was assumed to follow pseudo-first order dependence with respect to triglycerides. The pre-exponential factor (0.5574 s^{-1}) and the activation energy (30,700 J/mol) were determined through regression of experimental data, considering Arrhenius Equation.

The transesterification of triglycerides with methanol over CaO/Al_2O_3 catalyst produces methyl oleate and glycerol, as represented by the following stoichiometry:

$$OOO + 3\ MEOH \xrightarrow{CaO/Al_2O_3} 3\ FAME + GLY \qquad (10)$$

3.2 Case Studies

Based on previous studies in literature, three case studies were proposed to evaluate the impact of PI in biodiesel production, which are described below. In each case study, it was evaluated the performance of RD and HPRD Configuration (denoted as Configurations A and B, respectively). The flowsheets of Configuration A and its operational conditions was adapted from Boon-Anuwat *et al*. (2015) and Gaurav *et al*. (2013), while Configuration B was proposed by this work. In all case studies, the diameter of each distillation column (modeled with RADFRAC block) was determined through tray sizing calculations performed in Aspen Plus and the h_{weir} and L_{DS}/D_{col} were set to 10.16 cm and 0.1, respectively, based on heuristics to avoid high pressure drops and operating problems such as weeping and flooding (Lee; Hsiao, 2017). All corresponding Aspen Plus flowsheets for each case study are provided in Appendix A.

3.2.1 Case Study 1 (CS-1)

In this first scenario, the biodiesel production process is analyzed considering as the only quality specification the methyl oleate mass fraction, which must be higher than 96.5 wt.%. No additional specifications are imposed on the biodiesel or on the produced glycerol, which is assumed to be commercialized as crude glycerol with a mass purity ranging from 70 wt.% to 99.5 wt.%. This assumption is consistent with previous studies in the literature (Bose *et al*., 2024; Mondal *et al*., 2021; Mondal; Rangaiah; Jana, 2022), which also focused exclusively on the process technology, without addressing glycerol purification or imposing strict standards for biodiesel quality.

In Configuration A (CS-1A), represented in Figure 17, the feed stream consists of soybean oil (SBO-IN) with a molar flow rate of 4.5 kmol/h and methanol (MEOH-IN) at 15.0 kmol/h. These are mixed with recycled methanol stream (REC-MEOH) and pumped into a reactive distillation column (RDC-1) at 4th stage, operating at 1 atm. The RDC-1 is modeled with 8 theoretical stages, a total condenser, a kettle-type reboiler, a reflux ratio of 0.6, and distillate-to-feed flow rate ratio of 0.31. A pressure drop of 0.1 atm per stage is considered. The design variables are adapted from the configuration proposed by Gaurav *et al.* (2013), who modeled a similar column using 7 stages and adopted a reflux ratio of 0.6 with 0.1 atm pressure drop per stage. The decision to operate at 1 atm, rather than the 3 atm used in Gaurav *et al.* (2013) is to avoid excessive temperatures, which could lead to thermal degradation of components. The bottom stream flows into a decanter (DEC-1), which separates the organic

phase from the glycerol and unreacted methanol mixture, due to density difference between methyl oleate and glycerol.

Figure 17 – Schematic Representation of CS-1A.

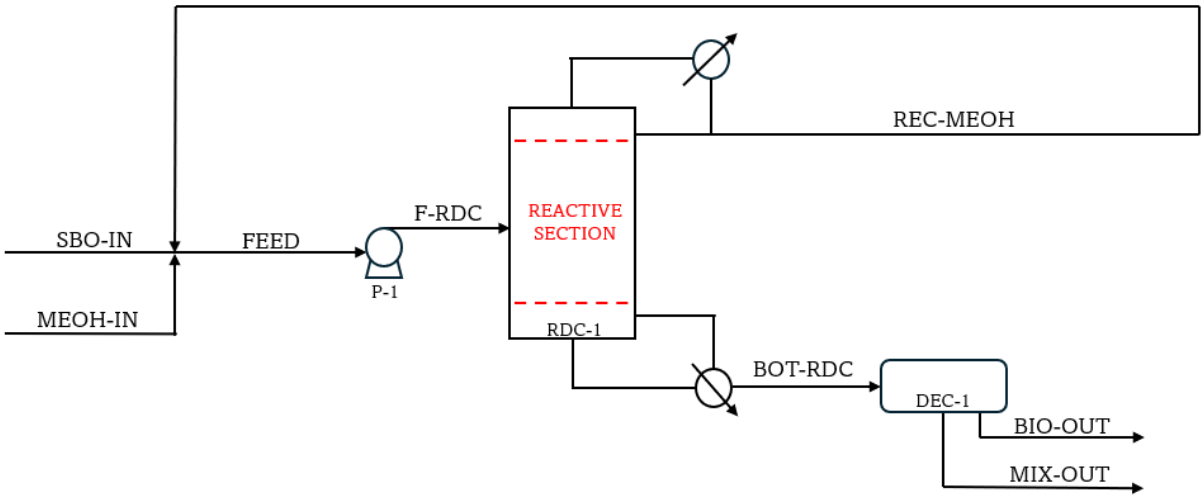

Source: Adapted from Gaurav *et al*. (2013).

In Configuration B (CS-1B) (Figure 18) the heat duty of RDC-1 is supplied by an internal VR system, replacing the use of conventional hot utilities. In this device, the distillate stream (DIST-RDC) is compressed to 15 atm (80% isentropic efficiency), increasing its temperature to serve as heat source in the reboiler (HX).

Figure 18 – Schematic Representation of CS-1B.

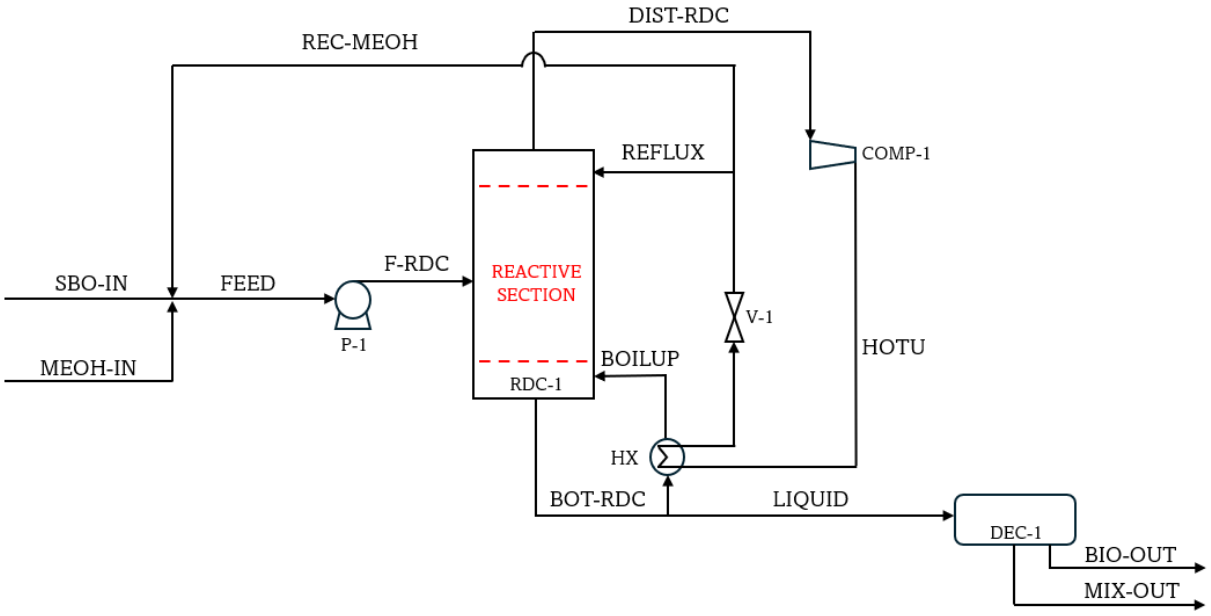

Source: Author.

To model HX in Aspen Plus, a traditional HPRD modelling approach was used, with a combination of *HeatX* block (HEAT) and *Flash2* separator (SEP) , as expressed in Valvassore and Costa (2025). The minimum temperature in the reboiler is set to 5 °C, and 66% of the bottom stream (BOT-RDC) is vaporized. The cooled vapor stream is partially recycled, with 60% refluxed to RDC-1 (REFLUX), and the remainder returned to the feed stream (REC-MEOH). The liquid outlet of HEAT is directed to DEC-1 for phase separation. The detailed modelling of HX is represented in Figure 19.

Figure 19 – Detailed Modelling of RDC Reboiler in HPRD system.

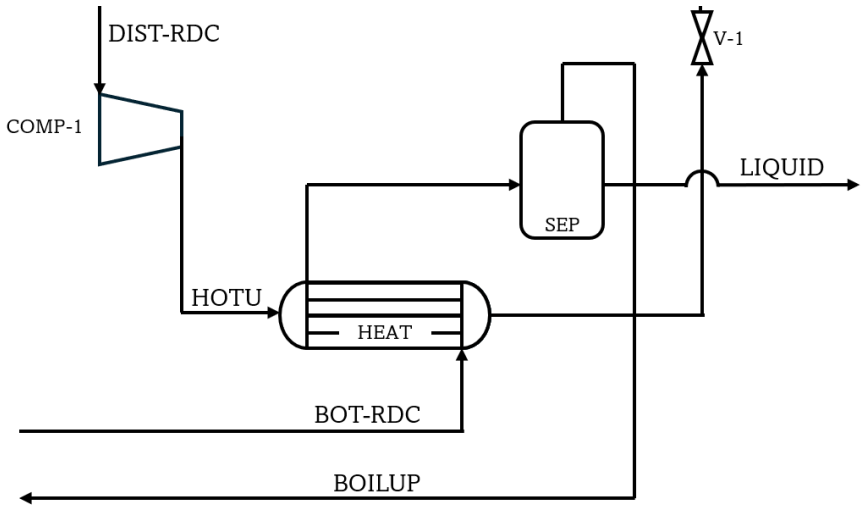

Source: Author.

3.2.2 Case Study 2 (CS-2)

The second case study (CS-2) is driven by the growing demand for crude glycerol valorization as strategy improve the economic viability of biodiesel production. The glycerol phase obtained from conventional transesterification processes, such as those obtained in CS-1, is typically contaminated with significant amounts of methanol, inorganic salts, soaps, and other organic residues, which make it unsuitable for applications in the pharmaceutical and food industries without further refinement. As highlighted by Ciriminna *et al*. (2014), vacuum distillation is the most adopted method for achieving high-purity glycerol, giving that its boiling point is approximately 290 °C under atmospheric conditions. Nonetheless, this separation technique is energy-intensive and economically justified only at large processing capacities.

Despite the technical and operational disadvantages, the substantial increase in commercial value achieved by upgrading crude glycerol to United States Pharmacopeia (USP) grade (purity above 99.5 wt.%), suitable for pharmaceutical use, may compensate additional

investment and energy requirements. Accordingly, in CS-2, a vacuum distillation column (DC-1), operating at 0.1 atm to mitigate thermal degradation, is integrated into the flowsheets of CS-1 to evaluate the feasibility of crude glycerol purification. The modified process diagrams for configurations CS-2A and CS-2B are depicted in Figure 20.

Figure 20 – Schematic Representation of (a) CS-2A and (b) CS-2B.

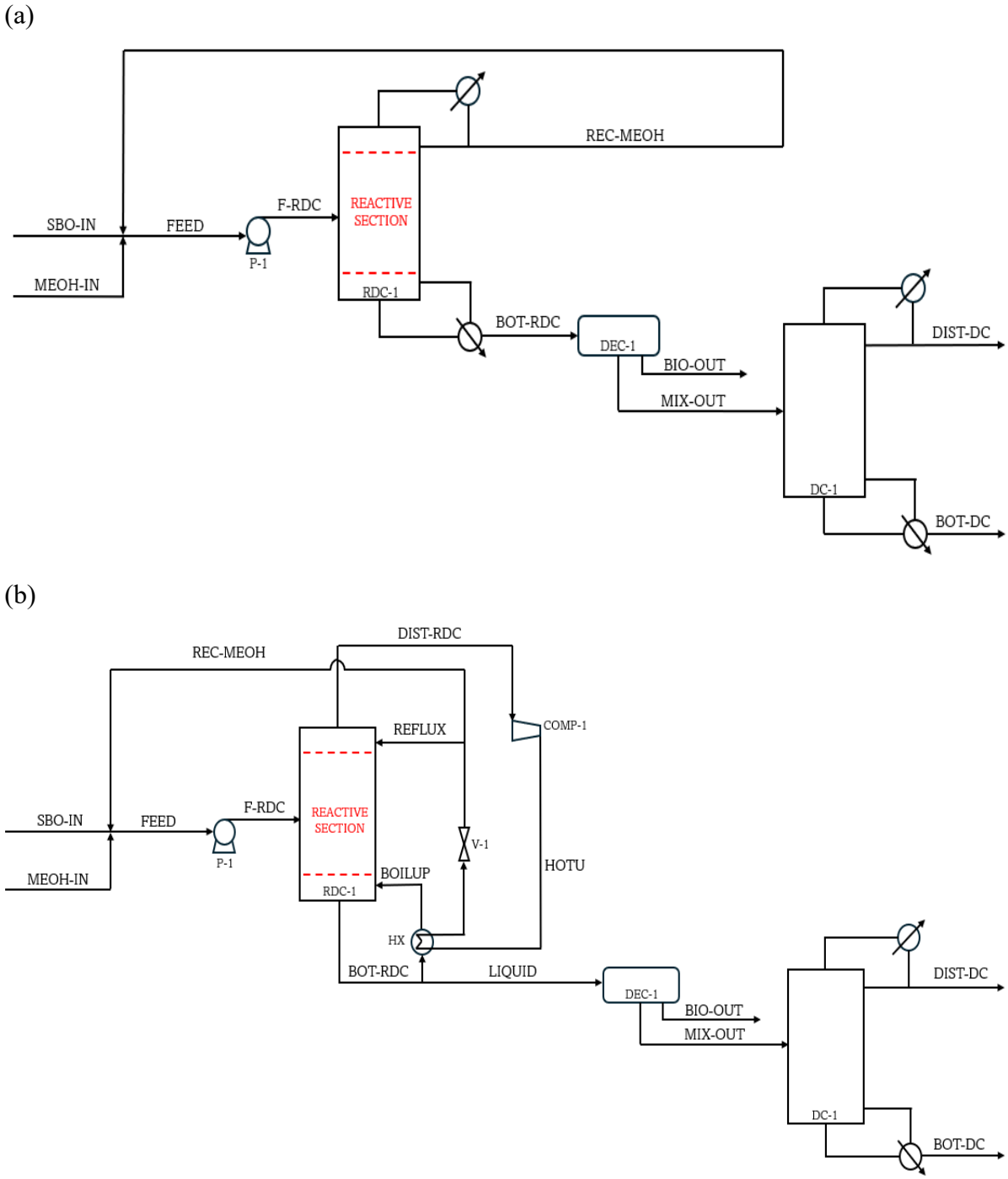

Source: (a) Adapted from Boon-Anuwat *et al*. (2015) and (b) Author.

3.2.3 Case Study 3 (CS-3)

The third case study (CS-3) explores a scenario where the biodiesel product must attend all quality specifications established by ANP. Unlike the previous cases, where only FAME mass fraction was controlled, this configuration imposes strict quality constraints aligned with ANP Resolution No. 920/2023, which regulates the commercial purity of biodiesel for fuel applications in Brazil. In this scenario, the biodiesel stream must present a minimum FAME mass fraction of 96.5 wt.%, glycerol, while the content of each impurity (glycerol, methanol and triolein) must be individually lower than 0.2 wt.%.

To facilitate convergence and ensure simulations robustness within the feasible operating region during optimization problem resolution, a methanol purge strategy is implemented in both configurations. Specifically, 95% of methanol recovered from RDC-1 is recycled to the feed stream, while 5% is purged from the system (MEOH-OUT). The adjustment prevents methanol accumulation in the recycle loop, which could otherwise lead to numerical instability of simulation under stringent separation and purity requirements. The modified flowsheets corresponding to CS-3A and CS-3B are presented in Figures 21 and 22.

Figure 21 – Schematic Representation of CS-3A.

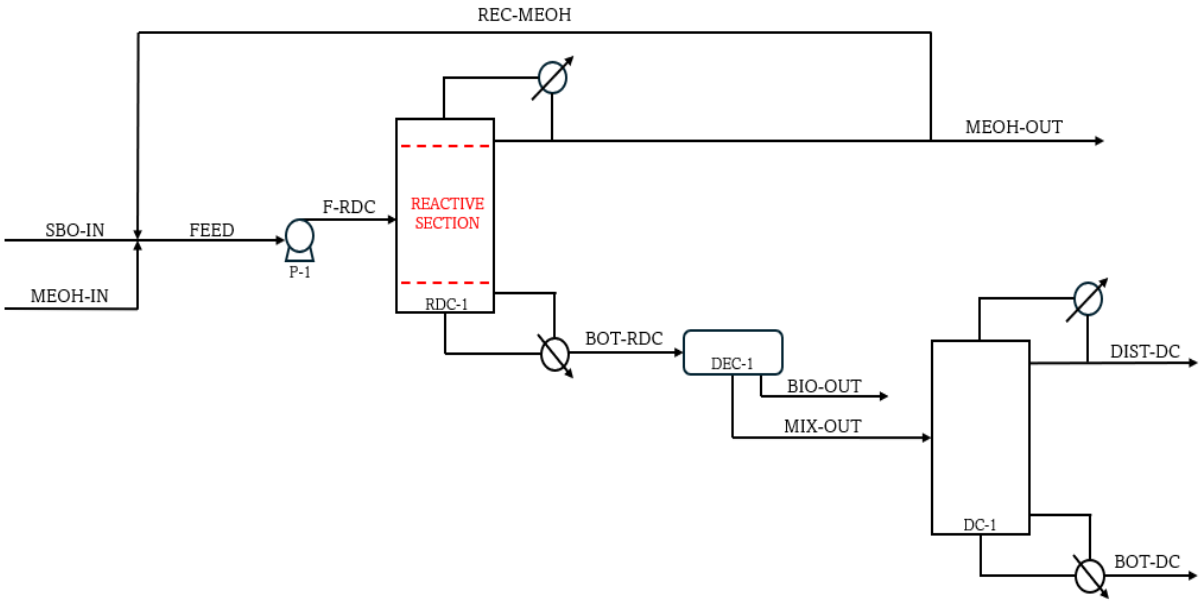

Source: Author.

Figure 22 – Schematic Representation of CS-3B.

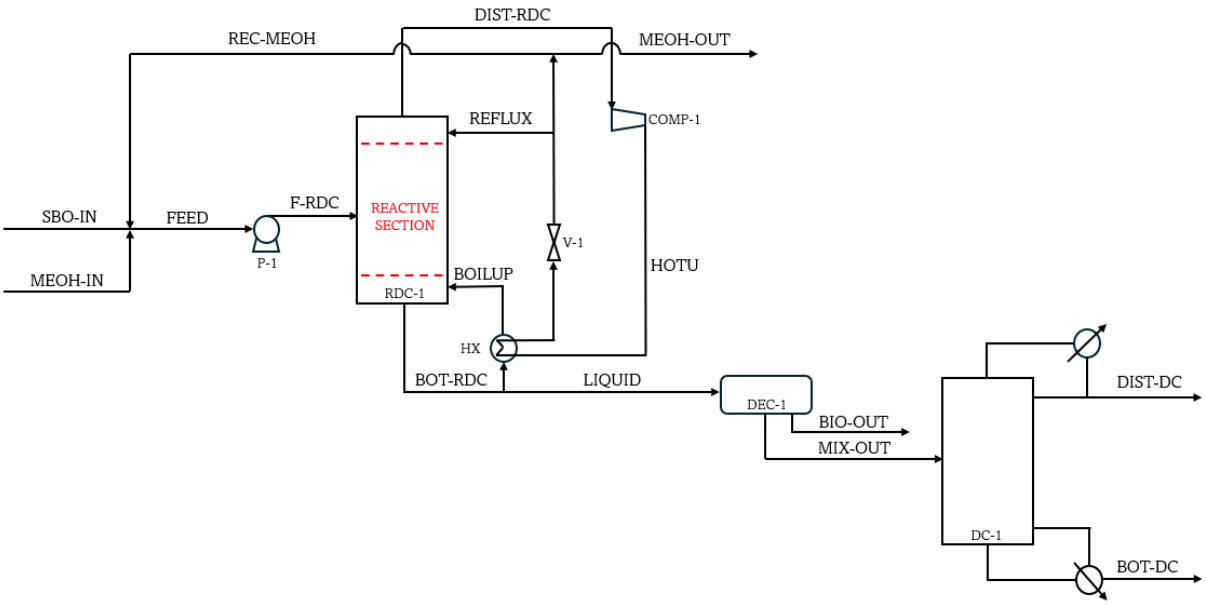

Source: Author.

3.3 Multi-Objective Optimization (MOO) Problem

This subsection describes the formulation of the MOO problem developed to assess the intensified process configurations in each case study. In MOO, the concept of non-dominance is fundamental: in two conflicting objectives, a non-dominated solution cannot be improved in one objective without deteriorating the other. The goal here is thus to determine the set of non-dominated solutions regarding maximizing economic profitability and minimizing environmental impact, while accounting for the main constraints observed in real operations. The set of non-dominated solutions is typically referred to as the Pareto front. The methodology adopted for the quantification of each performance indicator, as well as the penalization strategy and solution approach in the MOO algorithm, is described in detail.

3.3.1 Economic Indicator

Although the TAC is commonly adopted in literature as the main indicator of economic performance, this study employs the Yearly Gross Profit (YGP) as the economic objective function. This choice reflects the understanding that, in real industrial scenarios, profitability is not exclusively determined by cost minimization but also influenced by revenue generation (an aspect not captured by TAC). A similar economic perspective has been adopted by several studies (Chiou *et al*., 2023; Wu *et al*., 2024; Yu, 2020). It is important to note that, different from reported literature for intensified process configurations evaluations and in

accordance with the methodology adopted by Siqueira and Pavão (2025), the total capital expenditure of the chemical plant was estimated using Lang Factor method. For fluid-processing plants, Turton *et al.* (2018) recommend a Lang Factor (F_{lang}) of 4.74, which is applied to *TIC* to determine the overall investment required.

The considered costs are related to equipment acquisition and installation, utility consumption, catalyst use, and raw material costs as in previous studies (Babaie; Esfahany, 2021; Mondal *et al*., 2021; Mondal; Rangaiah; Jana, 2022; Sun *et al*., 2023; Wang *et al*., 2019). The mathematical formulation of YGP is defined by Equations 11 – 14.

$$YGP = TR - TC \tag{11}$$

$$TR = t_{op} \sum_{i}^{n_{rea}} P_i \dot{m}_i \tag{12}$$

$$TC = \left(F_{lang} \frac{TIC}{PBP}\right) + TOC + RC \tag{13}$$

$$RC = t_{op} \sum_{j}^{n_{prod}} P_j \dot{m}_j \tag{14}$$

Where:

- TR: total revenue
- TC: total costs
- t_{op}: operational time (8000 h)
- P: unit price (index *i* is related to feedstock and *j* to product)
- $\dot{m}$: mass flowrate (index *i* is related to feedstock and *j* to product)
- n_{rea}: number of reactants
- n_{prod}: number of products
- F_{lang}: Lang factor
- TIC: total installed costs
- PBP: payback period (5 years as considered in Mondal, Rangaiah and Jana (2022))
- TOC: total operating costs
- RC: raw materials cost

In this work, TIC was calculated as the sum of the installed costs for each equipment used in the chemical process following the equations proposed by Douglas (1988) and data regression for pumps derived from a manufacturer's catalog (Inverter, 2022) presented in detail

in Appendix B. The Marshall and Swift (M&S) index used in this study was 2031.9 (correspondent to 2022), as reported by Go, Chu and McFarland (2023). Following the calculations based on the 2022 M&S index, the individual equipment costs were updated using the Chemical Engineering Plant Cost Index (CEPCI) values for October 2024 (793.1), 2022 (797.6) and 2018 (615.9) (CE Plant Cost Index Report, 2025). The cost adjustment was performed using the following equation:

$$Cost_{2024} = \left(\frac{CEPCI_{2024}}{CEPCI_{2022}}\right) Cost_{2022} \quad (15)$$

On the other hand, TOC includes the costs of catalysts, utilities and electricity. The cost estimation of CaO supported on alumina catalyst was conducted using Catcost, a free and user-friendly tool developed by Chemical Catalysis for Bioenergy Consortium composed by several US national laboratories (Van Allsburg *et al*., 2022). The detailed estimation is provided by Appendix C and it is assumed a lifetime of 1 year (Gaurav *et al*., 2013). Prices of reactants, products and catalyst are expressed in Table 8, and utilities used in Table 9.

Table 8 – Prices of reactants, products and catalyst used in biodiesel production.

Material	Price (USD/kg or USD/L)
Biodiesel (in USD/L)	1.00
Methanol	0.79
Soybean Oil	0.97
Crude glycerol (< 99.5% wt.)	0.30
USP grade glycerol (> 99.5% wt.)	1.58
CaO/Al_2O_3	53.50

Source: ANP (2024d); Imarc (2023); IMEA (2024); MDIC (2024); Methanex (2024).

Table 9 – Utility prices used in the process configurations.

Utility	Price (USD/GJ)
Low-pressure Steam (6 bar, 160 °C)	4.54
Medium-pressure Steam (11 bar, 184 °C)	4.77
High-pressure Steam (42 bar, 254 °C)	5.66
Cooling water (inlet = 30 °C and outlet = 45 °C)	0.378
Chilled water (inlet = 5 °C and outlet = 15 °C)	4.43
Electricity	16.90

Source: Turton *et al.* (2018).

3.3.2 Environmental Indicator

The environmental impact associated with each configuration was quantified based on the equivalent CO_2e resulting from the combustion of fossil fuels used for steam generation (main source of greenhouse gas emissions in distillation processes). Since no biomass waste is produced to support energy recovery through combustion, it is assumed that natural gas is the fuel for steam generation. The estimation of CO_2e was conducted using the methodology proposed by Gadalla *et al*. (2005), which is based on the application of energy balances in steam boilers. The mathematical formulation of CO_2e is expressed by Equations 16 and 17.

$$CO_2e = \left(\frac{Q_{fuel}}{NHV}\right)\left(\frac{C\%}{100}\right)\alpha \tag{16}$$

$$Q_{fuel} = \frac{Q_{proc}}{\lambda_{proc}}\left(H_{proc} - H_{water}\right)\left(\frac{T_{FTB} - T_o}{T_{FTB} - T_{stack}}\right) \tag{17}$$

Where:

- α: conversion factor representing the molar ratio of CO_2 to C.
- λ_{proc}: latent heat of process steam delivered to the process (kJ/kg)
- $C\%$: percentage of carbon present in the fuel composition (%)
- H_{proc}: enthalpy of steam delivered to the process (kJ/kg)
- H_{water}: enthalpy of boiler feedwater (419 kJ/kg at 100 °C)
- NHV: net heating value of fuel (kJ/kg)
- Q_{fuel}: thermal energy provided by the fuel through combustion for steam generation (kW).
- Q_{proc}: heat duty of the process (kW)
- T_{FTB}: flame temperature of the boiler flue gases (°C)
- T_o: ambient temperature (°C)
- T_{stack}: stack temperature (°C)

Table 10 provides the λ_{proc} and H_{proc} for each type of steam, while the variables required for Equation 16 and 17 (specific for natural gas) are listed in Table 11. CO_2e associated with electricity generation ($\widehat{CO_2e_{,ele}}$) from natural gas is 120.06 kg/GJ (Chiu; Yu, 2024).

Table 10 – Thermodynamic Parameters of Different Steam Types Used in the Process.

Steam	λ_{proc} (kJ/kg)	H_{proc} (kJ/kg)
Low-pressure Steam (6 bar, 160 °C)	2085.0	2755.5
Medium-pressure Steam (11 bar, 184 °C)	1995.2	2780.4
High-pressure Steam (42 bar, 254 °C)	1688.1	2798.4

Source: Kong *et al*. (2024).

Table 11 – Natural Gas Properties and Variables Applied in Equations 15 and 16.

Variable	Value
α	3.67
$C\%$	75.38
H_{water} (kJ/kg)	419
NHV (kJ/kg)	51600
T_{stack} (°C)	160
T_{FTB} (°C)	1800

Source: Gadalla *et al.* (2005).

3.3.3 Multi-objective Optimization Problem Formulation

In addition to economic and environmental criteria, biodiesel purity was incorporated as an objective function in the MOO problem of CS-3. Considering the regulatory constraints imposed in this case study, particularly the limit of 0.6 wt.% for the total content of impurities, a minimum methyl oleate content of 99.4 wt.% is required. While this could be formally considered as a problem constraint rather than an objective, in preliminary analysis it was noted that severe convergence issues arise when this is included as a design specification in a simulation/optimization environment. Therefore, maximizing FAME purity was adopted as a strategic objective to promote convergence by guiding the optimization toward operational regions more likely to satisfy the purity constraints. Moreover, the inclusion of purity as an objective also allows the observation of how it is affected by process variables. The objective functions of each case study are summarized in Table 12.

Table 12 – Objective Functions for each case study.

Indicator	Variable	Optimization Type	Case Study
Economic	YGP	Maximization	1, 2 and 3
Environmental	CO_2e	Minimization	1, 2 and 3
Product Quality	$x_{FAME}^{BIO-OUT}$	Maximization	3

Source: Author.

The complete mathematical formulation of the metrics in each case study is present in Appendix D. For clarity, Tables 13 – 15 provide an overview of the main considerations of costs and emissions sources from natural gas combustion. It is worth highlight that, although catalyst costs are accounted for in the TOC across all configurations, they are not explicitly shown in the Table 14 to enhance readability.

Table 13 – Equipment considered for installed cost estimation in each case study.

Device	Case Study					
	CS-1A	CS-1B	CS-2A	CS-2B	CS-3A	CS-3B
P-1	X	X	X	X	X	X
DEC-1	X	X	X	X	X	X
RDC-1 (Vessel and Plates)	X	X	X	X	X	X
RDC-1 (Condenser)	X		X		X	
RDC-1 (Reboiler)	X	X	X	X	X	X
COMP-1		X		X		X
DC-1 (All components)			X	X	X	X

Source: Author.

Table 14 – Considerations in operational cost estimation in each case study.

Electricity / Utility	Device	Case Study					
		CS-1A	CS-1B	CS-2A	CS-2B	CS-3A	CS-3B
Eletricity	P-1	X	X	X	X	X	X
Cold	RDC-1	X		X		X	
Hot	RDC-1	X		X		X	
Eletricity	COMP-1		X		X		X
Cold and Hot	DC-1			X	X	X	X

Source: Author.

Table 15 – Source of Emissions from Natural Gas Combustion in each case study.

Device	Case Study					
	CS-1A	CS-1B	CS-2A	CS-2B	CS-3A	CS-3B
P-1	X	X	X	X	X	X
RDC-1	X		X		X	
COMP-1		X		X		X
DC-1			X	X	X	X

Source: Author.

For reference and comparison purposes, Table 16 offers a summary of the main design decisions, technical constraints, and process adaptations in each scenario, streamlining the interpretation of their differences.

Table 16 – Comparative summary of specifications and objectives for each case study.

Aspect	CS-1	CS-2	CS-3
Biodiesel purity specification	FAME ≥ 96.5 wt.%	FAME ≥ 96.5 wt.%	ANP-compliant (FAME ≥ 96.5 wt.%, impurities ≤ 0.2 wt.%)
Glycerol purity requirement	Crude glycerol (≥ 70.0 wt.%)	USP grade (≥ 99.5 wt.%)	USP grade (≥ 99.5 wt.%)
Glycerol purification step	Not included	Included	Included
Summary	Innovation: VR replacing reboiler utility (HPRD) Objective: Evaluate VR as energy-saving alternative	Innovation: Glycerol purification integration Objective: Assess purification feasibility	Innovation: Strict compliance with ANP specification Objective: Ensure regulatory fuel quality

Source: Author.

In all case studies, the operational constraints are associated with thermal degradation of the species (Bose *et al.*, 2024), a minimum methanol-to-oil molar ratio to validate the assumption of pseudo-first order kinetics and ensure high conversion efficiency in

transesterification reaction (Pasupulety *et al*., 2013) and production capacity of the *Be8* plant located in Marialva (metropolitan area of Maringá) (ANP, 2024a). These restrictions are formalized through the following inequality constraints, represented by Equations 18 – 20.

$$T_{reb}^{RDC-1/DC-1} < 280\ °\text{C} \tag{18}$$

$$R_{in}^{RDC-1} = \frac{\dot{n}^{F-SBO}}{\dot{n}^{F-MEOH}} > 5 \tag{19}$$

$$\dot{q}_{BIO-OUT} < 54170\ \text{L/h} \tag{20}$$

In addition to above limits, biodiesel quality requirements are incorporated based on the specific purposes of each case study. It is important to note that when glycerol stream achieves a purity between 75.0 and 99.5 %wt., it is considered crude glycerol, however in purities above 99.5 %wt., it is designated as USP grade glycerol, suitable for pharmaceutical applications. The inequalities constraints related to biodiesel and biodiesel quality are represented by Equations 21 – 25.

$$x_{FAME}^{BIO-OUT} > 96.5\ wt.\% \tag{21}$$

$$x_{GLY}^{MIX-OUT/BOT-DC} > 75.0\ \%wt. \tag{22}$$

$$x_{OOO}^{BIO-OUT,CS-3} < 0.2\ \%wt. \tag{23}$$

$$x_{MEOH}^{BIO-OUT,CS-3} < 0.2\ \%wt. \tag{24}$$

$$x_{GLY}^{BIO-OUT,CS-3} < 0.2\ \%wt. \tag{25}$$

The decision variables and their respective search intervals used in the optimization problems are detailed in Table 17, while the specific set of variables selected for each configuration is presented in Table 18.

Table 17 – Decision Variables and Search Intervals Used in the Optimization Problems.

Variable	Description	Search Interval	
		Lower Bound	Upper Bound
P^{COMP-1} (atm)	Compressor discharge pressure	5.5	30.0
P^{RDC-1} (atm)	RDC Condenser pressure	1.0	3.0
P^{DC-1} (atm)	Vacuum DC Condenser pressure	0.05	0.4
FS^{RDC-1}	RDC feed stage	1	38
FS^{DC-1}	DC feed stage	1	38
$\dot{n}_{SBO-IN}$ (kmol/h)	Soybean oil flow rate	35.0	55.0
N_R^{RDC-1}	Number of rectifying stages in RDC	1	16
N_T^{RDC-1}	Number of stages in RDC	8	38
N_T^{DC-1}	Number of stages in DC	8	38
N_S^{RDC-1}	Number of stripping stages in RDC	1	16
P^{V-1} (atm)	Valve Outlet Pressure	3.1	30.0
P^{P-1} (atm)	Pump Outlet Pressure	1.5	4.0
$R_{in}^{process}$	Molar process Inlet methanol-to-oil ratio	2.0	7.0
f_{holdup}^{RDC-1}	Reactive holdup factor in RDC	0.5	1.0
DF^{RDC-1}	RDC molar distillate to feed ratio	0.05	0.95
DF^{DC-1}	DC molar distillate to feed ratio	0.05	0.95
RR^{RDC-1}	Molar Reflux Ratio in RDC	0.05	6.00
RR^{DC-1}	Molar Reflux Ratio in DC	0.05	6.00
RF^{RDC-1}	Reflux split to enter in RDC	0.1	0.9
VF^{RDC-1}	Vapor fraction in RDC Reboiler	0.3	0.8

Source: Author.

Table 18 – Selected Decision Variables for Each Process Configuration.

Variable	Case Study					
	CS-1A	CS-1B	CS-2A	CS-2B	CS-3A	CS-3B
P^{COMP-1} (atm)		X		X		X
P^{RDC-1} (atm)	X	X	X	X	X	X
P^{DC-1} (atm)			X	X	X	X
FS^{RDC-1}	X	X	X	X	X	X
FS^{DC-1}			X	X	X	X
$\dot{n}_{SBO-IN}$ (kmol/h)	X	X	X	X	X	X
N_R^{RDC-1}	X	X	X	X	X	X
N_T^{RDC-1}	X	X	X	X	X	X
N_T^{DC-1}			X	X	X	X
N_S^{RDC-1}	X	X	X	X	X	X
P^{V-1} (atm)		X		X		X
P^{P-1} (atm)	X	X	X	X	X	X
$R_{in}^{process}$	X	X	X	X	X	X
f_{holdup}^{RDC-1}	X	X	X	X	X	X
DF^{RDC-1}	X		X		X	
DF^{DC-1}			X	X	X	X
RR^{RDC-1}	X		X		X	
RR^{DC-1}			X	X	X	X
RF^{RDC-1}		X		X		X
VF^{RDC-1}		X		X		X

Source: Author.

The optimization problems were solved using NSGA-II implemented via the "Pymoo" library in Python, integrated with Aspen Plus simulations. The same algorithm hyperparameters reported by Stander, Woolway and Van Zyl (2025) were adopted. NSGA-II was configured with a population size of 60 and executed over 60 generations. It employed the Simulated Binary Crossover operator (η = 30, μ = 1.0), with η controlling the distribution spread of the offsprings around the parent solutions. The Polynomial Mutation operator was applied with η

= 20. A crossover probability of 1.0 was used, meaning that all variables participated in the recombination phase. The Tournament Selection strategy was employed for parent selection. Further details on the crossover operator are provided in Deb, Sindhya and Okabe (2007).

Figure 23 illustrates the workflow for the optimization process, where the Python and Aspen Plus symbols indicate the respective platforms used for executing each step. Initially, the algorithm generates a population of candidate solutions, which are iteratively updated using the crossover and mutation operators. For each individual, the corresponding decision variables are sent to Aspen Plus, where process simulations are conducted. The outputs are then used to evaluate the objective functions. If the solution fails to converge or is infeasible, penalty functions are applied accordingly. The cycle continues with the generation of new offspring until the termination criterion is satisfied, at which point the Pareto front with optimal trade-off solutions is generated.

Figure 23 – Optimization Algorithm Steps using Integration between Aspen Plus and Python.

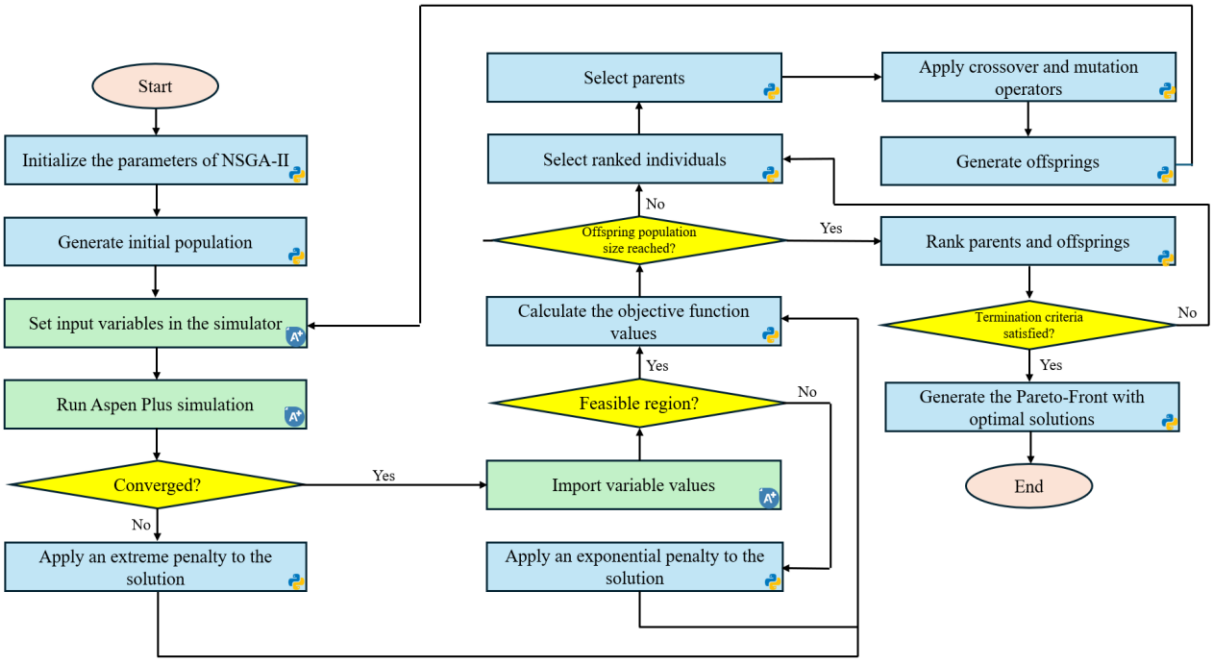

Source: Author.

The total penalty applied to the objective functions (Pen_{tot}) is the sum of exponential penalties associated with violations of process constraints, as shown in Equation 26:

$$Pen_{tot} = \sum_{i=1}^{n_c} Pen_i = \sum_{i=1}^{n_c} k_0 \exp\left(\frac{\Delta_i}{tol_i}\right) \tag{26}$$

Where k_0 is a penalty scaling factor, Δ_i represents the deviation from the constraint limit for i-th constraints and tol_i is the tolerance of constraint violation. Each penalty term is only applied when the corresponding constraint is violated. Otherwise, Pen_i = 0 for that constraint. The values adopted for k_0 and tol_i are shown in Table 19. These parameters were defined based on preliminary sensitivity analysis in MOO problems resolution.

Table 19 – Penalty Parameters adopted in optimization problems.

Parameter	Value
$\boldsymbol{k_0}$	50000000
$\boldsymbol{tol_{temp}}$ (°C)	1
$\boldsymbol{tol_{comp}}$	0.01
$\boldsymbol{tol_{prod}}$ (L/h)	500
$\boldsymbol{tol_{ex}}$	0.1

Source: Author.

4 Results and Discussion

To investigate and quantify the influence of decision variables on economic and environmental indicators, as well as on constraint variable values, Spearman correlation matrices were generated based on 360 samples obtained through Latin Hypercube Sampling (LHS) for each process configuration and visualized using heatmap plots from the Seaborn library in Python (Waskom, 2021). To improve the readability of this work, the matrices are presented in detail in Appendix E, while the detailed results of each obtained non-dominated solution in Appendix F.

4.1 Case Study 1

In both CS-1 configurations, a trade-off is observed between YGP and CO_2e, where higher profitability is accompanied by increased environmental impact. For CS-1A (Figure 24), the most profitable solutions, those exceeding 80 million USD/year, are associated with emissions above 3700 t/year. In contrast, environmentally favorable alternatives (< 1500 t/year) are limited to less profitable scenarios (< 65 million USD/year), demonstrating the challenge in optimizing both objectives simultaneously.

Figure 24 – Pareto Front (CS-1A).

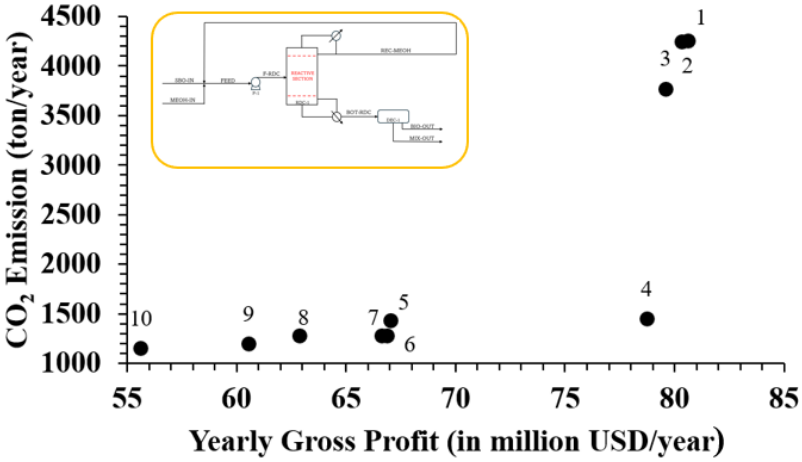

Source: Author.

To enable a more detailed evaluation of individual solution performance, Figure 25 identifies each non-dominated alternative obtained in the optimization. In CS-1A, Solutions 1 to 3 generate high profits but incur substantial emissions, while Solutions 5 through 10 present reduced emissions at the expense of economic performance. An exception to this trend is the

Solution 4, which reaches YGP close to 79 million USD/year with CO_2e around 1500 t/year. Despite this favorable balance, Solution 4 appears as an isolated point.

Figure 25 – Objective Function Values per Solution (CS-1A).

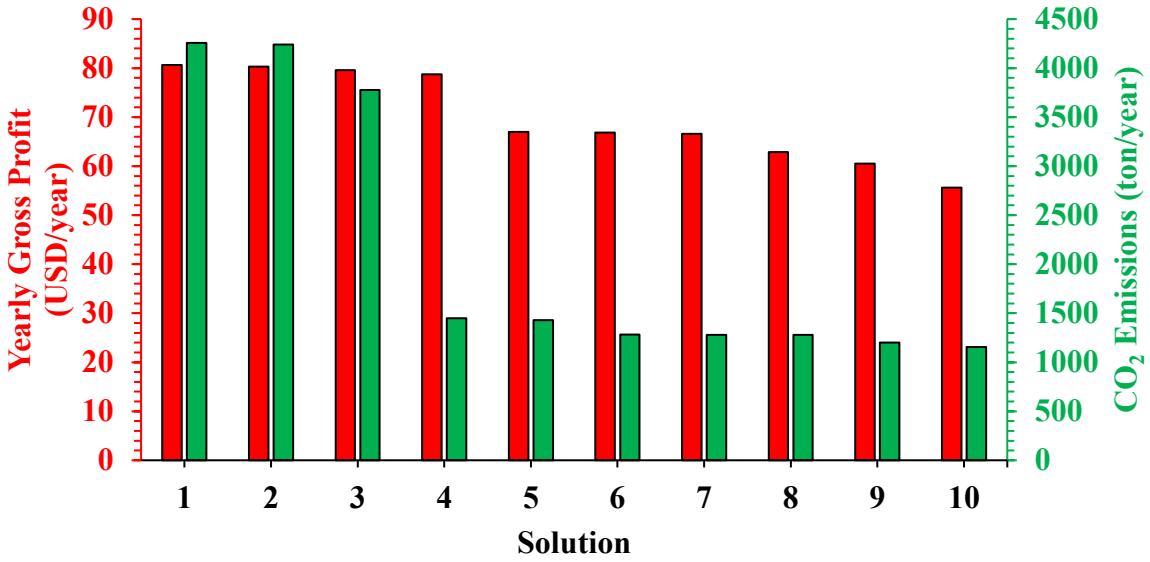

Source: Author.

As represented in Figures 26 and 27, CS-1B configuration shows a performance shift in the biodiesel production. Several non-dominated solutions combine high profitability with lower emissions. While the most profitable (> 75 million USD/year) present moderate emissions (900–1000 t/year), this still represents a substantial reduction compared to CS-1A. Additionally, intermediate profitable solutions (YGP between 60 and 75 million USD/year) reach emissions below 500 t/year. Particularly, Solutions 1, 2 and 3 achieve profits comparable to the best economic alternatives of CS-1A, while clearly dominating them from an environmental standpoint. These results confirm the effectiveness of VR in eliminating hot utility demand, revealing that the energy integration in HPRD enhances environmental performance without compromising economic viability, underscoring the potential of this PI strategy in biodiesel production.

To elucidate the behavior in variations of YGP, the contribution of each component was analyzed for the non-dominated solutions in both CS-1A and CS-1B. By definition, YGP corresponds to the difference between total annual revenue from product sales and aggregated costs of raw materials, capital recovery and operation. When considering an annual horizon evaluation, it is evident that reactant costs emerge as the dominant factor, surpassing capital

and utility costs by at least one order of magnitude. Therefore, the analysis begins with an examination of these elements. Figures 28 and 29 show the reactant costs and product revenues for each solution for CS-1A, while 30 and 31 present the same analysis for CS-1B.

Figure 26 – Pareto Front (CS-1B).

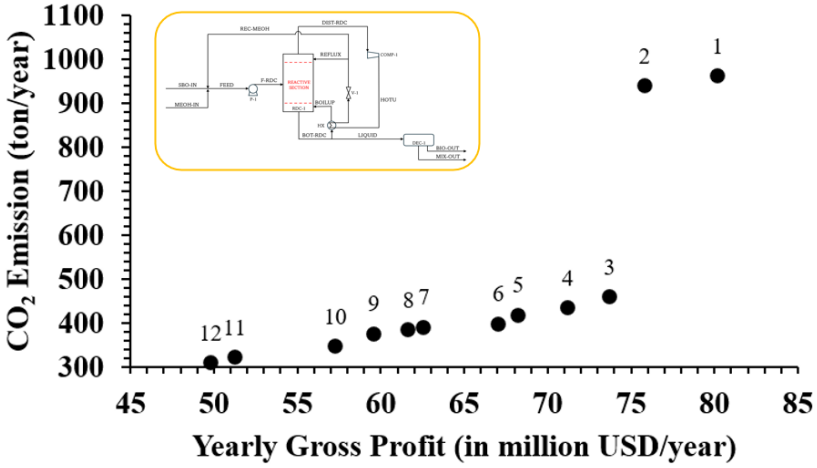

Source: Author.

Figure 27 – Objective Function Values per Solution (CS-1B).

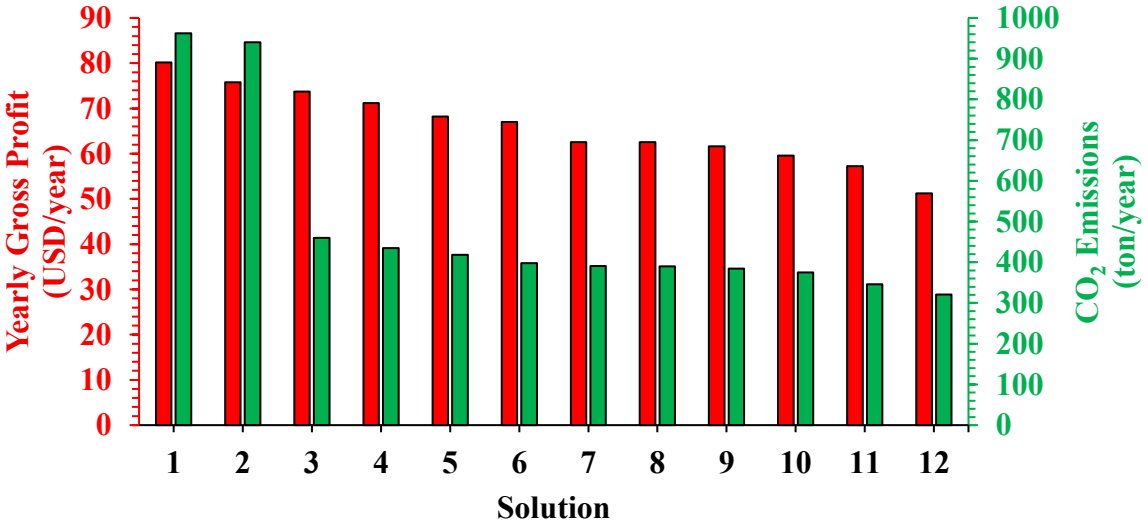

Source: Author.

Figure 28 – Annual Biodiesel and Glycerol Revenue per Solution (CS-1A).

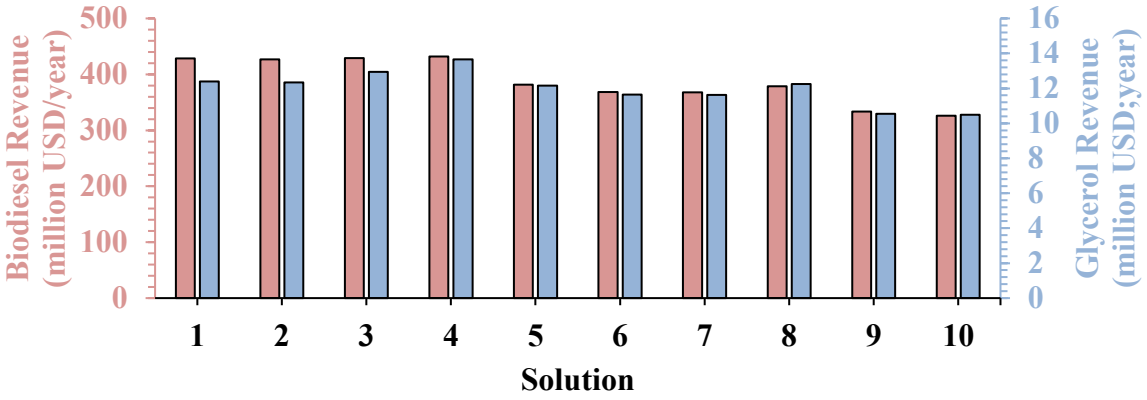

Source: Author.

Figure 29 – Annual Soybean Oil and Methanol Costs per Solution (CS-1A).

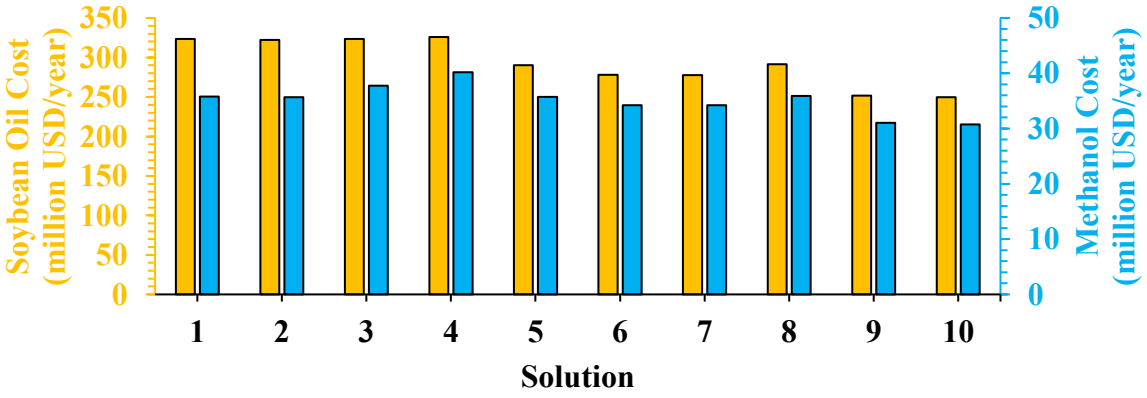

Source: Author.

Figure 30 – Annual Biodiesel and Glycerol Revenue per Solution (CS-1B).

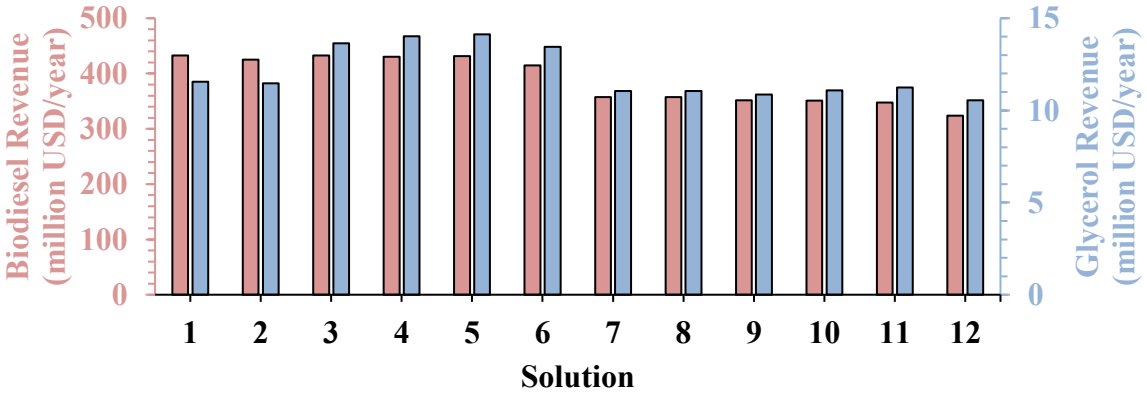

Source: Author.

Figure 31 – Annual Soybean Oil and Methanol Costs per Solution (CS-1B).

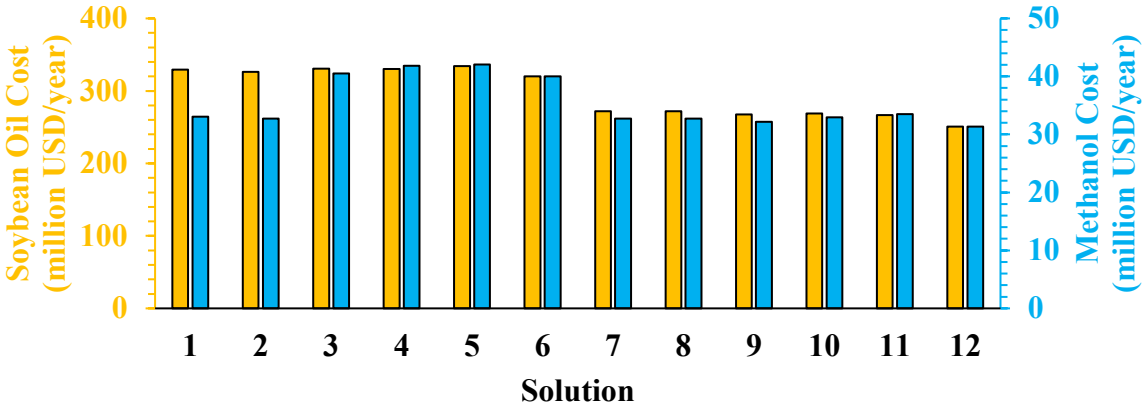

Source: Author.

As shown in Figures 28 – 31, Solutions 1 – 4 (for CS-1A) and 1 – 5 (for CS-1B) exhibited the highest YGP values and revenues from biodiesel sales, which are directly attributable to increased soybean oil consumption, which was expected. The higher availability of triglycerides favors methyl oleate formation, as each mole of triglycerides yields three moles of methyl oleate and one mole of glycerol under complete conversion (which aligns with the obtained solutions, where FAME yields are above 95%). Simultaneously, solutions with higher methanol feed rates tend to show slightly higher revenues of crude glycerol, as a portion of unreacted methanol is carried over with glycerol in the decanter, thereby increasing the total mass of the bottom phase sold. However, since glycerol is sold as a crude product in CS-1, the additional methanol is economically marginal and does not offset the increased reactant cost.

When analyzing the emission distribution per configuration, a distinction emerges between CS-1A and CS-1B, driven by the respective utility consumption strategies. In CS-1A (Figure 32), emissions originate from the RDC reboiler, with only a negligible contribution from the feed pump, emphasizing that in the absence of any heat integration, the environmental impact of the process is governed by the thermal duty required in the reboiler. In contrast, the CS-1B shifts the main emission source from steam generation to electricity consumption (Figure 33). The compressor is responsible for 85 – 95% of the total CO_2e across the solution set, while the pump contributes the remaining fraction. This change in emission origin also leads to different mitigation strategies: while CS-1A relies on reducing RDC thermal duty or fuel switching in steam boilers, CS-1B benefits from cleaner electricity matrices or from improvements in compressor efficiency.

Figure 32 – CO_2e Distribution by Equipment (CS-1A).

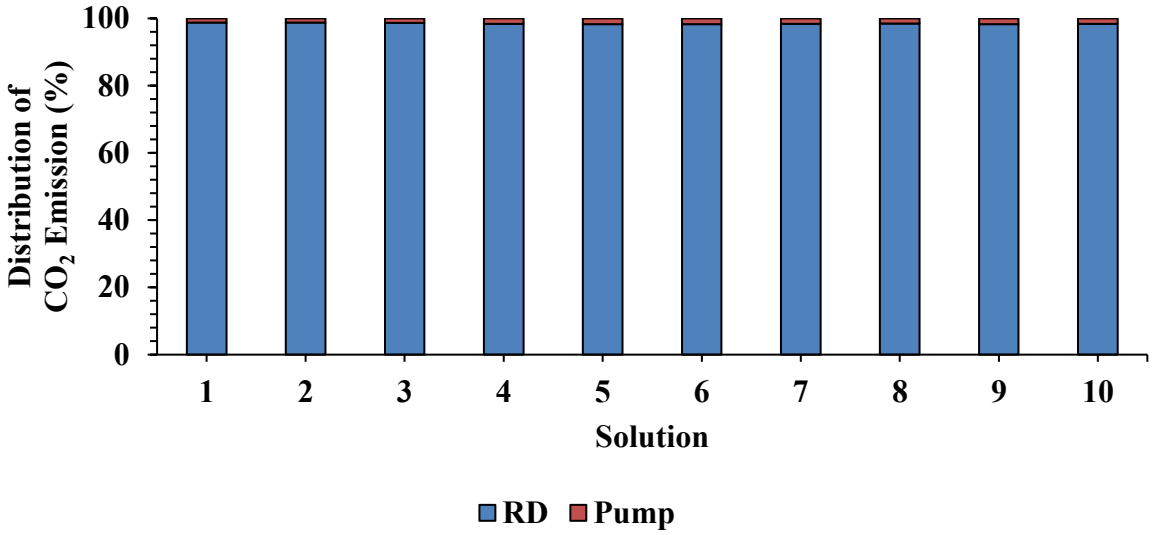

Source: Author.

Figure 33 – CO_2e Distribution by Equipment (CS-1B).

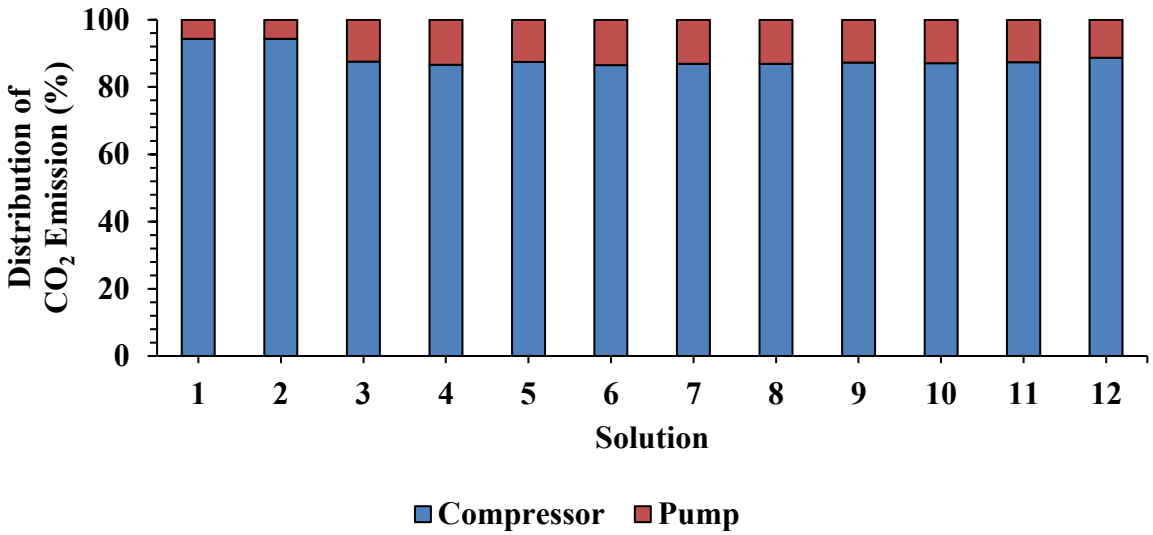

Source: Author.

4.1.1 Effect of Decision Variables

This subsection analyzes the influence of decision variables on the economic and environmental performance of configurations CS-1A and CS-1B. The discussion is supported by the correlations between decision variables, objective functions, and process constraints, providing insights into the operational strategies (Appendix E and F).

The matrices analysis reveals consistent operational patterns across both configurations (Figures E.1 and E.2). Moderate and strong Sperman correlations indicate that the soybean oil feed flow rate ($\dot{n}_{SBO-IN}$) is an important variable governing the YGP (r = 0.30 for CS-1A and r = 0.65 for CS-1B). Operationally, the most profitable solutions (1 – 4 for CS-1A and CS-1B) are characterized by $\dot{n}_{SBO-IN}$ above 46 kmol/h, supporting biodiesel production rates exceeding 53000 L/h, close to the maximum process capacity (Table F.2 and F.4).

The methanol-to-oil molar ratio at the process inlet ($R_{in}^{process}$) is also significant for economic performance. In CS-1A, the most profitable solutions (in exception of Solution 4) operated with $R_{in}^{process}$ below 4.0. Although it reduces reactant costs, it requires greater internal recovery of methanol to guarantee the excess necessary for the pseudo-first order regime adopted in the reactive section of RDC. The operation dependence is reinforced by the strong correlation between distillate to feed ratio (DF^{RDC-1}) and R_{in}^{RDC-1} (r = 0.91). A comparative pattern is observed in CS-1B, particularly for Solutions 1 and 2, which employed lower $R_{in}^{process}$ (3.40) and achieved higher profits in the solution set. The feasibility of operation with reduced methanol input is supported by higher vapor fractions in the RDC reboiler (VF^{RDC-1} = 0.53), which increased methanol recovery from bottom stream (as evidenced by correlation of 0.79 between VF^{RDC-1} and R_{in}^{RDC-1}).

While reducing external methanol consumption increases YGP, it imposes environmental and purity penalties in each configuration. In CS-1A, the increased demand for methanol recovery results in higher reflux ratios (RR^{RDC-1}) and DF^{RDC-1}, elevating the thermal load of the reboiler (as reflected by correlations between emissions, RR^{RDC-1}, and DF^{RDC-1} – $r =$ 0.34 and 0.90). The VF^{RDC-1} is the most influential variable affecting emissions (r = 0.84) in CS-1B, as higher vapor generation increases the required work in the compressor, which is the main consumer of electricity in the system. This effect is clearly demonstrated by Solutions 1 and 2, which exhibit both the highest VF^{RDC-1} and emission levels within the CS-1B solution set.

The thermodynamic formulation of compressor power in isentropic conditions, defined by Equation 26 (Çengel; Boles, 2011), can explain the aforementioned behavior. According to it, the compressor power (W_{comp}) increases with the molar inlet flow rate ($\dot{n}_{in}^{COMP-1}$) and temperature (T_{in}), while the effect of the pressure ratio is governed by the exponent $(k-1)/k$, where $k = C_p/C_v$.

$$W_{comp} = \dot{n}_{in}^{COMP-1} \frac{kRT_{in}}{k-1} \left[\left(\frac{P_{out}}{P_{in}} \right)^{\frac{k-1}{k}} - 1 \right] \quad (26)$$

For methanol with $k \approx 1.2$, the exponent is approximately 0.17, meaning that the influence of pressure variation on compressor workload is comparatively weaker than that of vapor flowrate. The sensitivity analysis in industrial production (Figure 34) supports this interpretation. In the system under study, higher values of VF^{RDC-1} lead to increased vapor flow entering the RDC. As a result, the amount of vapor reaching the top of the column (and consequently entering in the compressor) also increases. It is important to note that the compressor operates with dry vapor; thus, VF^{RDC-1} here refers to the conditions at the reboiler outlet, not within the compressor itself. At lower vapor loads, variations in pressure ratio produce minimal changes in compressor work. However, as vapor flow rate increases, the effect of pressure becomes more relevant, although it still secondary compared to the influence of VF^{RDC-1} (which dominates the effect in operating costs and emissions). Under these fixed conditions, Spearman correlation validates the influence of vapor flow rate values, where r between W^{COMP-1} and VF^{RDC-1} is almost three times higher when compared to P^{COMP-1}.

Figure 34 – Effect of Compressor Pressure and Vapor Fraction on Compressor Power.

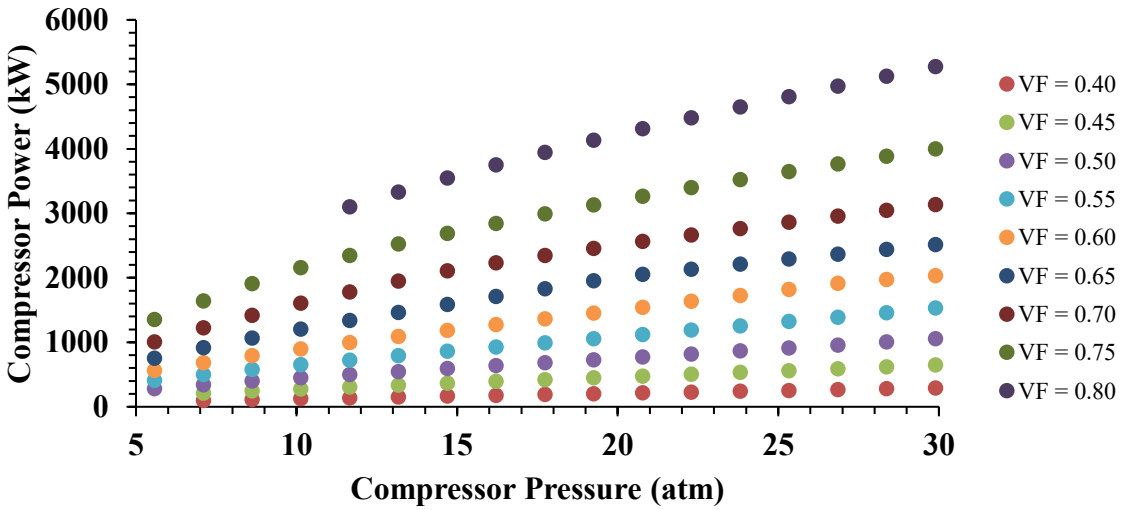

Source: Author.

4.1.2 Installed and Operating Costs

Following the analysis of revenues and reactant costs, this subsection examines the contribution of capital investment and operating expenses related to catalyst, utility, and

electricity consumption to the overall economic performance of the CS-1 configurations. For CS-1A, Figures 35 and 36 illustrate the absolute TIC for each non-dominated solution and the distribution across the equipment.

Figure 35 – TIC per Solution (CS-1A).

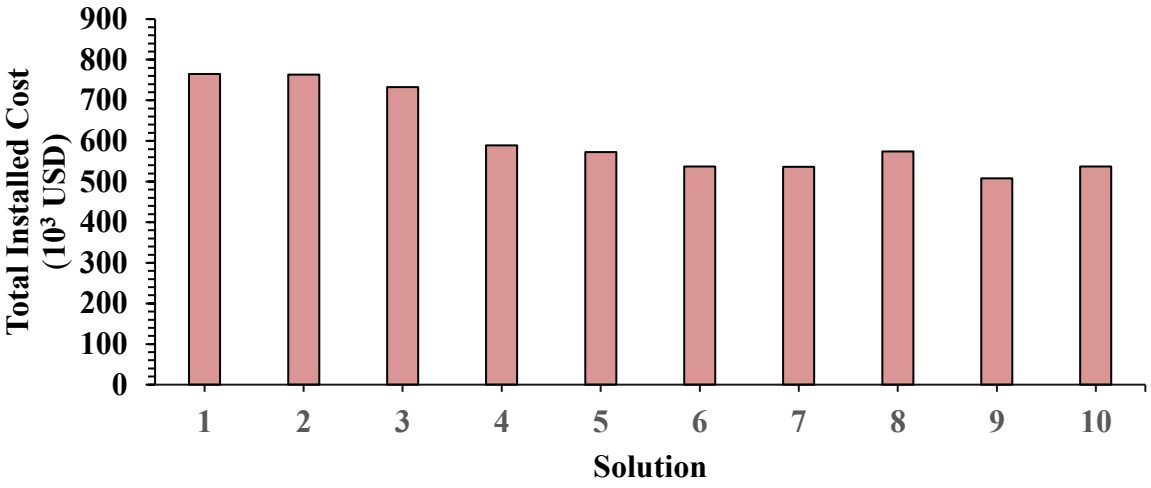

Source: Author.

Figure 36 – Distribution of TIC by Equipment (CS-1A).

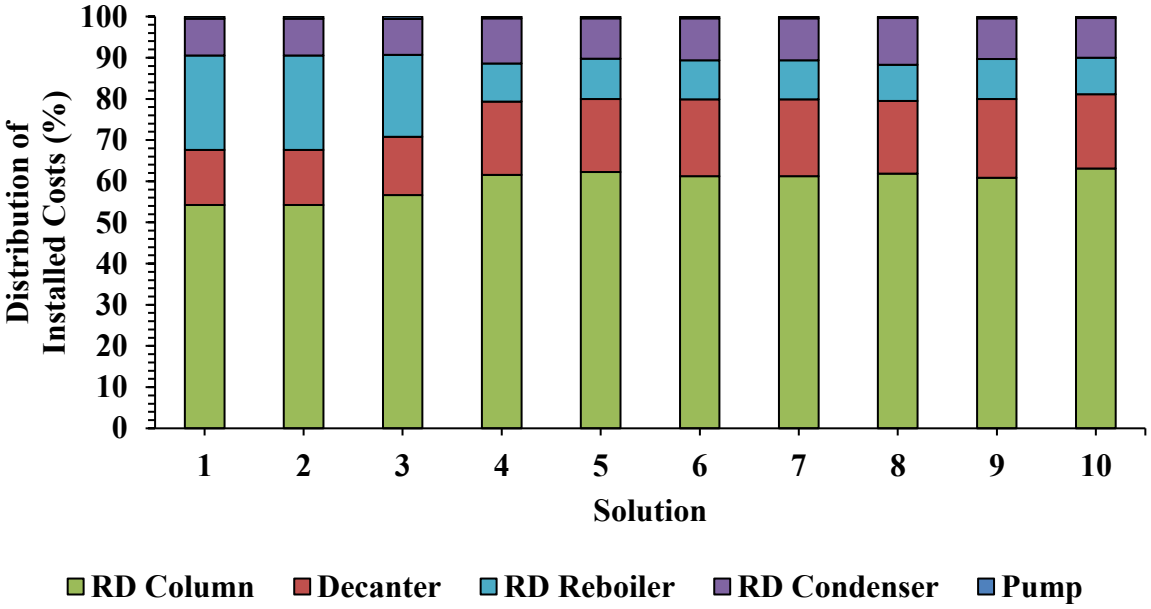

Source: Author.

As observed, the largest contributions to TIC are attributed to the RDC, the decanter and heat exchangers. The decanter cost exhibits strong correlations with the $\dot{n}_{SBO-IN}$ ($r = 0.54$)

and the $R_{in}^{process}$ (r = 0.85) linked to the decanter sizing equation, which depends on the flow rate of the inlet streams.

For the RDC vessel, the cost increases proportionally with the total number of stages – N_T^{RDC-1} (r = 0.45), and the DF^{RDC-1} (r = 0.80). While N_T^{RDC-1} determines the column height, RR^{RDC-1} and DF^{RDC-1} affect internal vapor and liquid flow rates, influencing the diameter calculated by Aspen Plus. The costs of the RDC heat exchangers are similarly impacted by the column operating conditions, specifically RR^{RDC-1} (r = 0.34 for the condenser and reboiler) and DF^{RDC-1} (r = 0.89 for the condenser and r = 0.81 for the reboiler). These values reflect the increase in thermal duties required to enhance methanol recovery, which in turn demands larger heat exchange areas.

Among all evaluated solutions, the TIC ranges from 500 to 800 thousand USD. Solution 1, 2, and 3 present the highest TICs, directly associated with their higher N_T^{RDC-1} and DF^{RDC-1}, when compared to the remaining solutions. Solution 4 holds the 4th highest TIC, mainly due to its operation with a higher RR^{RDC-1} (0.10) and n_{SBO-IN} (47.41 kmol/h) than less profitable solutions (similar effect with Solution 8). At the lower end, while Solution 9 (lowest TIC ~ 500 thousand USD) shares similar operating conditions with Solutions 6 and 7, its reduced TIC is attributed to a lower $\dot{n}_{SBO-IN}$ (weak correlation, but still present).

For CS-1B, Figure 37 shows the absolute TIC for each non-dominated solution, while Figure 38 presents the distribution of TIC among the main equipment. Compared to CS-1A, the adoption of VR results in a substantial increase in TIC, ranging from 900 thousand to 1.7 million USD. The higher investment is associated with the introduction of the compressor as a major cost contributor to the process, particularly under high vapor fraction in the reboiler (VF^{RDC-1} = 0.53), as observed in Solutions 1 and 2, which exhibit the highest TIC values (above 1.6 million USD) and a larger proportion of compressor contribution.

The Spearman correlation matrix (Figure E.2) reinforces the observations. For the RDC vessel, the installed cost maintains a strong dependence on N_T^{RDC-1} (r = 0.68) and VF^{RDC-1} (r = 0.64), analogous to the trends in RDC height and diameter observed in CS-1A. For the compressor, VF^{RDC-1} emerges as the dominant factor, showing a strong correlation with compressor cost (r = 0.84) and overall TIC (r = 0.86). As previously discussed, higher VF^{RDC-1} increase the vapor flow that must be compressed and, consequently, required compressor power.

Figure 37 – TIC per Solution (CS-1B).

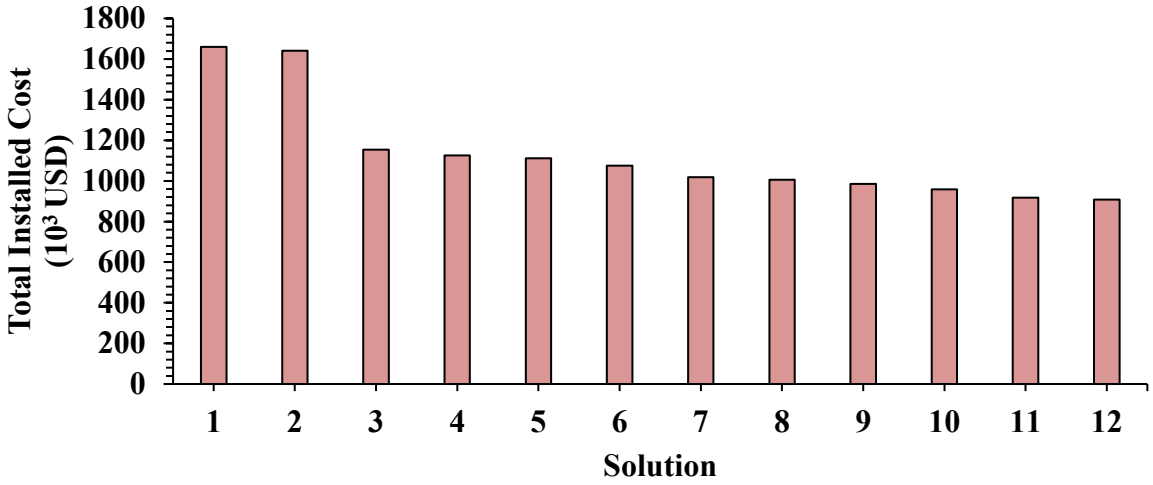

Source: Author.

Figure 38 – Distribution of TIC by Equipment (CS-1B).

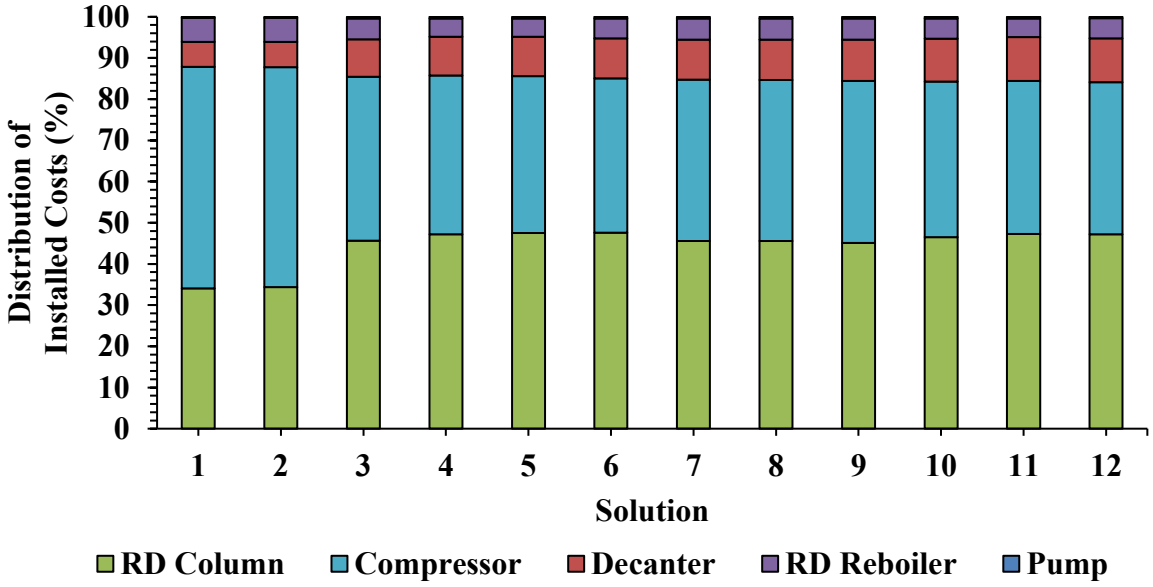

Source: Author.

For CS-1A, the Total Operating Cost (TOC) varies between 150 and 450 thousand USD/year (Figure 39), predominantly driven by hot utility consumption (Figure 40). In Solutions 1, 2, and 3, which exhibit the highest TOC values, steam accounts for approximately 85% of the total. In contrast, for the remaining configurations, its contribution decreases to around 70%. This behavior aligns with the trends previously discussed in the emissions analysis, where the impact of decision variables on thermal demand was thoroughly examined.

Consequently, the influence of decision variables will not be further detailed again in this subsection.

Figure 39 – TOC per Solution (CS-1A).

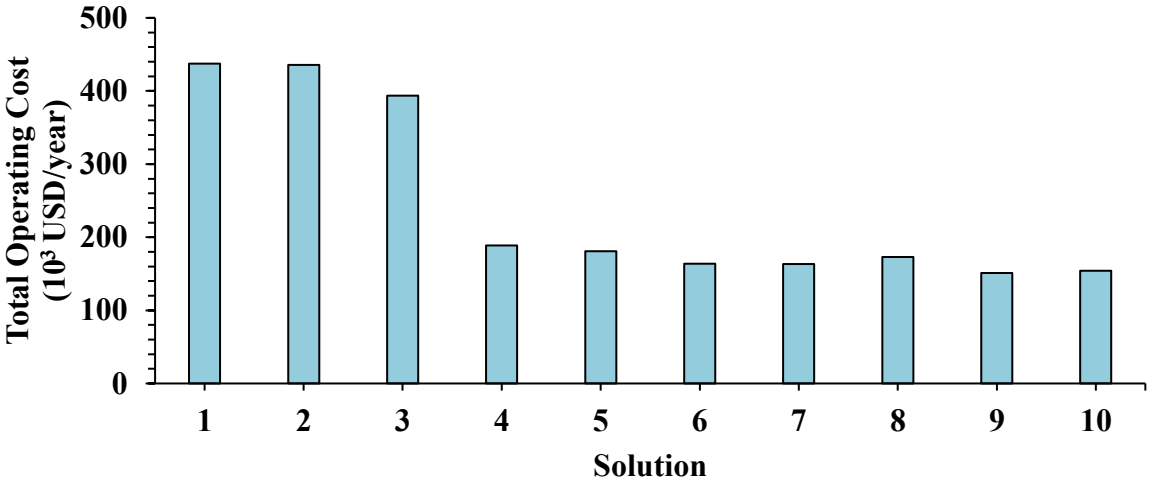

Source: Author.

Figure 40 – Distribution of TOC by Equipment (CS-1A).

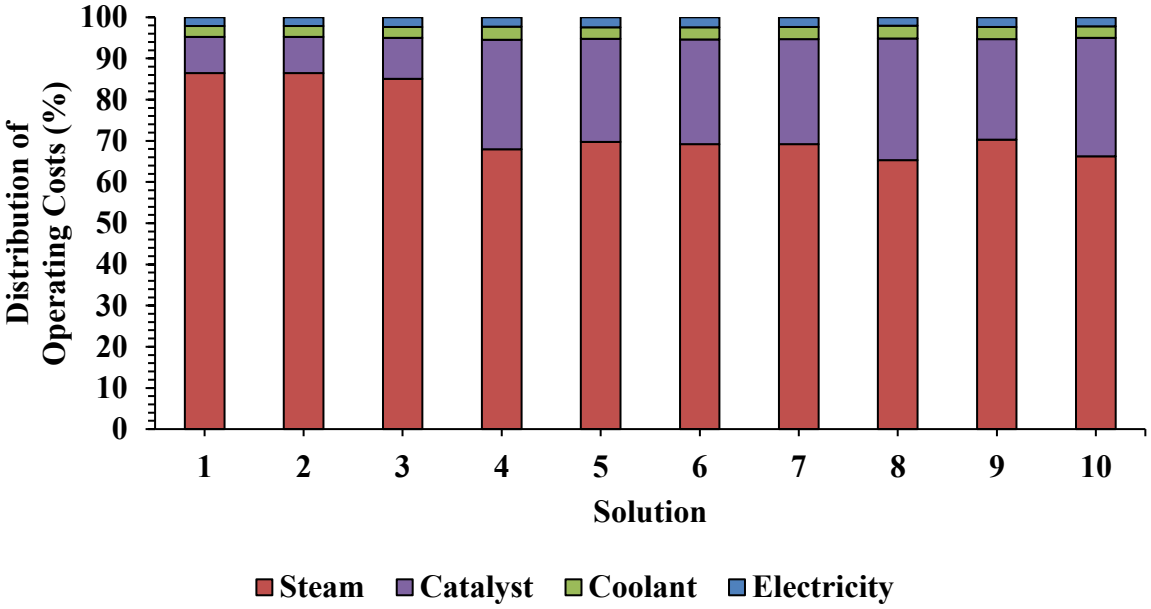

Source: Author.

A comparable pattern is observed for CS-1B, where TOC is primarily governed by electricity consumption related to compressor operation. As shown in Figure 41 and 42, solutions with higher operating costs exhibit a larger proportion of expenses associated with electrical demand. Another relevant aspect in CS-1B is the increased contribution of catalyst

costs, ranging from 33% to 56% of TOC across the non-dominated solutions as a direct consequence of eliminating external steam and coolant requirements, and elimination of the relative share of utilities in the TOC.

Figure 41 – TOC per Solution (CS-1B).

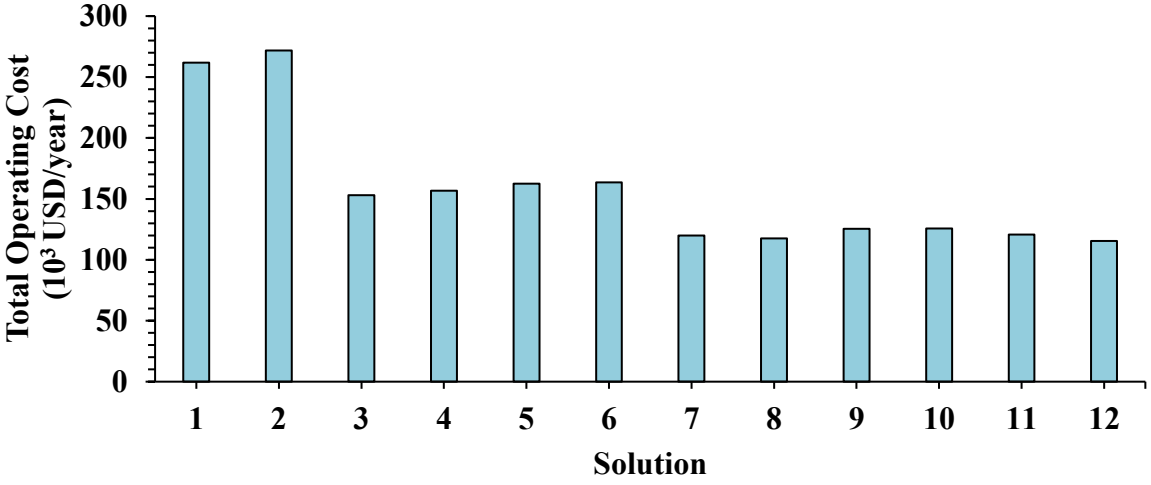

Source: Author.

Figure 42 – Distribution of TOC by Equipment (CS-1B).

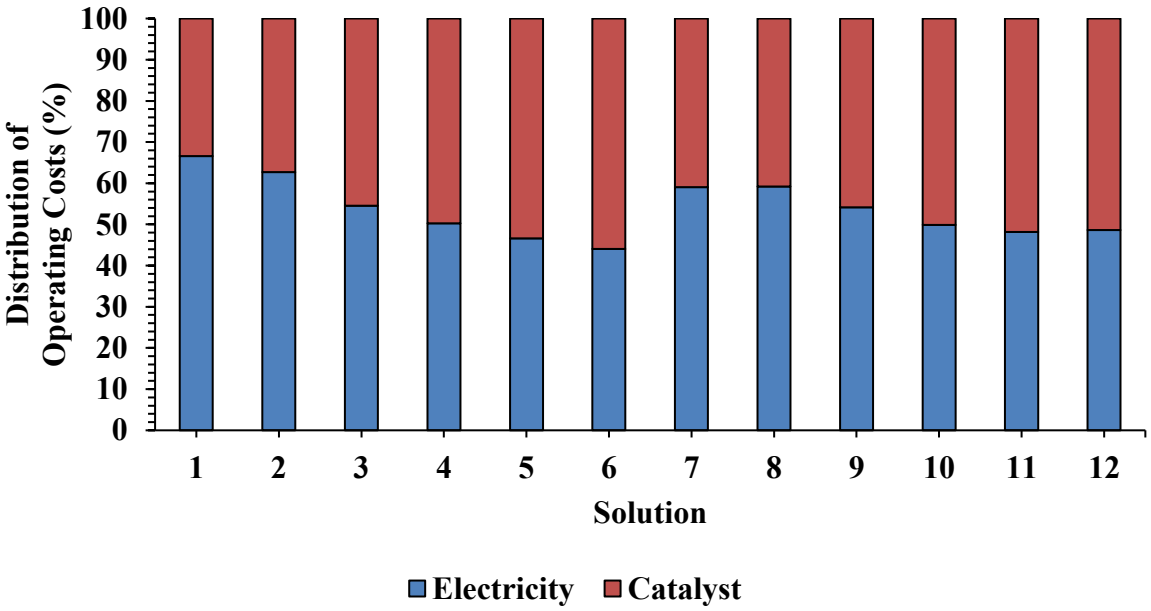

Source: Author.

The absolute TOC values (Figure 41) vary from 115 to 280 thousand USD/year, significantly lower than those observed in CS-1A. Despite the increase in capital investment due to compressor implementation, the removal of external hot and cold utilities leads to a

considerable reduction in operating costs, confirming the effectiveness of VR in improving economic performance from an operational standpoint. Since electricity usage is inherently tied to compressor performance, variations in TOC follow the same trends identified in the emissions analysis.

4.1.3 Overall Comparative Analysis

A comparative analysis between CS-1A (reference) and CS-1B is carried out in this subsection to evaluate their economic and environmental trade-offs. The assessment is based on the non-dominated solutions obtained from the MOO. Table 20 and Table 21 summarize the relative differences in TIC and TOC, considering the highest and lowest values within each configuration.

Table 20 – Relative Difference of Lowest and Highest TIC Solutions in CS-1A and CS-1B.

Situation	Lowest TIC solution (CS-1A)	Highest TIC solution (CS-1A)
Lowest TIC solution (CS-1B)	+79%	+19%
Highest TIC solution (CS-1B)	+227%	+117%

Source: Author.

Table 21 – Relative Difference of Lowest and Highest TOC Solutions in CS-1A and CS-1B.

	Lowest TOC solution (CS-1A)	Highest TOC solution (CS-1A)
Lowest TOC solution (CS-1B)	-24%	-74%
Highest TOC solution (CS-1B)	+80%	-38%

Source: Author.

The tables indicate a clear economic trade-off between CS-1A and CS-1B. Capital costs in CS-1B are considerably higher, with TIC increasing between 19% and 227% compared to CS-1A, mainly due to compressor acquisition. On the other hand, CS-1B achieves significant reductions in TOC (up to 74%), driven by the elimination of external steam consumption. Despite this, configurations with high VF^{RDC-1} can result in TOC up to 80% higher than the lowest TOC in CS-1A, reflecting the impact of compressor energy demand under certain conditions.

Overall, the transition from CS-1A to CS-1B leads to an increase in TIC, counterbalanced by a reduction in TOC. The Total Annual Cost (TAC), illustrated in Figure 43,

was calculated as the sum of annualized TIC (TIC/PBP) and TOC, following established methodologies in the literature. Despite the increase in TIC, the reduction in TOC compensates for a large part of this investment. As a result, CS-1B achieves a lower TAC when compared to most thermally demanding solutions from CS-1A (Solutions 1, 2, and 3), where high steam consumption drives operational costs to dominate total expenses. It is reflected in Table 22, where the highest TAC for CS-1B is nearly equivalent to the highest TAC in CS-1A (+2%), while the lowest TAC for CS-1B for CS-1B is 50% lower than the highest TAC in CS-1A.

Figure 43 –TAC Distribution for Non-Dominated Solutions in CS-1A and CS-1B.

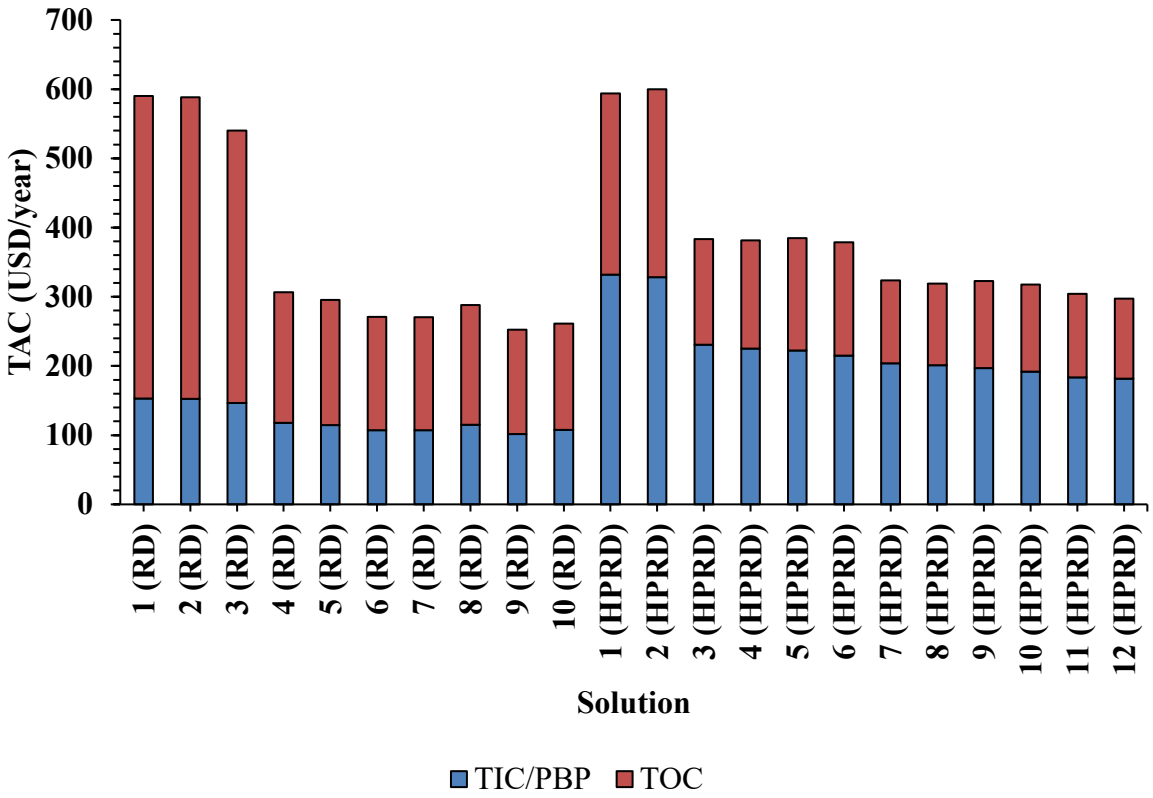

Source: Author.

Nevertheless, when compared to most economical solutions in CS-1A, CS-1B shows less favorable results. Its lowest TAC is still 18% higher than the lowest TAC in CS-1A and its highest TAC exceeds the lowest in CS-1A by 138%, indicating that, despite lower operating costs, the high capital investment required for VR limits the economic competitiveness of CS-1B relative to the most economical RD configurations.

Table 22 – Relative Difference of Lowest and Highest TAC Solutions in CS-1A and CS-1B.

	Lowest TAC (CS-1A)	Highest TAC (CS-1A)
Lowest TAC (CS-1B)	+18%	-50%
Highest TAC (CS-1B)	+138%	+2%

Source: Author.

From an environmental perspective, however, the advantage of CS-1B is unequivocal even in the worst case for CS-1B in the best of CS-1A (reduction of 17%). As shown in Table 23, the lowest emissions from CS-1B are 73% lower than the lowest in CS-1A, and up to 93% lower when compared to the highest emission CS-1A solution. While CS-1A offers lower TAC under optimized conditions, CS-1B delivers far superior environmental performance, which becomes a decisive factor when the process evaluation prioritizes decarbonization targets.

Table 23 – Relative Difference of CO_2e in CS-1A and CS-1B.

	Lowest CO_2e (CS-1A)	Highest CO_2e (CS-1A)
Lowest CO_2e (CS-1B)	-73%	-93%
Highest CO_2e (CS-1B)	-17%	-77%

Source: Author.

In MOO problems, the Pareto Front provides a set of non-dominated solutions that represent the trade-offs among conflicting objectives. Nevertheless, for practical implemental, particularly in industrial applications, it is necessary to select a single operational point from the available alternatives. To support this decision-making process, the Technique for Order of Preference by Similarity to Ideal Solution (TOPSIS), Grey Relational Analysis (GRA), and Simple Additive Weighting (SAW) methods were employed due to their simplicity, robustness and applicability within the PSE field.

In the application of TOPSIS and SAW, it is necessary to assign weights to each objective function. Therefore, a sensitivity analysis was conducted by varying the weights in an interval of 0.2 and in addition to evaluating the scenario where all objectives were considered equally important. In contrast, the GRA does not require the definition of objective function weights, and the optimal solution is selected directly based on the GRC. Table 24 represents the selected solution ID across different scenarios of priority between the metrics.

Table 24 – Selected Solution IDs Across Different Methods (CS-1).

Weight of Objective Function		Selected Solution ID					
W_{YGP}	W_{CO_2e}	TOPSIS		SAW		GRA	
		CS-1A	CS-1B	CS-1A	CS-1B	CS-1A	CS-1B
0.2	0.8	10	12	10	12		
0.4	0.6	4	6	9	12		
0.6	0.4	4	3	4	3	4	3
0.8	0.2	4	3	4	3		
0.5	0.5	4	6	3	12		

Source: Author.

Based on the results presented in Table 24, the selection of the most representative solutions for each configuration was established by analyzing their recurrence across the different decision-making methods. For CS-1A, Solution 4 emerges as the most robust candidate, being selected in 7 scenarios (4 by TOPSIS, 2 by SAW and once by GRA), while in CS-1B, Solution 3 is more frequent chosen (5 times). The decision variables adopted for Solution 4 (CS-1A) and 3 (CS-1B), as its performance and constraint function values are presented in Table 24.

For comparison with other intensified processes reported in the literature, the chosen solutions were normalized based on the biodiesel production capacity for a direct and fair comparison between different technologies regardless of scale. It is important to note that in the compared studies, including the Side Vapor Recompression Reactive Distillation (SVRRD) proposed by Mondal *et al.* (2021), do not account for catalyst costs nor for CO_2e associated with electricity consumption. This omission may have a significant impact, especially for configurations that adopt a compressor (depending heavily on electrical energy), such as SVRRD and HPRD.

Therefore, to maintain consistency with the literature, catalyst costs were excluded from the economic analysis for comparison purposes in this section. However, CO_2e associated with electricity consumption are considered in this study, even though other works neglect them. This decision is justified since, if this type of emissions is omitted, CO_2e from CS-1B would be virtually zero due to the absence of external utility demand. Additionally, all cost data from the literature were updated to the same economic basis used in this work, applying CEPCI correlation factors for the respective years, as described in the *Literature Review* Section.

Table 25 – Decision Variables and Constraint Values for Selected Solutions (CS-1).

Variable	Solution	
	4 (CS-1A)	3 (CS-1B)
$\dot{n}_{SBO-IN}$ (kmol/h)	47.41	48.11
$R_{in}^{process}$	4.18	4.16
P^{P-1} (atm)	2.10	3.78
P^{RDC-1} (atm)	1.15	1.95
P^{V-1} (atm)	--	8.88
P^{COMP-1} (atm)	--	9.08
f_{holdup}^{RDC-1}	0.96	0.80
N_T^{RDC-1}	10	15
N_R^{RDC-1}	2	4
N_S^{RDC-1}	1	3
FS^{RDC-1}	2	9
RR^{RDC-1}	0.10	--
DF^{RDC-1}	0.14	--
RF^{RDC-1}	--	0.38
VF^{RDC-1}	--	0.43
YGP (million USD/year)	78.71	73.71
CO_2e (ton/year)	1451	460
$\dot{q}_{BIO-OUT}$ (L/h)	53967	54050
$x_{FAME}^{BIO-OUT}$ (wt.%)	96.5	97.6
$x_{GLY}^{MIX-OUT}$ (wt.%)	75.0	77.0
T_{reb}^{RDC-1} (°C)	110	121
R_{in}^{RDC-1}	5.03	5.00

Source: Author.

Figures 44 and 45 present a comparative analysis of cost and environmental performance between the chosen solutions for CS-1A and CS-1B and alternative intensified processes reported in the literature, including SVRRD (Mondal *et al.*, 2021), TCRD (Mondal; Rangaiah; Jana, 2022), Supercritical RD (Bose *et al.*, 2024), and conventional RD benchmarks.

Figure 44 – Comparison of Normalized TIC/PBP and TOC Across Process Intensified Biodiesel Processes.

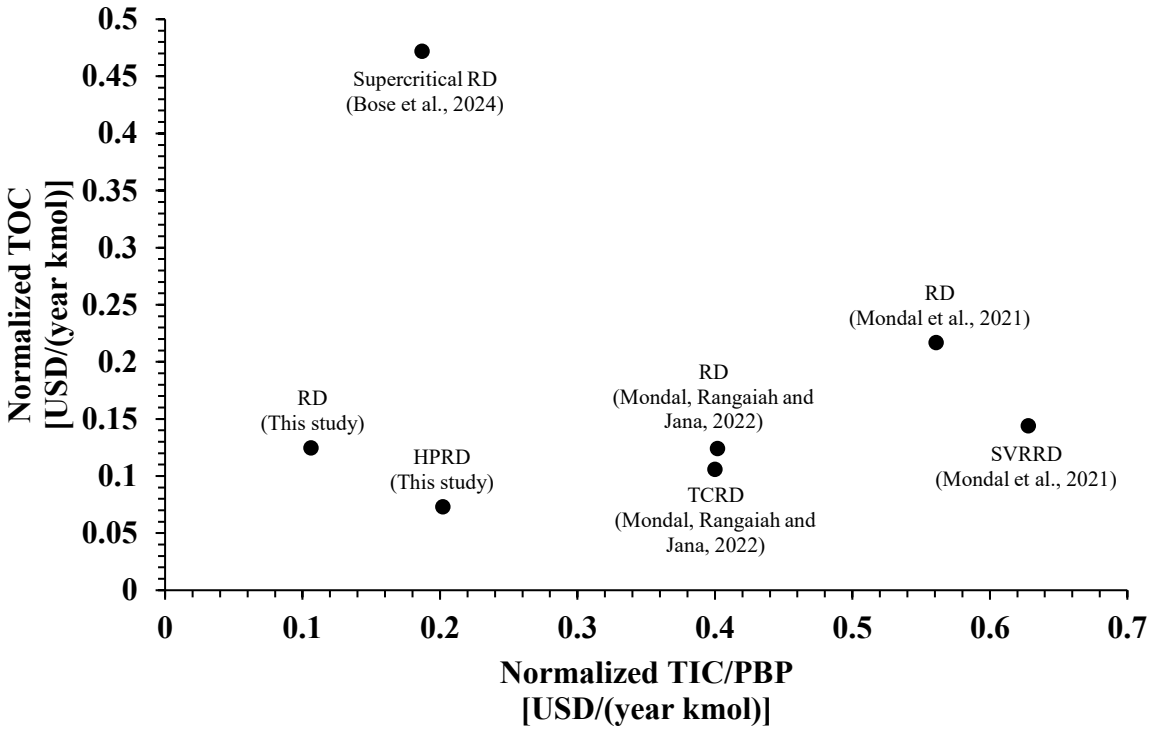

Source: Author.

The results indicate that the RD configuration proposed in this work achieves the lowest normalized TIC/PBP among all evaluated processes. Conversely, the HPRD presents the lowest normalized TOC, as a direct consequence of eliminating external hot utility demand through full VR. These results are also better when analyzed the TAC.

In contrast, the SVRRD process proposed by Mondal *et al*. (2021), although incorporating VR, still requires additional external heat input and a condenser, since the heat recovered from the compressed vapor is not sufficient to fully supply the reboiler duty. A similar limitation is observed in the TCRD configuration developed by Mondal, Rangaiah and Jana (2022), which also depends on supplementary steam in the reboiler to complement the heat supplied by the pumped liquid stream. As a result, both configurations exhibit higher operating costs and CO_2e compared to HPRD, which operates without any external heat source.

The Supercritical RD process reported by Bose *et al*. (2024) exhibits the highest TOC among all analyzed processes, primarily due to the extreme energy requirements inherent to supercritical operation. Additionally, this process reports a biodiesel purity of only 75 wt.%, as the design does not include a decanter for phase separation after RD. It is also important to note that the RD and TCRD configurations proposed by Mondal, Rangaiah and Jana (2022) target a

FAME purity of 99.45 wt.%, which imposes stricter operational demands compared to the 95 wt.% and 75 wt.% in SVRRD (Mondal *et al*., 2021) and supercritical process (Bose *et al.*, 2024), respectively.

Figure 45 – Comparison of Normalized TAC and Emissions Across Process Intensified Biodiesel Processes.

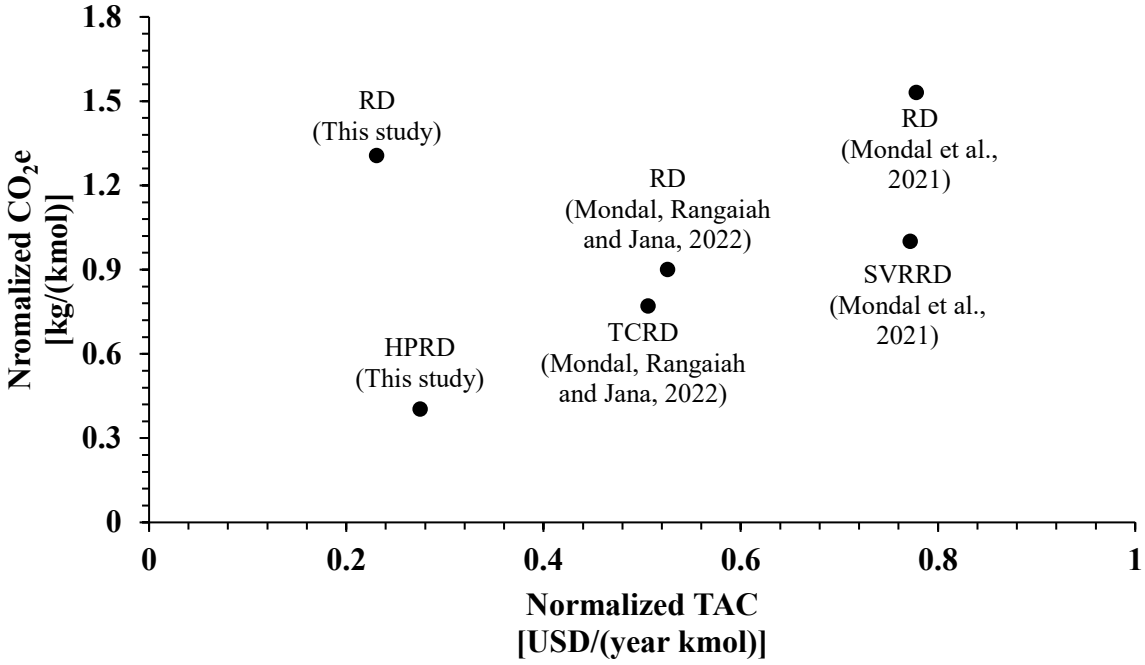

Source: Author.

4.2 Case Study 2

The implementation of the vacuum distillation column (DC-1) for glycerol purification in CS-2 significantly impacts economic and environmental performance when compared to CS-1. From an economic perspective, the increase in YGP is evident in both configurations. While in CS-1, the maximum YGP reached approximately 80 million USD/year, in CS-2, increases to nearly 120 million USD/year, as can be observed in the Pareto Fronts for CS-2A and CS-2B (Figures 46 – 49).

Profitability is enhanced by the revenue from pharmaceutical grade (USP) glycerol instead of crude. This effect is evident in CS-2A when comparing Solutions 5 and 8. Although Solution 8 produces more biodiesel (~ 53000 L/h) than Solution 5 (~ 48000 L/h), the latter achieves glycerol purity of 99.8 wt.%, resulting in a higher YGP (105 vs 78 million USD/year). A similar trend is observed in CS-2B, where Solution 4 operates with 10000 L/h less biodiesel than Solution 7 (43070 L/h vs. 53771 L/h) but achieves a profit nearly 20 million USD/year

higher driven by glycerol purification (99.6 wt.% vs. 87.3 wt.%). As shown in Figures 50 to 53, solutions that satisfy the USP specification generate substantially higher glycerol revenues, with values approaching 50 million USD/year, compared to around 10 million USD/year for crude glycerol.

Figure 46 – Pareto Front (CS-2A).

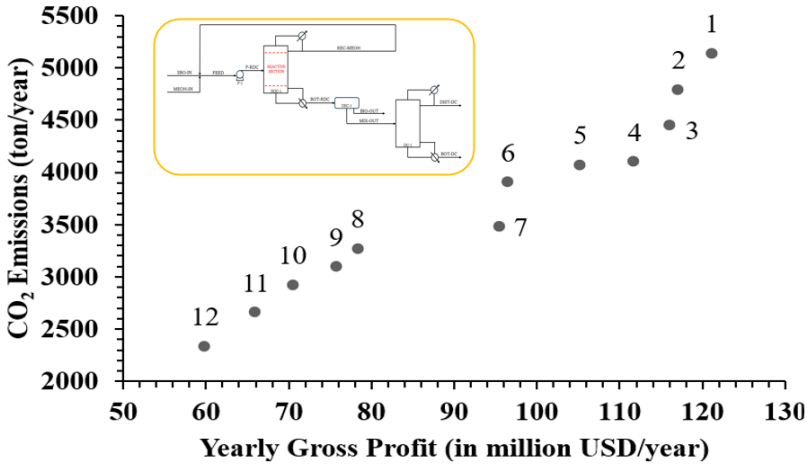

Source: Author.

Figure 47 – Pareto Front (CS-2B).

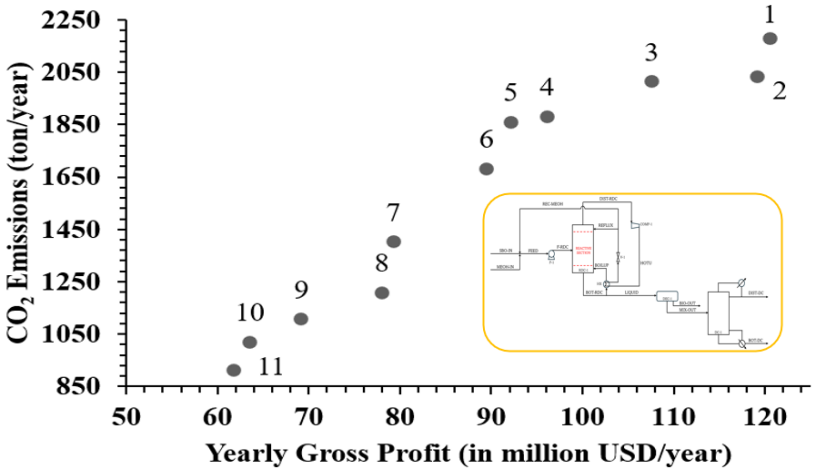

Source: Author.

Figure 48 – Objective Function Values per Solution (CS-2A).

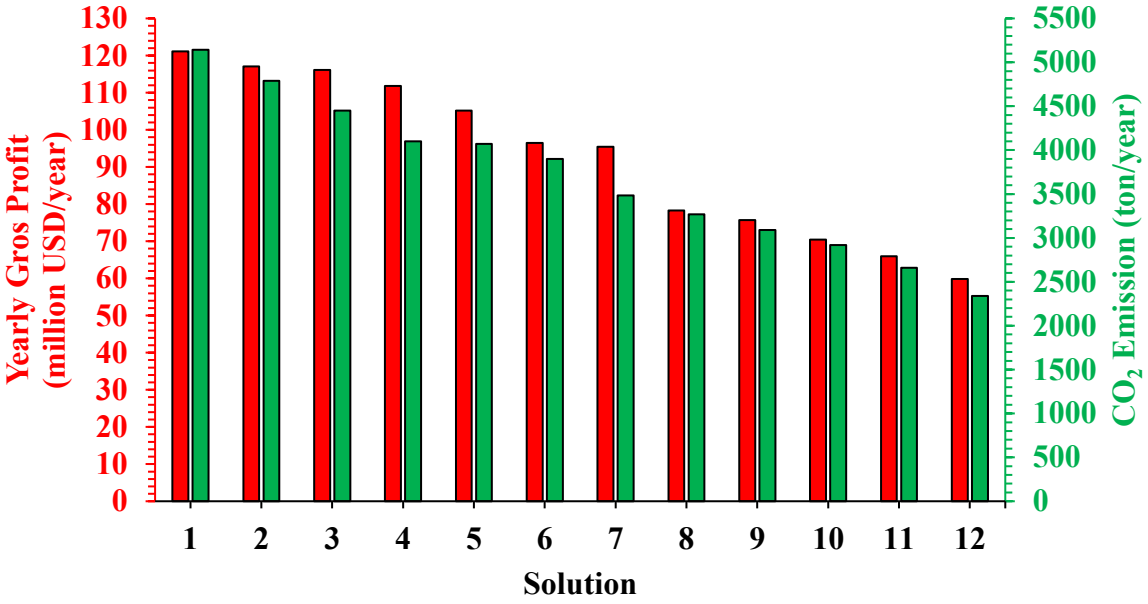

Source: Author.

Figure 49 – Objective Function Values per Solution (CS-2B).

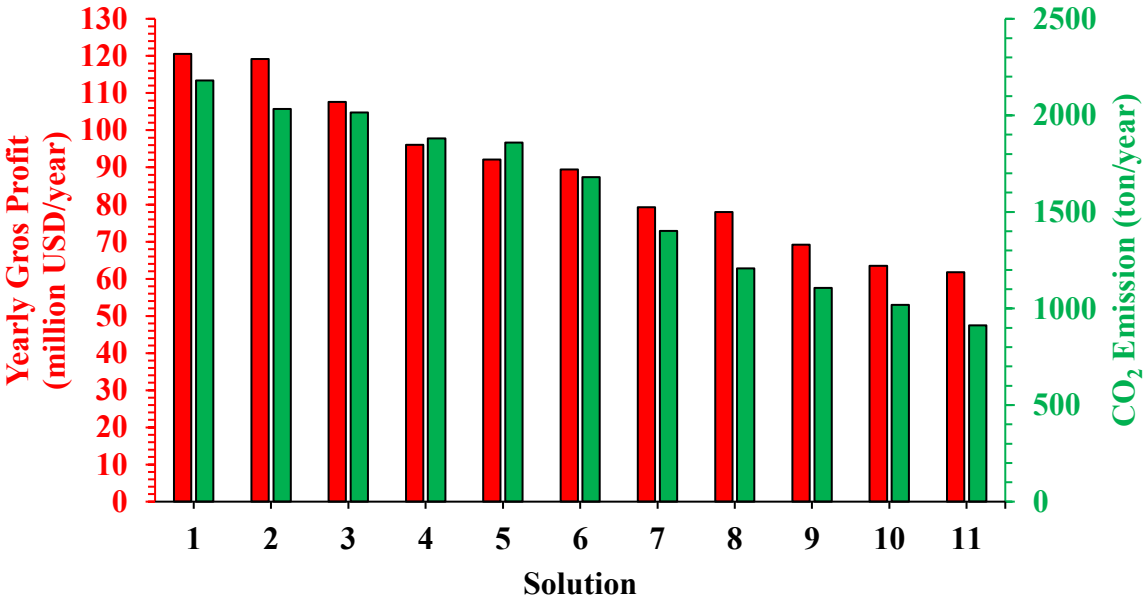

Source: Author.

Figure 50 – Annual Biodiesel and Glycerol Revenue per Solution (CS-2A).

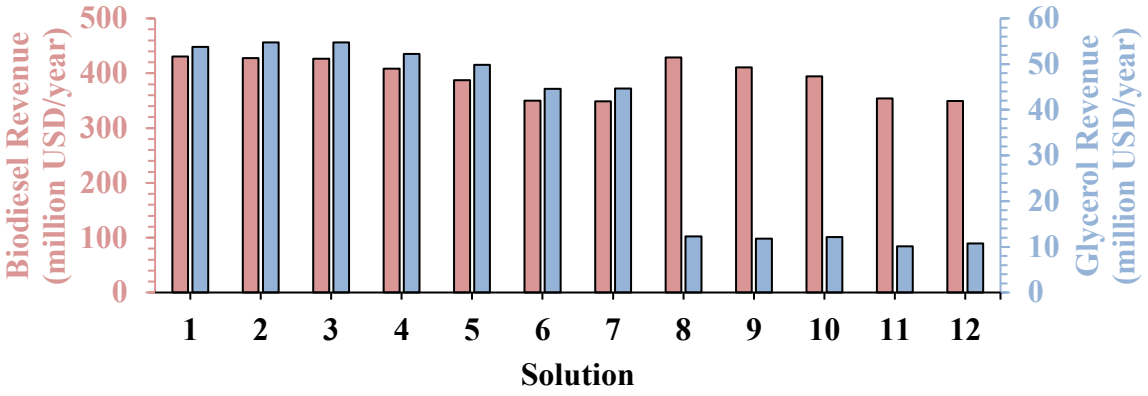

Source: Author.

Figure 51 – Annual Biodiesel and Glycerol Revenue per Solution (CS-2B).

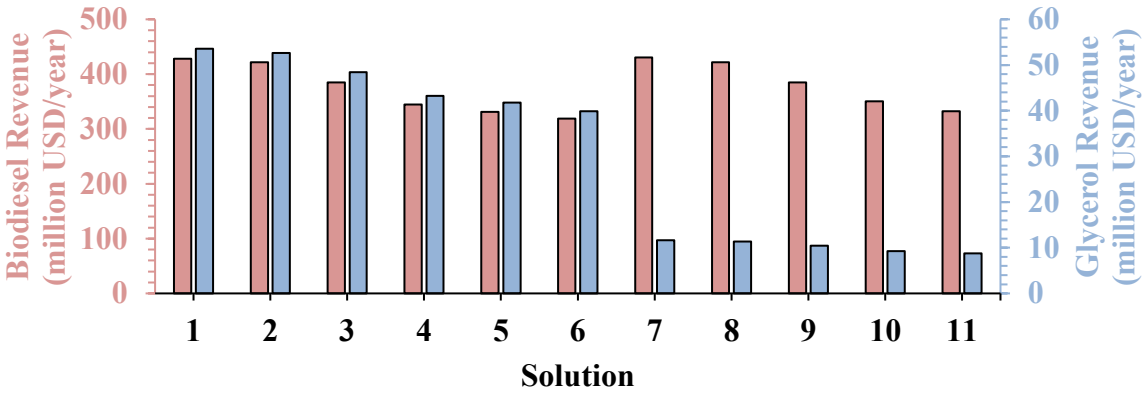

Source: Author.

Figure 52 – Glycerol Purity for Non-Dominated Solutions in CS-2A.

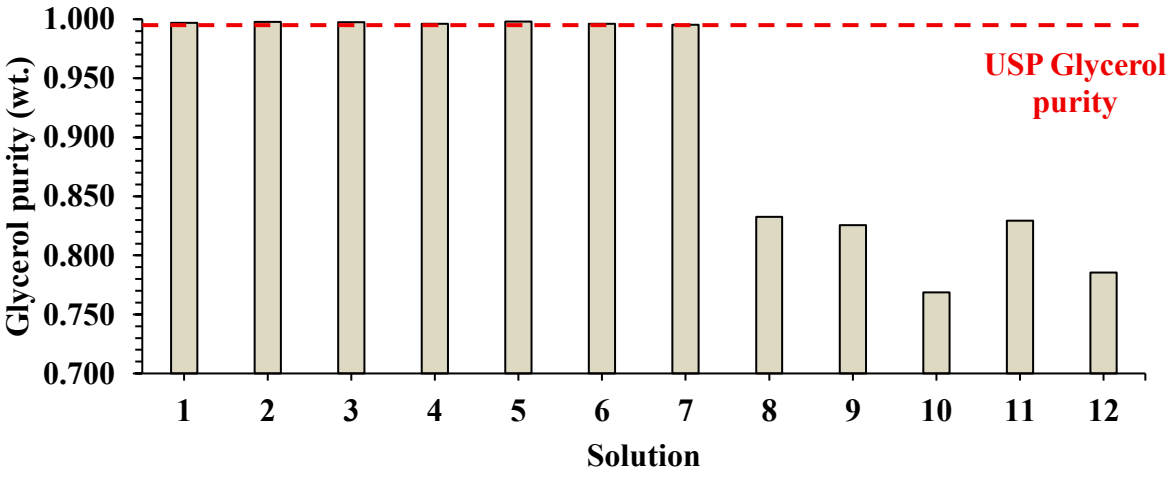

Source: Author.

Figure 53 – Glycerol Purity for Non-Dominated Solutions in CS-2B.

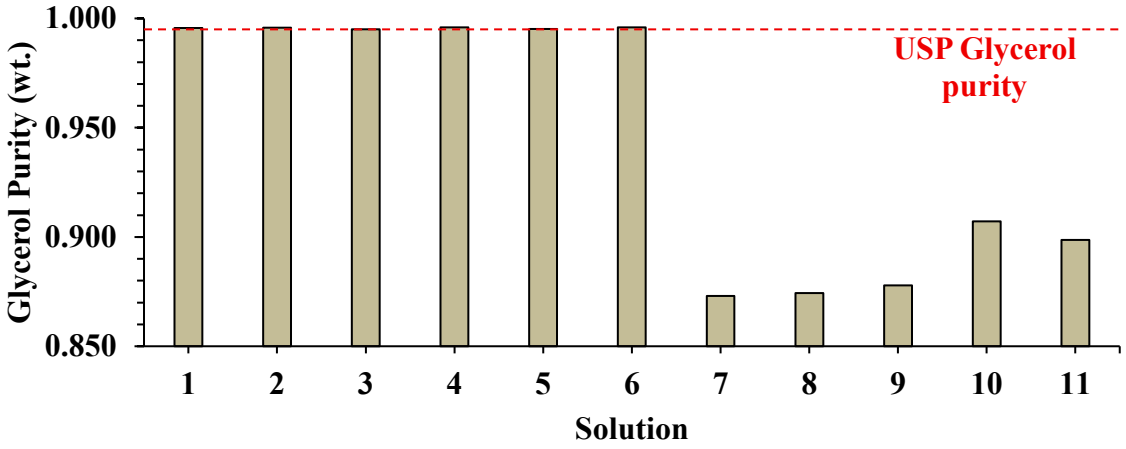

Source: Author.

On the environmental side, the addition of DC-1 leads to a grow in CO_2e, primarily due to the additional thermal demand supplied by external steam as illustrated by Figures 54 and 55. In CS-2A, emissions for solutions which obtains USP glycerol exceed 3500 t/year. In contrast, in CS-1A, only the three most profitable solutions approached this level, with most configurations operating between 1000 and 1500 t/year. Similarly, in CS-2B, emissions rise to over 2000 t/year, compared to approximately 1000 t/year in CS-1B. When glycerol is purified, steam from natural gas combustion (in DC-1) accounts for 27–33% of total emissions in CS-2A and 52–57% in CS-2B. On the other hand, when glycerol is sold as crude, the contribution of DC-1 drops to 5–11% and 24–28% respectively.

When analyzing the correlation matrices (Figure E.3 and E.4), DF^{DC-1} appears as a relevant variable in this context. In both configurations, DF^{DC-1} exhibits a strong correlation with the glycerol purity (x_{GLY}^{BOT-DC}) with r = 0.69 for CS-2A and r = 0.62 for CS-2B. This is consistent with process behavior, as higher distillate flow rates reduce methanol concentration in the bottom stream, enhancing the glycerol purity. At the same time, the increased separation efficiency of DC-1 leads to higher thermal loads in reboiler, which can be confirmed by strong correlation between $CO_2e_{HU}^{DC-1}$ and DF^{DC-1} (r = 0.77 and 0.88 for CS-2A and CS-2B).

Figure 54 – CO_2e Distribution by Equipment (CS-2A).

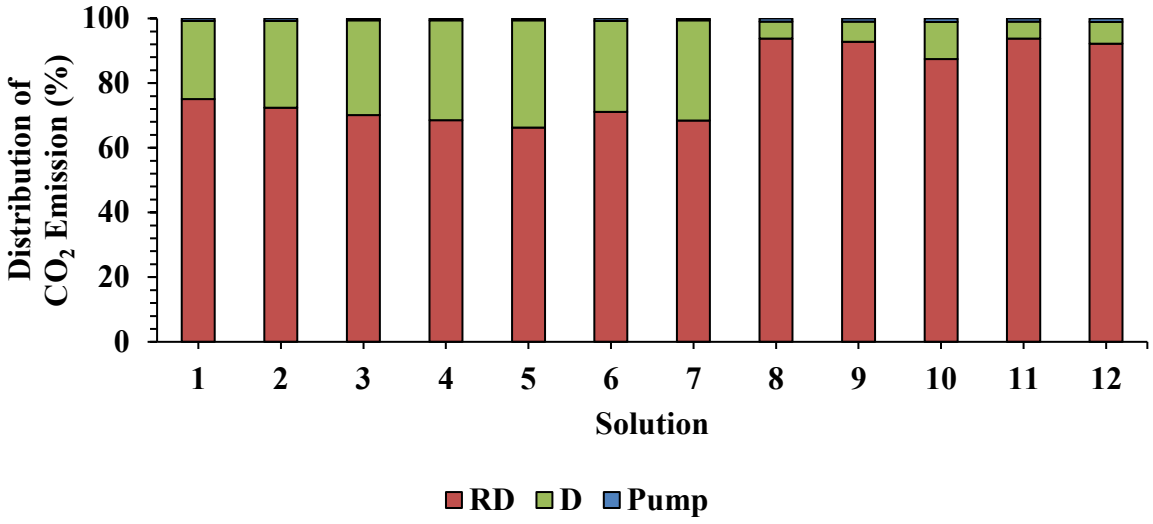

Source: Author.

Figure 55 – CO_2e Distribution by Equipment (CS-2B).

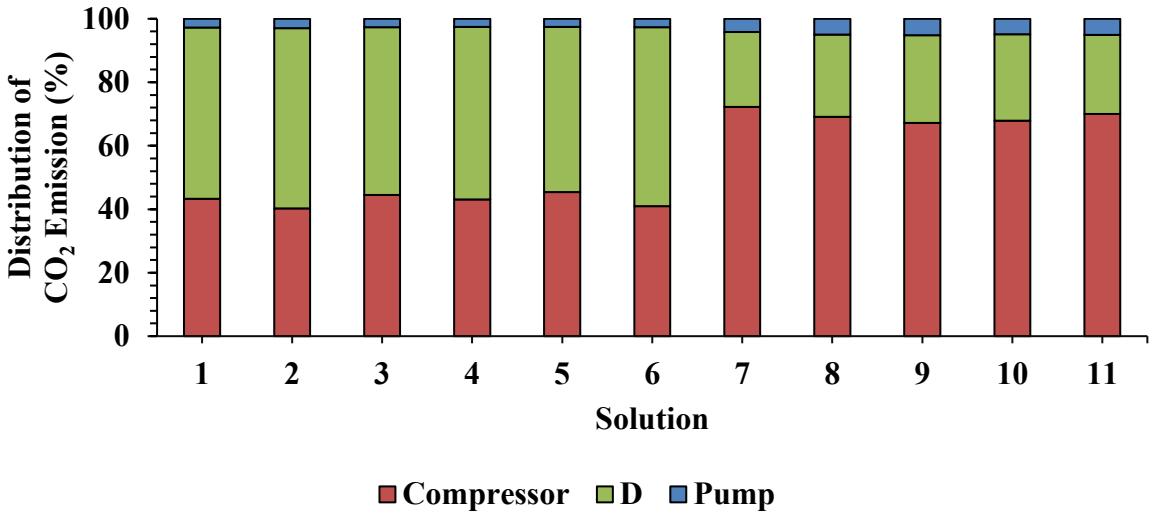

Source: Author.

Solutions designed for glycerol purification above 99.5 wt.% exhibit higher TIC, exceeding 1 million USD (Figure 56). As depicted in Figure 57, the main contribution comes from distillation column vessels, which represent approximately 60% of the total investment. The highest TICs are observed in Solutions 1, 4, and 7. When analyzing the correlation matrix (Figure E.3), it is noted that the most influential variable for TIC is DF^{RDC-1}, with r = 0.68. However, this variable remains nearly constant across all non-dominated solutions, as strategy to mitigate the environmental impact.

Given this, secondary variables with near moderate correlation can explain the TIC variation. Solutions 4 and 7 operates DF^{DC-1} around 0.40 (r = 0.24) and 26 stages (in DC-1). In the case of Solution 1, the elevated TIC results from a combination of higher reflux ratio in RDC-1 and DF^{DC-1}. Generally, DC-1 alone contributes to over 30% of the TIC in scenarios with glycerol purification, reinforcing the economic impact introduced by this purification step.

Figure 56 – TIC per Solution (CS-2A).

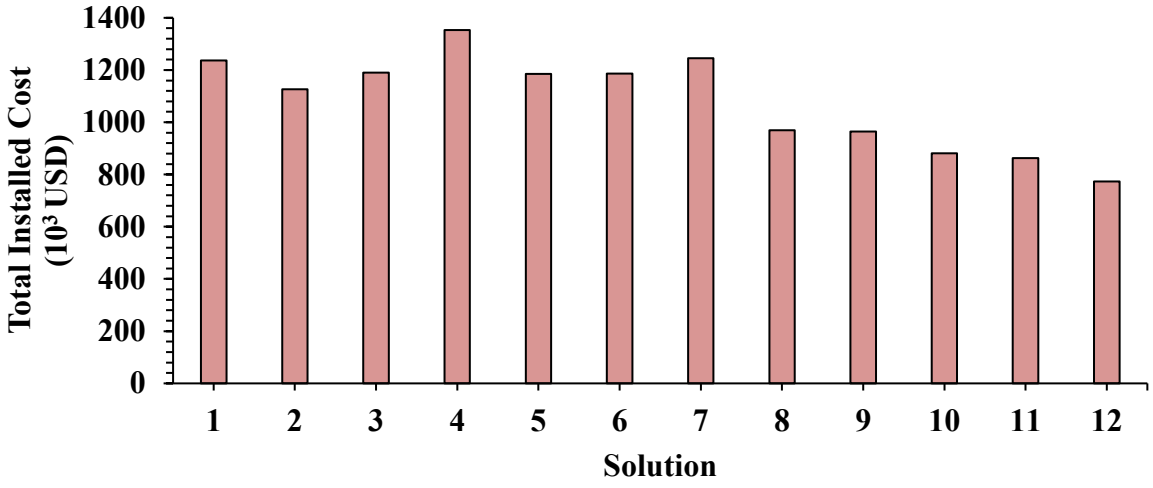

Source: Author.

Figure 57 – Distribution of TIC by Equipment (CS-2A).

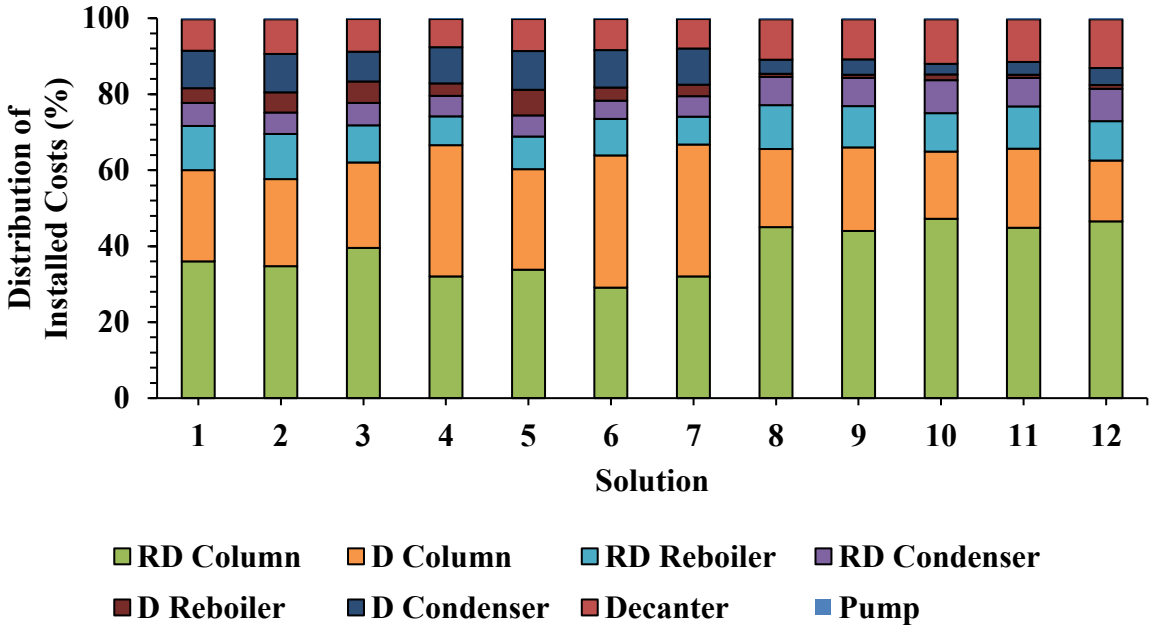

Source: Author.

The TOC in CS-2A is predominantly driven by RDC, as confirmed by the strong correlation between TOC and DF^{RDC-1} (r = 0.82), followed by a moderate influence from RR^{RDC-1} (r = 0.36). In contrast, variables associated with DC-1 have a secondary impact on TOC, despite its strong individual correlations with utility costs of DC-1 itself. This happens because the thermal demand from RDC significantly outweighs that of DC-1, as reflected in the TOC distribution shown in Figure 58. The RDC reboiler accounts for above 56% of the total, while the highest contribution observed for DC-1 reaches only 28%. Solutions focused on achieving USP glycerol present TOC above 380 thousand USD/year (Figure 59), with vacuum distillation column contributing between 21% and 29% to the operating costs. In contrast, for solutions that sell crude glycerol, this contribution drops, ranging from 5% to 12%. Among all evaluated alternatives, Solution 1 exhibits the highest TOC, directly associated with its highest RR^{RDC-1} (0.41).

Figure 58 – Distribution of TOC by Equipment (CS-2A).

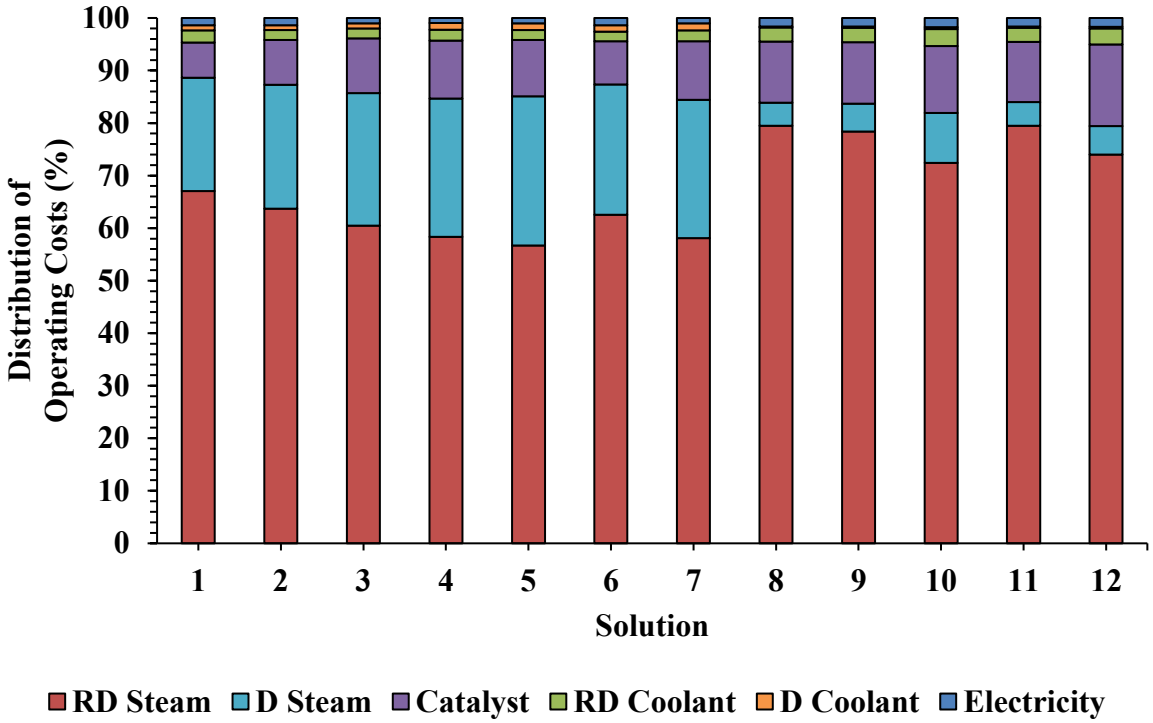

Source: Author.

Figure 59 – TOC per Solution (CS-2A).

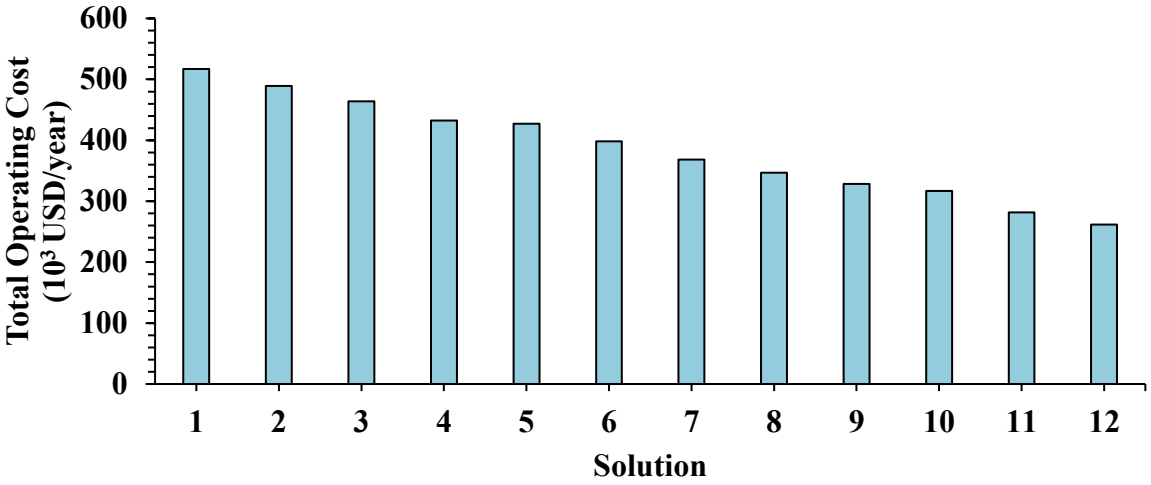

Source: Author.

In CS-2B, the TIC ranges from 1.6 to 2.2 million USD (Figure 60), with the compressors remaining the most significant contributors, representing 40–50% of the total (Figure 61), followed by the costs associated with the RDC. The addition of the DC-1 has a low to moderate impact, accounting for 4–20% of TIC.

Figure 60 – TIC per Solution (CS-2B).

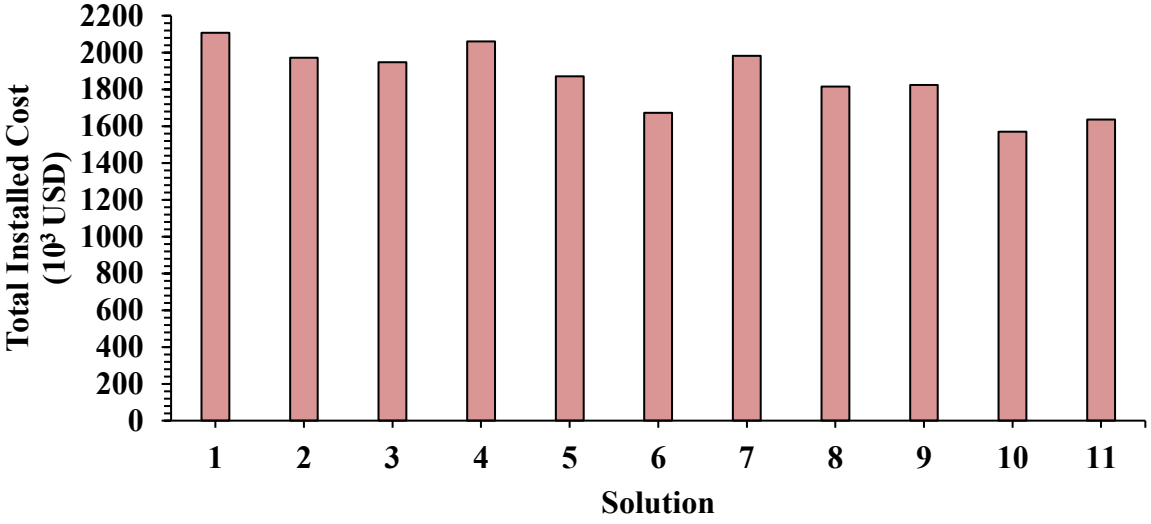

Source: Author.

Figure 61 – Distribution of TIC by Equipment (CS-2B).

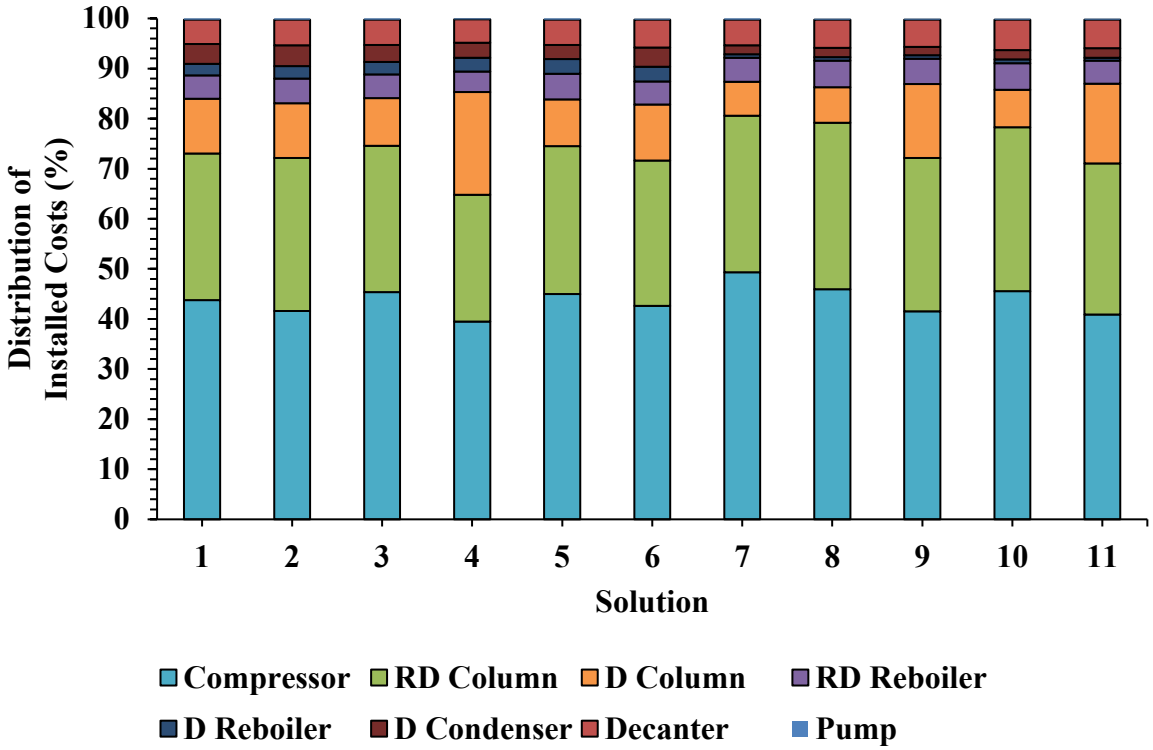

Source: Author.

Analyzing the correlation matrix (Figure E.4), it is observed that VF^{RDC-1} ($r = 0.86$), DF^{DC-1} ($r = 0.34$), RR^{DC-1} ($r = 0.29$), and P^{COMP-1} ($r = 0.26$) are the main variables that influence the TIC. While VF^{RDC-1} and P^{COMP-1} affect the compressor cost as discussed in Equation 26 analysis, DF^{DC-1} and RR^{DC-1} impact the investment cost of the vacuum distillation column and the associated heat exchangers. Overall, since compressors dominate the capital investment in CS-2B, the integration of the vacuum distillation column imposes a lower proportional influence on TIC compared to CS-2A.

In CS-2B, the TOC ranges from 200 to 450 million USD/year (Figure 62). Correlation analysis indicates that the most significant variables influencing TOC are DF^{DC-1} ($r = 0.70$), VF^{RDC-1} ($r = 0.59$), and RR^{DC-1} ($r = 0.41$). As illustrated in Figure 63, electricity remains the primary operational expense, representing 43–60% of the total, followed by the steam consumption associated with the DC-1. Solutions that achieve glycerol purification consistently present a higher contribution from steam, close to 26%, whereas scenarios selling crude glycerol show a reduced contribution, around 10%. Overall, the analysis confirms that glycerol purification exerts a more pronounced influence on TOC than on TIC for CS-2B. While the addition of DC-1 leads to a moderate increase in TIC, due to the capital already dominated by

compressor and RDC, the thermal load required for vacuum distillation has a more substantial impact on TOC, though still less significant than electricity consumption.

Figure 62 – TOC per Solution (CS-2B).

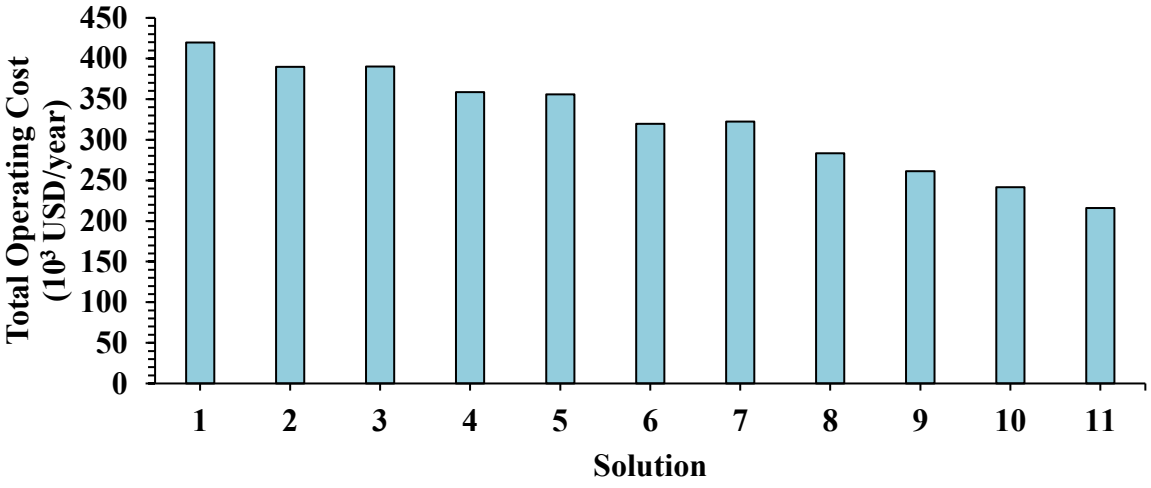

Source: Author.

Figure 63 – Distribution of TOC by Equipment (CS-2B).

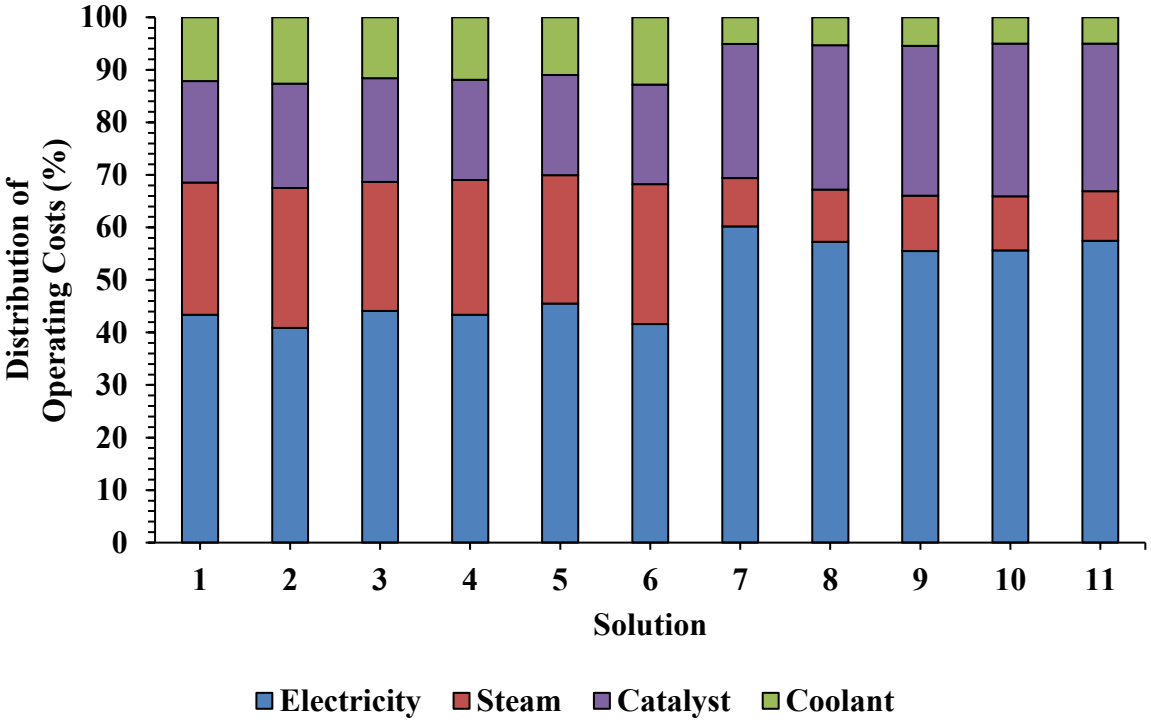

Source: Author.

Following the same selection methodology applied in CS-1 and considering only non-dominated solutions that meet the USP glycerol specification, Solution 7 (CS-2A) and Solution 2 (CS-2B) were identified as the most robust candidates for practical implementation, as summarized in Table 26. The corresponding decision, performance and constraint variable values are detailed in Table 27.

Table 26 – Selected Solution IDs Across Different Methods (CS-2).

Weight of Objective Function		Selected Solution ID					
W_{YGP}	W_{CO_2e}	TOPSIS		SAW		GRA	
		CS-2A	CS-2B	CS-2A	CS-2B	CS-2A	CS-2B
0.2	0.8	7	6	7	6		
0.4	0.6	7	2	7	6		
0.6	0.4	4	2	4	2	1	2
0.8	0.2	1	2	1	2		
0.5	0.5	4	2	7	2		

Source: Author.

To compare the economic and environmental metrics, the selected solutions of CS-2 and CS-1 were normalized using the biodiesel production. In Table 28, the comparison shows that the addition of DC-1 leads to a substantial increase in capital and operating costs in a normalized perspective. In RD configuration, the normalized TIC/PBP increases by 157% (from 0.106 to 0.272), while TOC increases in 222% (from 0.125 to 0.402), resulting in a TAC increase of 192% (from 0.231 to 0.674). In HPRD, the impact is also significant where TIC/PBP increases by 81%, TOC by 393%, and TAC by 164%.

From an environmental perspective, the adoption of DC-1 also leads to a significant increase in CO_2e. In RD, emissions rise by 190%, and in HPRD, by 370%. The difference in relative impact is explained by the absence of external steam use in CS-1B, where emissions are linked exclusively to electricity consumption in the pump and compressor. When DC-1 is added, it introduces an additional thermal load supplied by external steam, which was not previously part of the HPRD system.

Table 27 – Decision Variables and Constraint Values for Selected Solutions (CS-2).

Variable	Solution	
	7 (CS-2A)	2 (CS-2B)
$\dot{n}_{SBO-IN}$ (kmol/h)	38.81	46.31
$R_{in}^{process}$	3.80	3.72
P^{P-1} (atm)	2.13	4.12
P^{RDC-1} (atm)	1.49	2.09
P^{V-1} (atm)	--	2.89
P^{COMP-1} (atm)	--	9.40
f_{holdup}^{RDC-1}	0.82	0.76
N_T^{RDC-1}	12	18
N_R^{RDC-1}	2	4
N_S^{RDC-1}	3	5
FS^{RDC-1}	1	11
RR^{RDC-1}	0.08	--
DF^{RDC-1}	0.22	--
RF^{RDC-1}	--	0.49
VF^{RDC-1}	--	0.53
P^{DC-1} (atm)	0.13	0.17
N_T^{DC-1}	26	11
FS^{DC-1}	24	8
RR^{DC-1}	0.39	0.14
DF^{DC-1}	0.39	0.36
YGP (million USD/year)	95.42	119.19
CO_2e (ton/year)	3484	2033
$\dot{q}_{BIO-OUT}$ (L/h)	43606	52738
$x_{FAME}^{BIO-OUT}$ (wt.%)	97.7	96.5
$x_{GLY}^{MIX-OUT}$ (wt.%)	99.5	99.6
T_{reb}^{RDC-1} (°C)	129	127
T_{reb}^{DC-1} (°C)	124	143
R_{in}^{RDC-1}	5.17	5.21

Source: Author.

Table 28 – Relative Difference of Costs and Emissions Between Selected Solutions.

Metric	Selected Solution			
	4 (CS-1A)	7 (CS-2A)	3 (CS-1B)	2 (CS-2B)
Normalized TIC/PBP [USD/(year kmol)]	0.106	0.272 (+157%)	0.202	0.365 (+81%)
Normalized TOC [USD/(year kmol)]	0.125	0.402 (+222%)	0.073	0.360 (+393%)
Normalized TAC [USD/(year kmol)]	0.231	0.674 (+192%)	0.275	0.725 (+164%)
Normalized CO2e [kg/(year kmol)]	1.31	3.80 (+190%)	0.40	1.88 (+370%)

Source: Author.

It is important to highlight that the thermal duties associated with the glycerol purification column (DC-1) in this study are similar with the values present in literature (normalized by the purified glycerol flow rate). Specifically, the reboiler and condenser duties obtained in this work are 1.88 W/kmol (CS-2A), 1.66 W/kmol (CS-2B), and 1.14 W/kmol (CS-2A), 0.81 W/kmol (CS-2B) of purified glycerol. These results are close to the values reported by Braga (2023), which were 1.94 W/kmol for the reboiler and 1.24 W/kmol for the condenser.

4.3 Case Study 3

When the strict specifications established by ANP are applied (glycerol, methanol, and triolein below 0.2 wt.% and FAME above 96.5 wt.%), the Pareto Fronts for RD and HPRD configurations (Figures 64 – 67) shift towards higher CO_2e, without altering the inherent trade-off between economic and environmental objectives. Compared to CS-2, both CS-3A and CS-3B present a substantial increase in emissions, exceeding 6000 t/year in RD and 2700 t/year in HPRD. A reduction in YGP is also observed in both configurations. However, it is important to note that, despite the stricter specifications, multiple solutions still achieve YGP values above 100 million USD/year in CS-3, confirming the economic viability of the process under these conditions. Additionally, in all non-dominated solution, except for Solution 11 in CS-3A, the glycerol is sold as USP grade, as illustrated in Figures 68 and 69.

In CS-2A, RDC emissions accounted for 65–75% of the total (Figure 70), while in CS-3A this share rises to around 90% (Figure 71), driven by DF^{RDC-1} required to meet stricter purity targets. The DF^{RDC-1} increases from ~ 0.20 in CS-2A to ~ 0.30 in CS-3A, with strong correlation to CO_2e (r = 0.80), confirming its dominant function. To satisfy the pseudo-first-order kinetic model with $R_{in}^{process}$ above 5, the process must remove excess unreacted methanol that would otherwise compromise biodiesel and glycerol purity.

Figure 64 – Pareto Front (CS-3A).

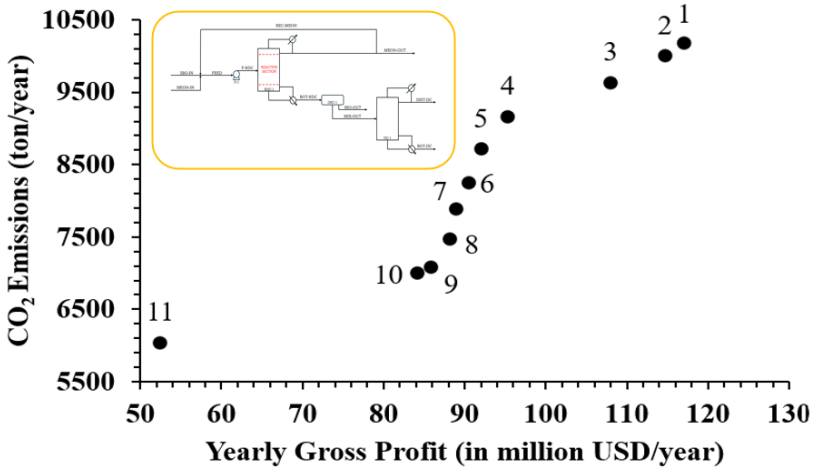

Source: Author.

Figure 65 – Pareto Front (CS-3B).

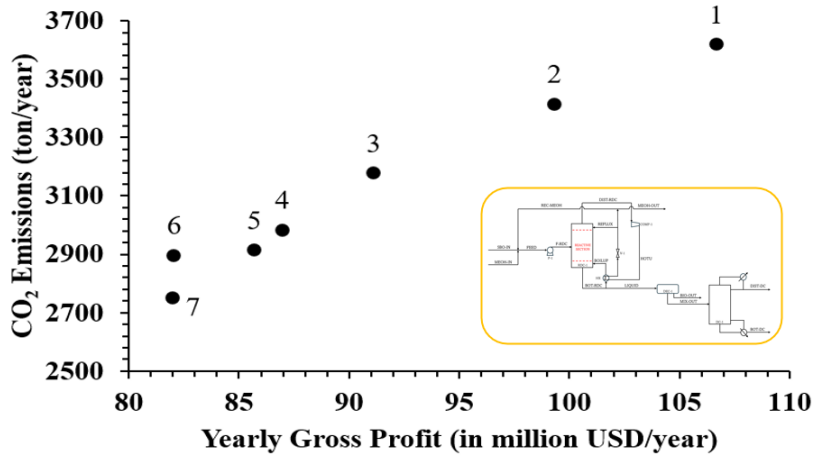

Source: Author.

Figure 66 – Objective Function Values per Solution (CS-3A).

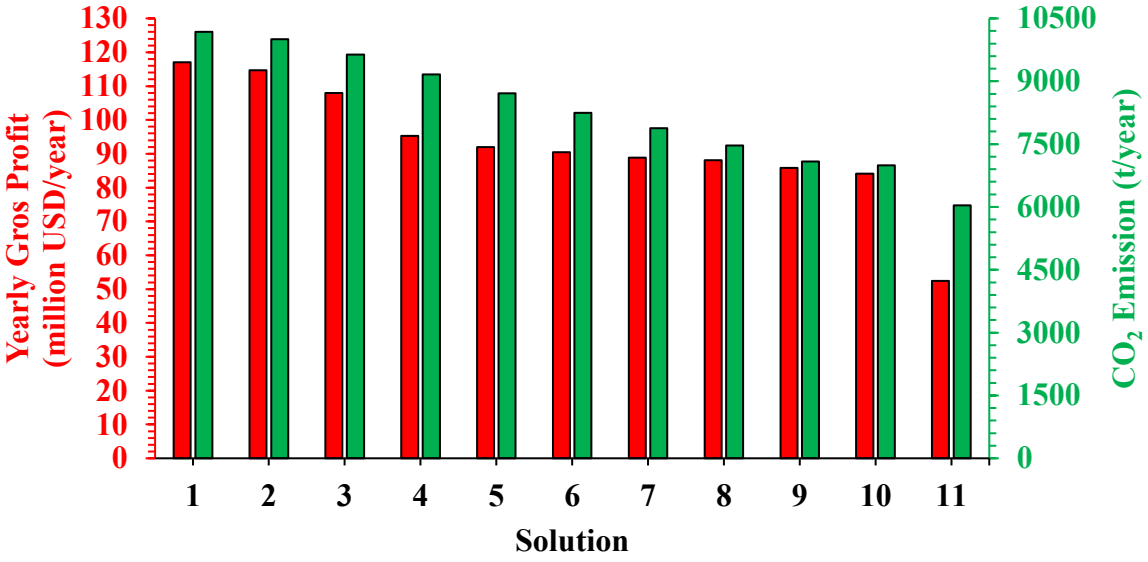

Source: Author.

Figure 67 – Objective Function Values per Solution (CS-3B).

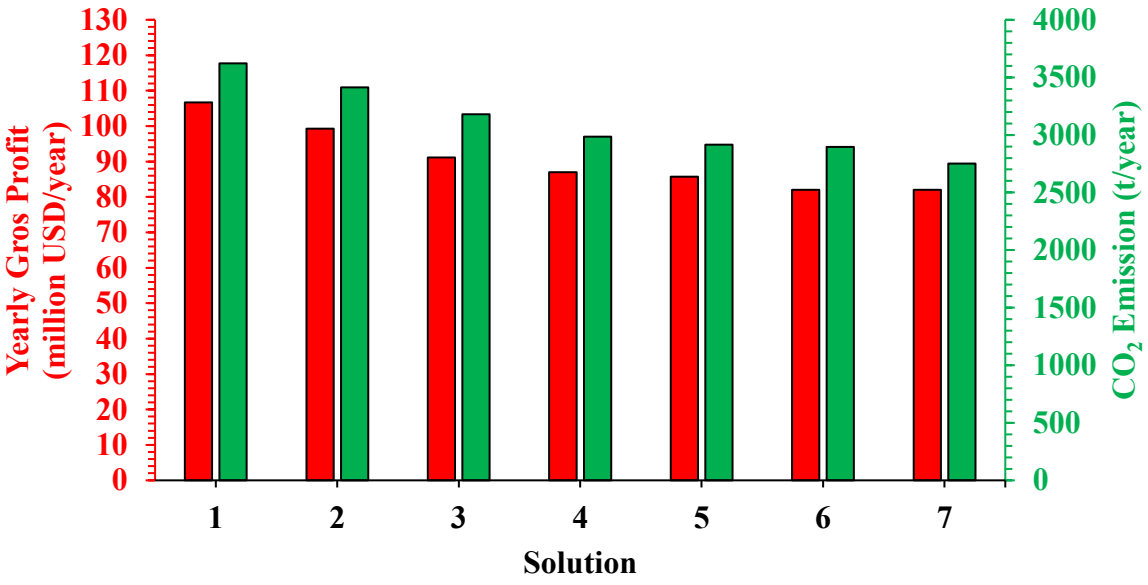

Source: Author.

Figure 68 – Glycerol Purity for Non-Dominated Solutions in CS-3A.

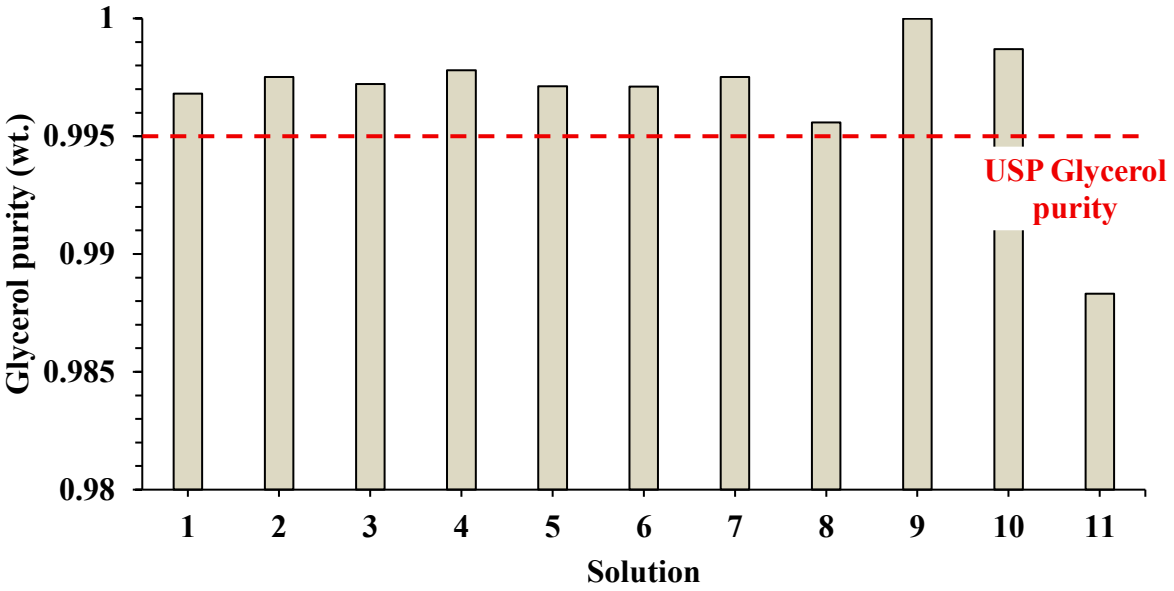

Source: Author

Figure 69 – Glycerol Purity for Non-Dominated Solutions in CS-3B.

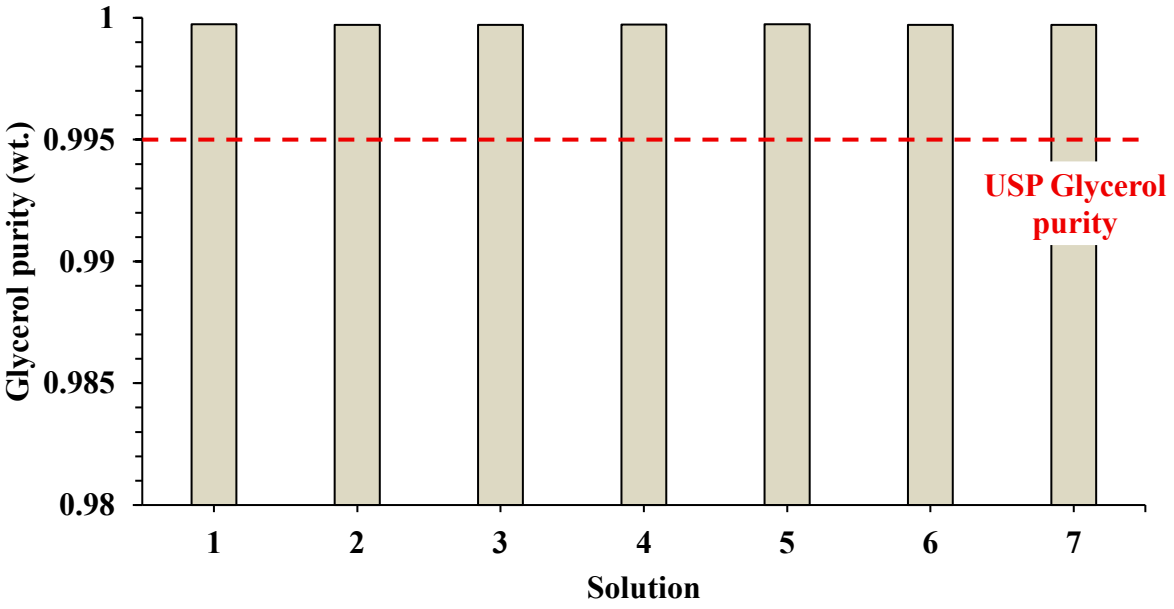

Source: Author.

In CS-3A, DF^{RDC-1} not only recovers methanol but also functions to purge 5% of recycled excess methanol to comply with ANP specifications. In CS-3B, CO_2e also increase compared to CS-2B, but the emission distribution remains similar, with RDC and compressor contributing between 53% and 65% in near totality of non-dominated solutions.

Figure 70 – CO_2e Distribution by Equipment (CS-3A).

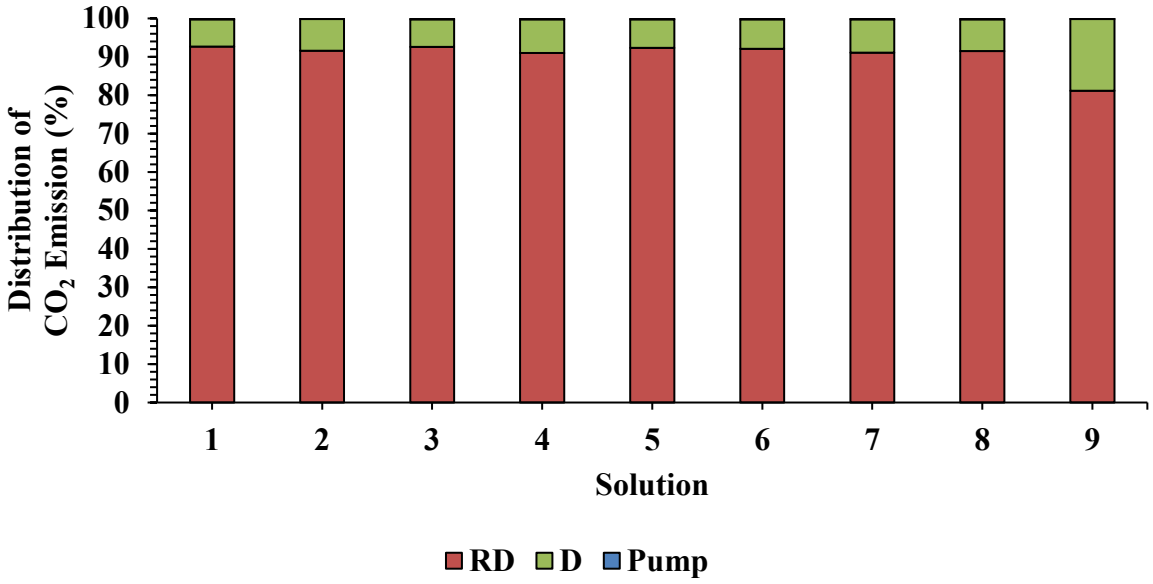

Source: Author.

Figure 71 – CO_2e Distribution by Equipment (CS-3B).

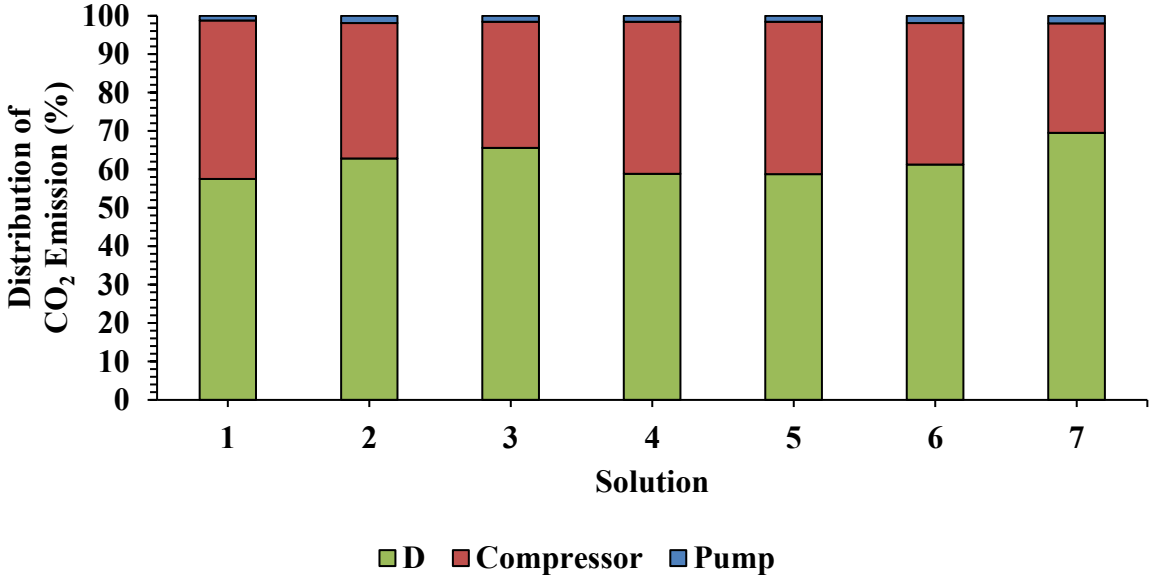

Source: Author.

The correlation values between decision variables and mass fractions constraints in the output streams indicate that N_T^{RDC-1} has a moderate positive correlation with $x_{FAME}^{BIO-OUT}$ and a strong negative with $x_{OOO}^{BIO-OUT}$. Increasing the number of stages enhances the contact between reactants and catalyst, improving the conversion of triolein to FAME. The impact on methanol and glycerol fractions are less significant, since methanol is fed in excess, leading to low

consumption relative to triolein, and glycerol is mainly removed in the decanter. Nevertheless, the correlation with $x_{GLY}^{BIO-OUT}$ remains moderate in CS-3B (r = 0.38), associated with the reaction under limited phase separation, as further discussed in the next paragraph.

The $R_{process}^{in}$ has a stronger impact. Higher $R_{process}^{in}$ raises $x_{MeOH}^{BIO-OUT}$ and simultaneously reduces x_{GLY}^{BOT-DC} with r = -0.44 in CS-3A and r = -0.52 in CS-3B. A relevant observation is the strong correlation between $R_{process}^{in}$ and $x_{GLY}^{BIO-OUT}$, with r = 0.83 in CS-3A and r = 0.67 in CS-3B. This reflects the reduced separation efficiency between biodiesel and glycerol phases caused by higher methanol content, which promotes mutual solubility. This behavior is consistent with experimental findings reported by Yang *et al*., (2024), demonstrating that excess methanol increases glycerol solubility in biodiesel under the decanter operating conditions used in this study. Figures 72 – 75 demonstrate that all solutions meet the ANP quality requirements, where red dashed line represents the imposed limits.

For CS-3A, TIC ranges from 880 thousand to 1.36 million USD (Figure 76), with a distribution (Figure 77) similar to the glycerol purification solutions from CS-2A. The main difference lies in the higher contribution from the RDC heat exchangers, reflecting the increased thermal demand for methanol removal. In CS-2A, the reboiler and condenser account for 7–12% and 4–6% of TIC, respectively, whereas in CS-3A, these contributions increase to 10–22% and 9–12%. For CS-3B, TIC varies between 1.67 and 2.10 million USD (Figure 78), maintaining a distribution pattern (Figure 79) comparable to CS-2B but with a higher cost share associated with the vacuum distillation column, ranging from 23% to 29%. Correlation analysis indicates similar trends to those observed in CS-2A and CS-2B, with an even stronger influence from DC-1 variables (CS-3A) and reactive holdup (CS-3B) within the convergence interval.

For CS-3A, TOC ranges from 603 thousand to 1 million USD/year (Figure 80), representing a substantial increase compared to CS-2A (398–517 thousand USD/year). This increase is mainly attributed to the sharp rise in steam demand for the RDC, whose contribution (Figure 81) grows from 58–67% in CS-2A to 71–83% in CS-3A, with most solutions concentrated near the upper limit. When considering both RDC and DC steam demand together, the total reaches approximately 90% of TOC. For CS-3B, TOC varies between 408 and 632 thousand USD/year (Figure 82), also higher than in CS-2B (319–419 thousand USD/year), but with a less pronounced relative increase compared to the RD case (Figure 83). In both configurations, the influence of decision variables on TOC remains consistent with the trends observed in CS-2.

Figure 72 – FAME Mass Fraction in Biodiesel Stream for All Obtained Solutions (CS-3A).

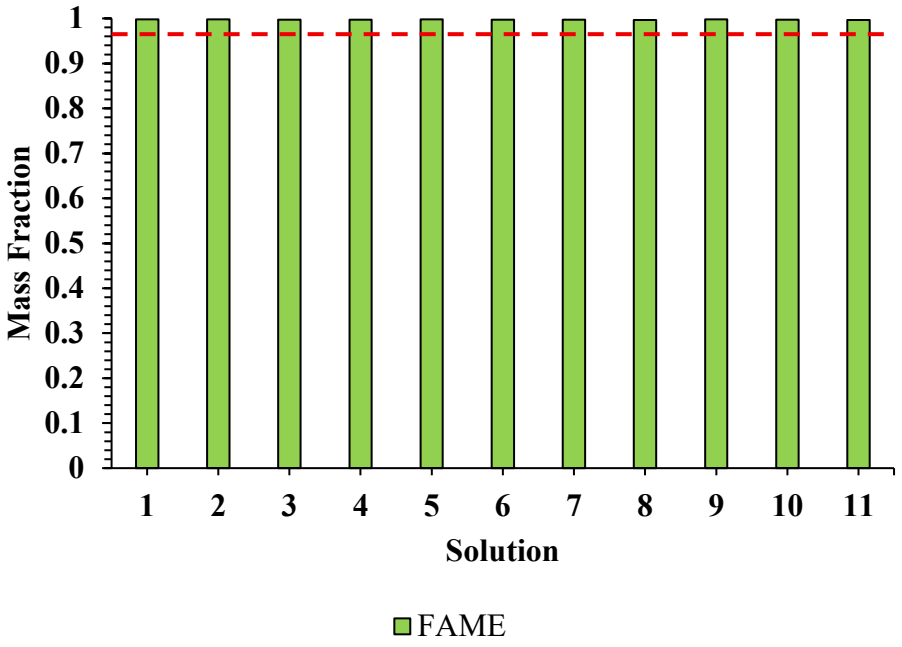

Source: Author.

Figure 73 – Mass Fraction in Biodiesel Stream for Residual Components (CS-3A).

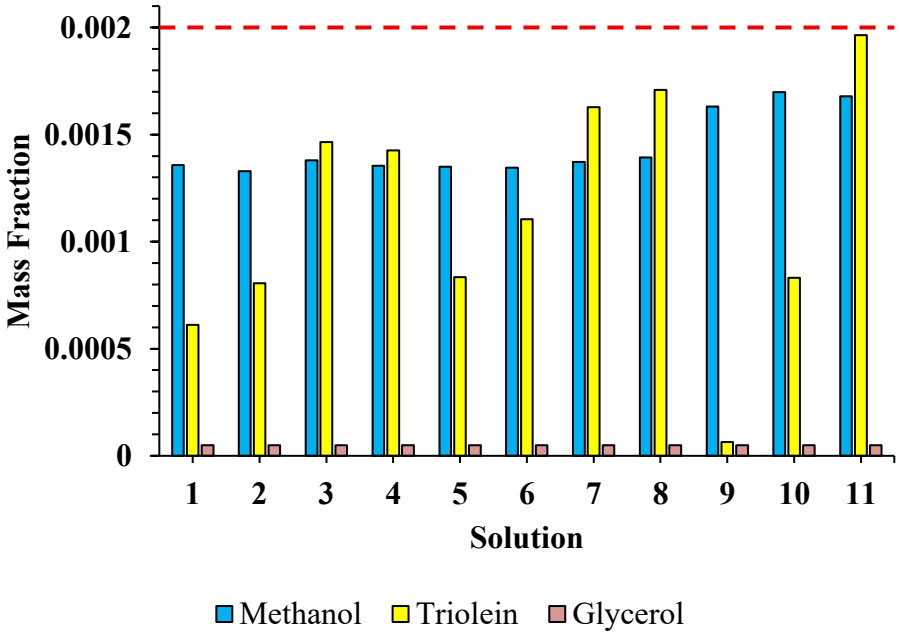

Source: Author.

Figure 74 – FAME Mass Fraction in Biodiesel Stream for All Obtained Solutions (CS-3B).

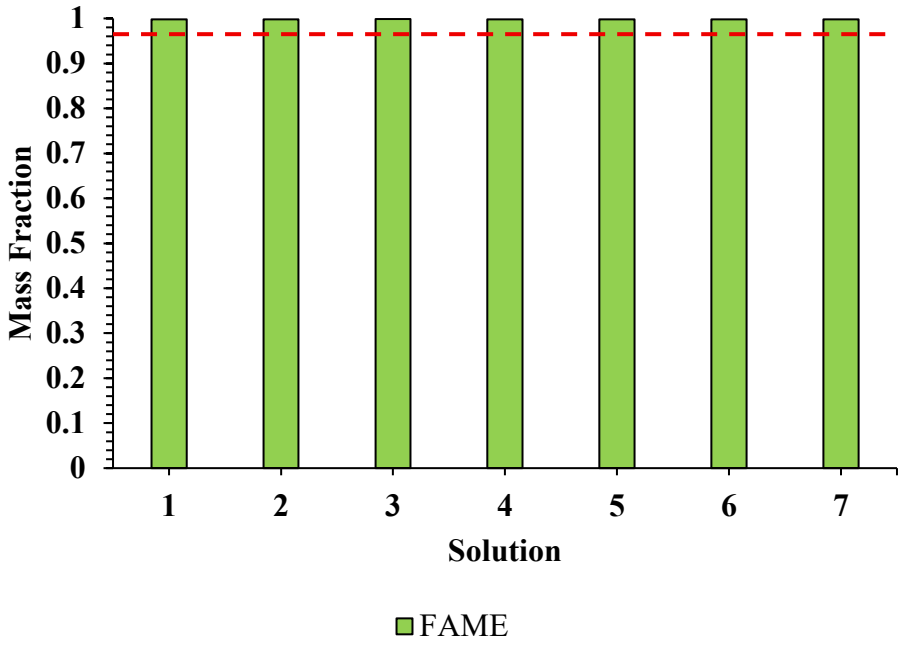

Source: Author.

Figure 75 – Mass Fraction in Biodiesel Stream for Residual Components (CS-3B).

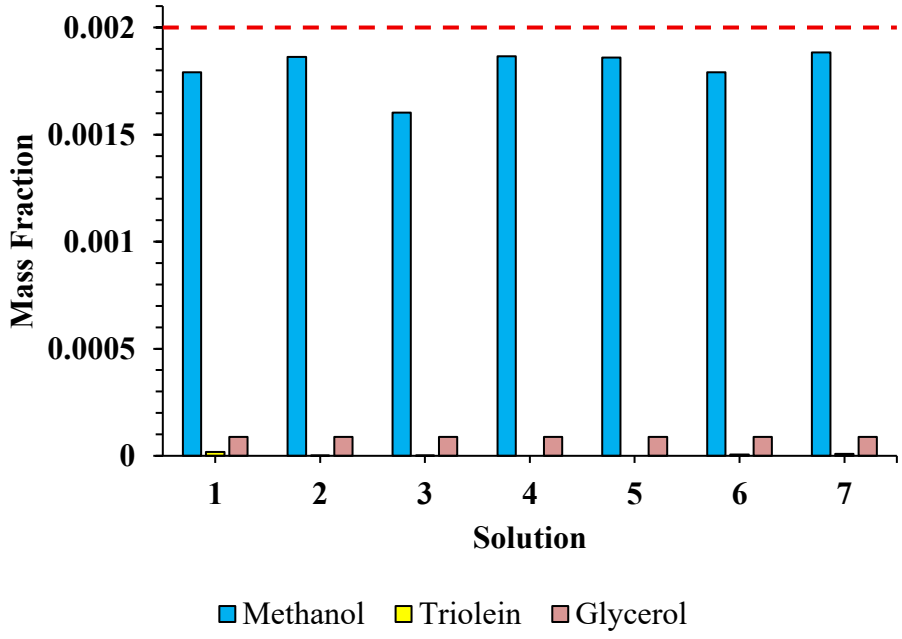

Source: Author.

Figure 76 – TIC per Solution (CS-3A).

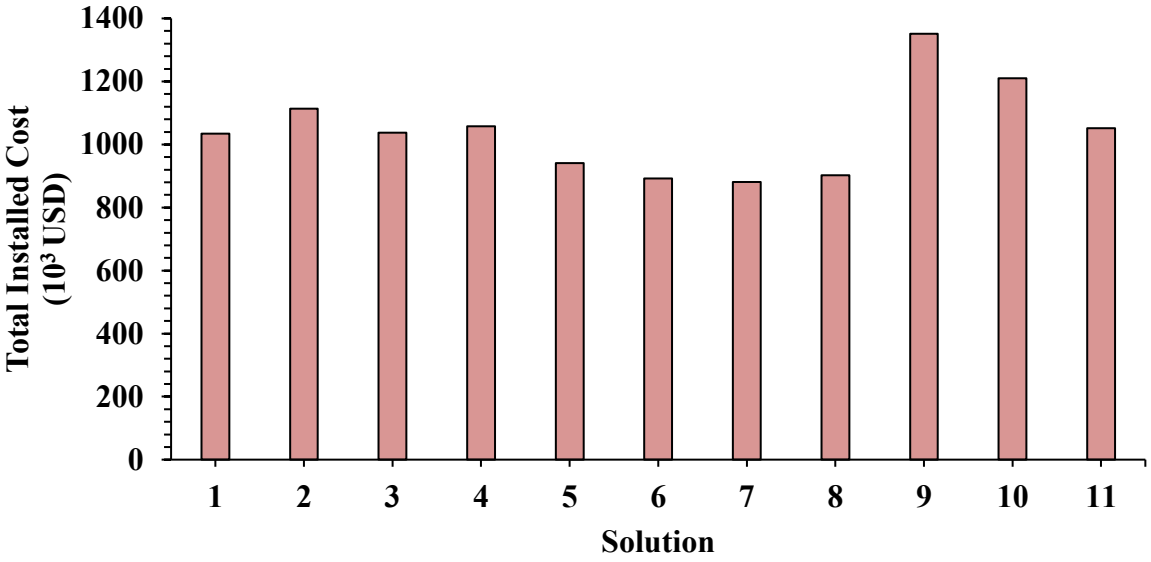

Source: Author.

Figure 77 – Distribution of TIC by Equipment (CS-3A).

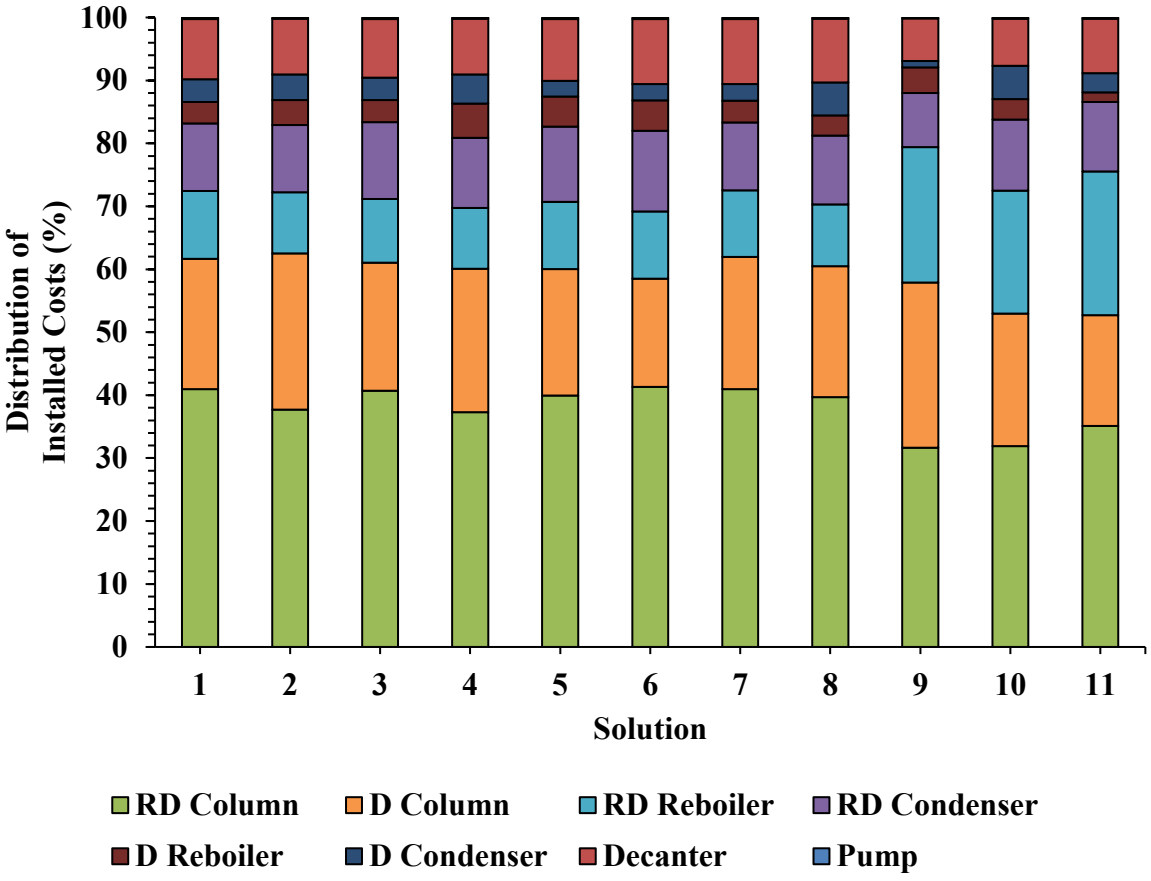

Source: Author.

Figure 78 – TIC per Solution (CS-3B).

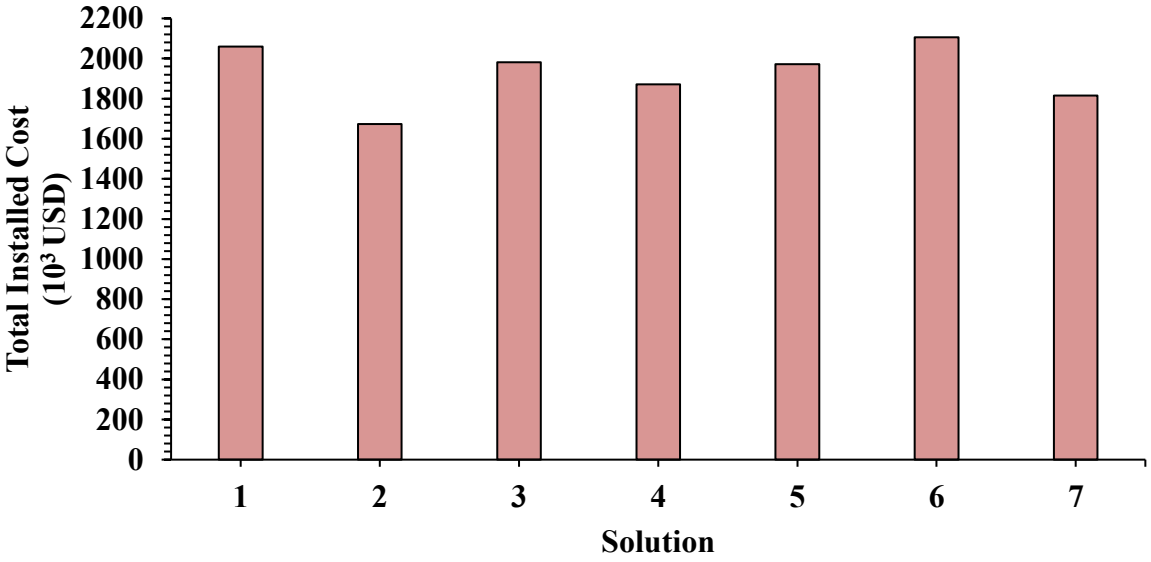

Source: Author.

Figure 79 – Distribution of TIC by Equipment (CS-3B).

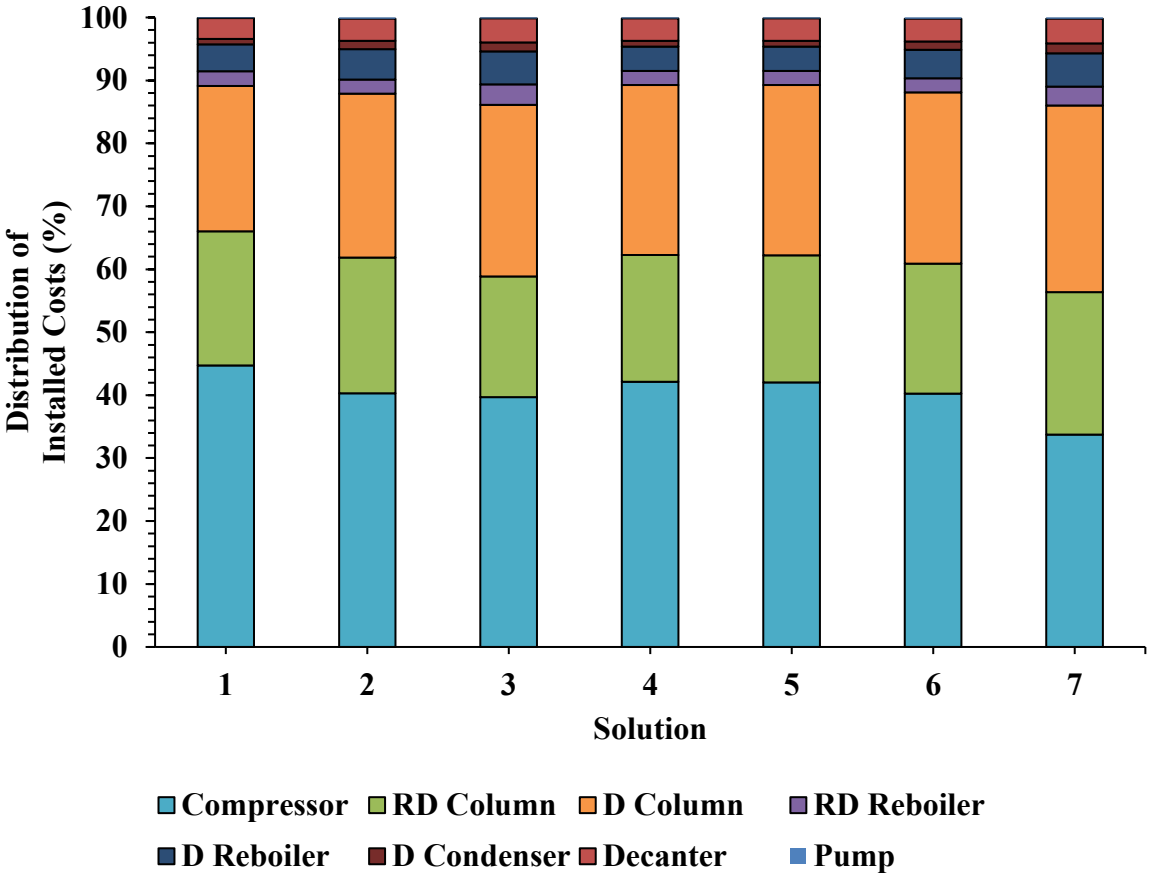

Source: Author.

Figure 80 – TOC per solution (CS-3A).

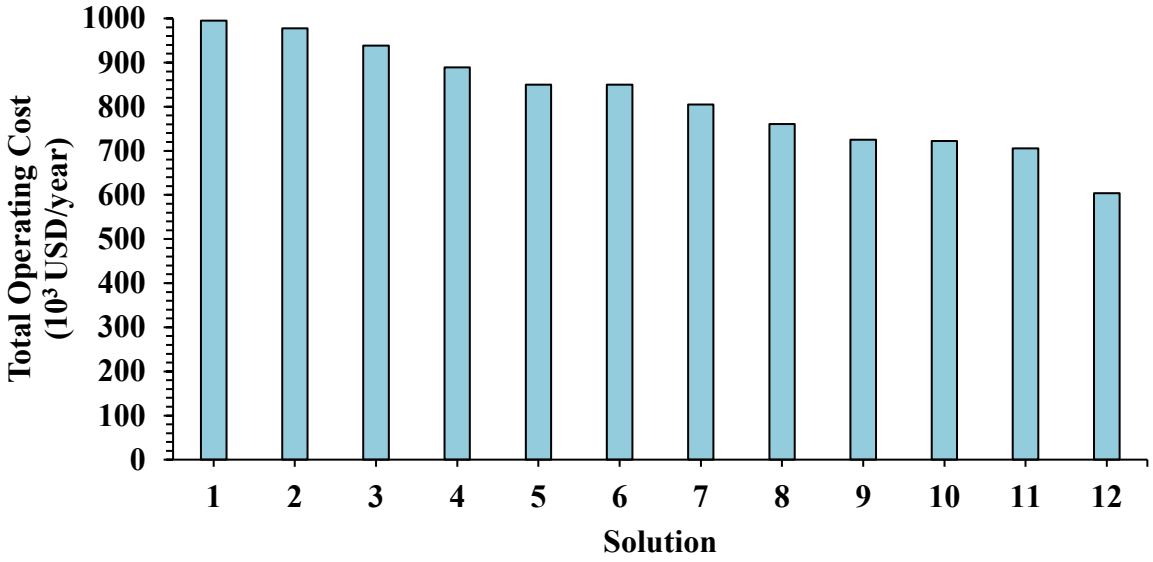

Source: Author.

Figure 81 – Distribution of TOC by component (CS-3A).

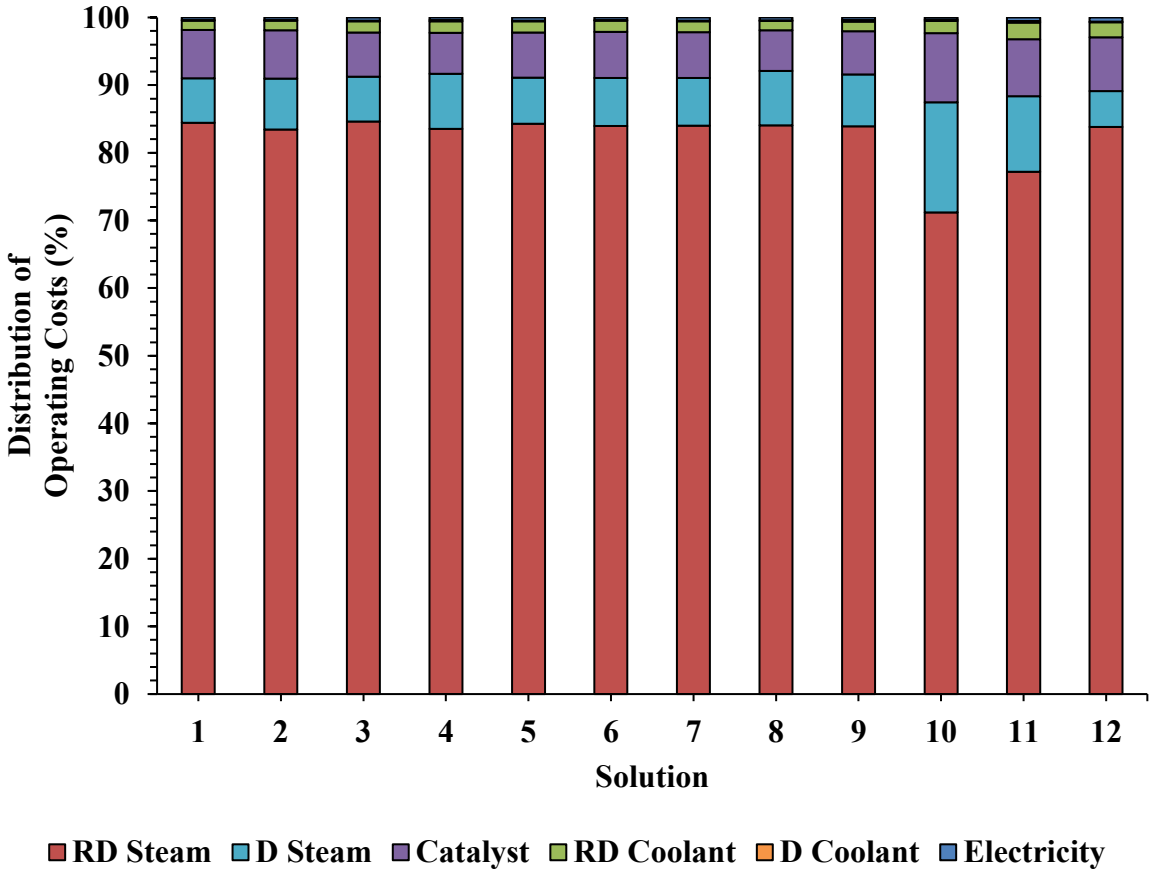

Source: Author.

Figure 82 – TOC per solution (CS-3B).

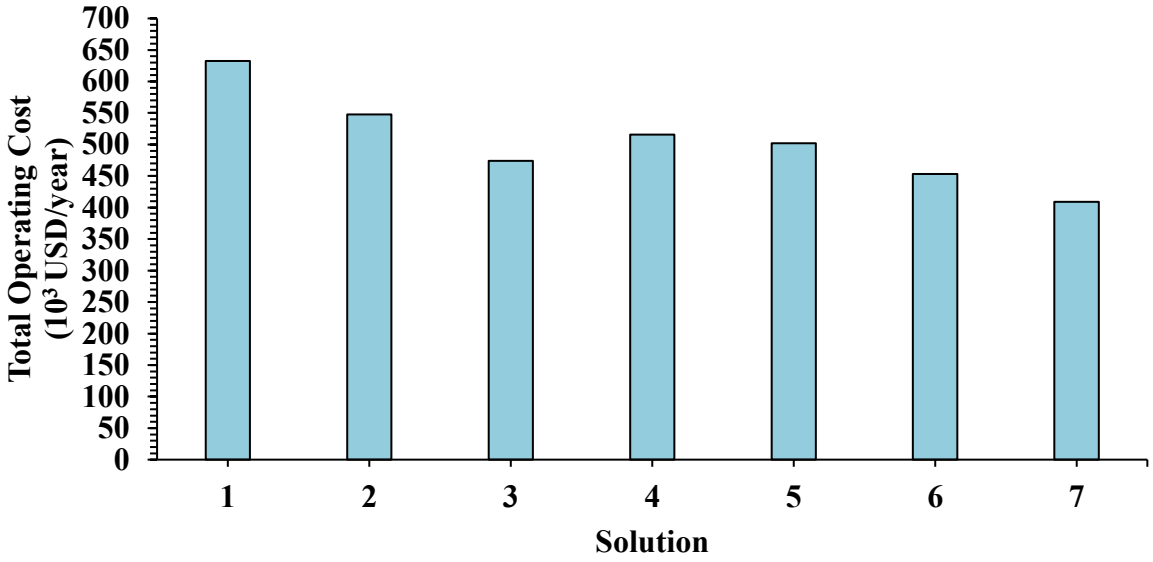

Source: Author.

Figure 83 – Distribution of TOC by component (CS-3B).

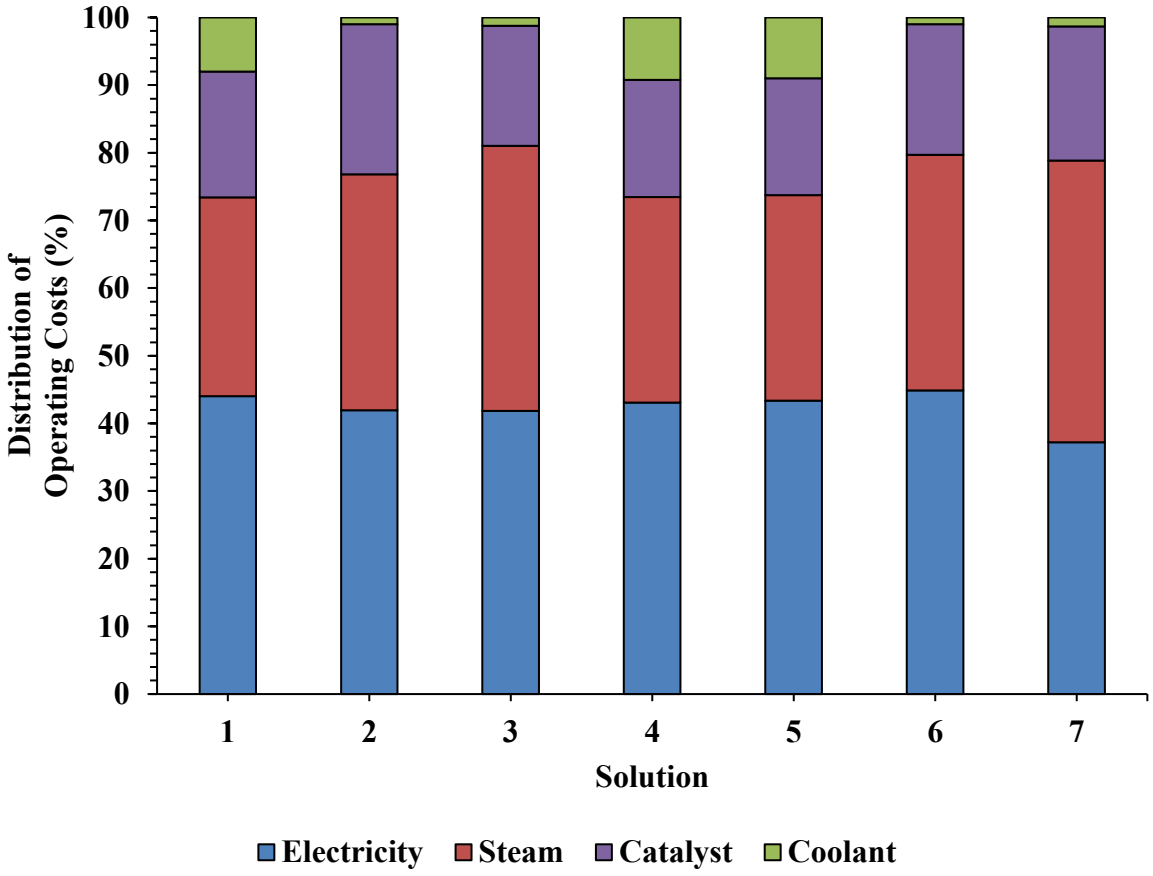

Source: Author.

Adopting the same selection criteria used in previous case studies, Solutions with ID 1 were identified as the most robust options for both CS-3A and CS-3B. These solutions achieve the highest profitability among the non-dominated alternatives while complying with all ANP and USP glycerol specifications (presenting the highest associated emissions). The selection results are summarized in Table 29, with detailed decision variables, process performances, and constraint values provided in Table 30.

To compare the economic and environmental metrics, the selected solutions of CS-2 and CS-3 were normalized using the biodiesel production. As shown in Table 31, the normalized TIC/PBP decreases by 35% in RD and increases by 43% in HPRD. On the other hand, TOC increases significantly, 110% for RD and 53% for HPRD, due to the additional energy demand. Consequently, TAC rises by 52% in RD and 48% in HPRD. From an environmental perspective, CO_2e show the most significant increase, with growth of 111% in RD and 67% in HPRD, directly associated with the higher thermal load required to meet ANP specifications.

Table 29 – Selected Solution IDs Across Different Methods (CS-3).

Weight of Objective Function		Selected Solution ID					
W_{YGP}	W_{CO_2e}	TOPSIS		SAW		GRA	
		CS-3A	CS-3B	CS-3A	CS-3B	CS-3A	CS-3B
0.2	0.8	11	7	11	7		
0.4	0.6	9	7	10	7		
0.6	0.4	1	1	1	1	1	1
0.8	0.2	1	1	1	1		
0.5	0.5	9	7	1	7		

Source: Author.

Table 30 – Decision Variables and Constraint Values for Selected Solutions (CS-3).

Variable	Solution	
	1 (CS-3A)	1 (CS-3B)
$\dot{n}_{SBO-IN}$ (kmol/h)	49.11	48.01
$R_{in}^{process}$	3.25	3.29
P^{P-1} (atm)	1.98	3.01
P^{RDC-1} (atm)	1.14	1.21
P^{V-1} (atm)	--	13.42
P^{COMP-1} (atm)	--	13.61
f_{holdup}^{RDC-1}	0.87	0.75
N_T^{RDC-1}	13	21
N_R^{RDC-1}	2	3
N_S^{RDC-1}	1	3
FS^{RDC-1}	3	12
RR^{RDC-1}	0.07	--
DF^{RDC-1}	0.31	--
RF^{RDC-1}	--	0.35
VF^{RDC-1}	--	0.52
P^{DC-1} (atm)	0.14	0.22
N_T^{DC-1}	22	35
FS^{DC-1}	20	21
RR^{DC-1}	0.11	0.40
DF^{DC-1}	0.10	0.19
YGP (million USD/year)	117.08	106.66
CO_2e (t/year)	10182.43	3620.25
$\dot{q}_{BIO-OUT}$ (L/h)	53935	52717
$x_{FAME}^{BIO-OUT}$ (wt.%)	99.8	99.8
x_{GLY}^{BOT-DC} (wt.%)	99.7	100.0
$x_{OOO}^{BIO-OUT}$ (wt.%)	0.06	0.00
$x_{MEOH}^{BIO-OUT}$ (wt.%)	0.14	0.18
$x_{GLY}^{BIO-OUT}$ (wt.%)	0.00	0.01
T_{reb}^{RDC-1} (°C)	195	130
T_{reb}^{DC-1} (°C)	138	237
R_{in}^{RDC-1}	5.06	5.17

Source: Author.

Table 31 –Relative Difference of Costs and Emissions Between Selected Solutions.

Metric	Selected Solution			
	7 (CS-2A)	1 (CS-3A)	1 (CS-3B)	1 (CS-2B)
Normalzed TIC/PBP [USD/(year kmol)]	0.272	0.175 (-35%)	0.365	0.521 (+43%)
Normalized TOC [USD/(year kmol)]	0.402	0.844 (+110%)	0.360	0.549 (+53%)
Normalized TAC [USD/(year kmol)]	0.674	1.020 (+52%)	0.725	1.070 (+48%)
Normalized CO2e [kg/(year kmol)]	3.80	8.01 (+111%)	1.88	3.14 (+67%)

Source: Author.

For consistency with the literature, catalyst costs and glycerol purification costs were excluded from the economic analysis in this section, since the compared studies do not consider glycerol purification. Figure 84 presents the comparison between the CS-3B solutions and alternative intensified processes reported by Mondal *et al*. (2021) and Mondal, Rangaiah, and Jana (2022). All CS-3B solutions achieve biodiesel purity of 99.8 wt.%, exceeding the specifications reached by the other processes. Among them, Solution 7 stands out for presenting the lowest normalized TAC and CO_2 emissions, even though it corresponds to the lowest profit within the non-dominated set. Despite this, its biodiesel production capacity is more than twice as high compared to the processes proposed in the literature. Additionally, when excluding emissions associated with electricity consumption (and steam for glycerol purification), CS-3B operates with zero direct CO_2 emissions due to the elimination of external heat utilities.

Figure 84 – Comparison of Normalized TAC and Emissions Across Process Intensified Biodiesel Processes and CS-3B Solutions.

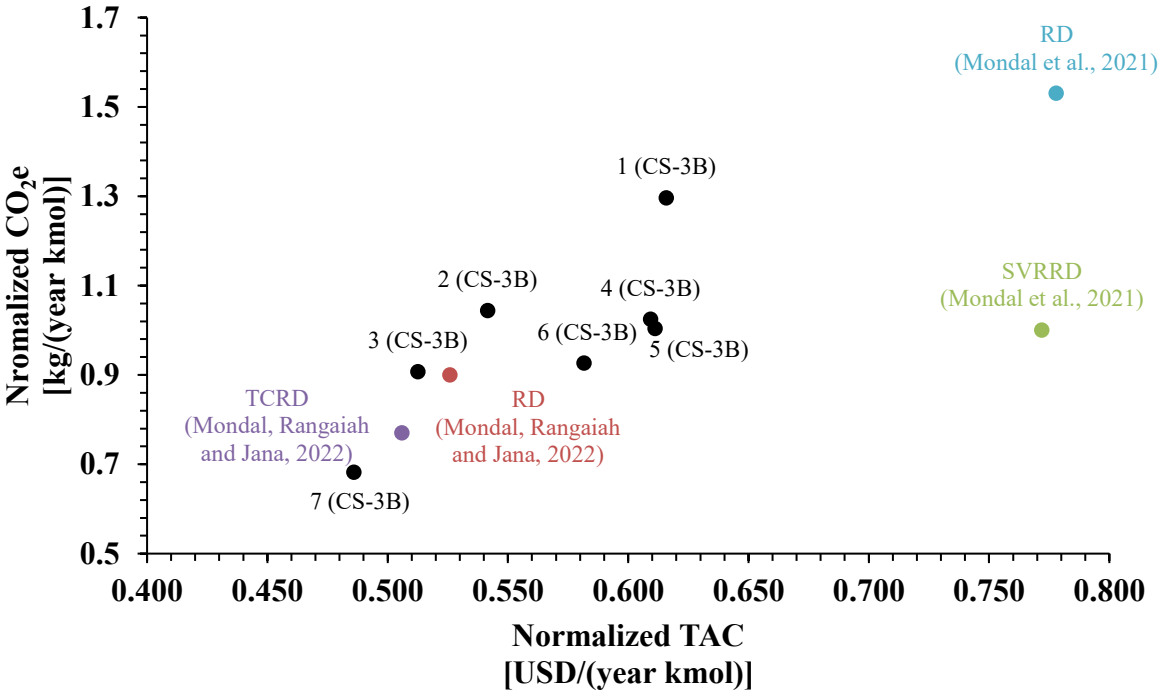

Source: Author.

5 Conclusion and Suggestions

This work proposed a novel intensified process configuration, Heat Pump Reactive Distillation (HPRD), for continuous biodiesel production at a Brazilian industrial scale. It also evaluated scenarios with different levels of glycerol purification and stricter biodiesel purity requirements (established by ANP Resolution No. 920/2023), considering both economic and environmental metrics. The equipment configurations defined for each strategy resulted in three case studies, in which the proposed configurations were directly compared with the conventional Reactive Distillation (RD). Multi-objective optimization (MOO) problems were solved using the NSGA-II algorithm to maximize Yearly Gross Profit (YGP), reduce CO_2 emissions (CO_2e), and improve final product quality.

In all case studies, the HPRD configuration achieved profitability levels compared to RD while significantly reducing CO_2e. Although TIC of CS-1B was considerably higher (ranging from 19% to 227%) due to compressor, the TOC was substantially reduced, with decreases of up to 74%. From an environmental perspective, the elimination of external utilities provided a clear advantage, with CO_2e reduced by up to 93%. Integrating a vacuum distillation column (DC-1) for glycerol purification to USP grade enabled revenue generation of up to 50 million USD/year, elevating YGP to nearly 120 million USD/year. However, this configuration also led to a marked increase in costs and emissions due to additional capital and thermal energy demands. In CS-3, the imposition of stricter biodiesel quality specifications increased emissions and reduced YGP compared to CS-2. Despite this, HPRD maintained its economic viability, with YGP remaining above 100 million USD/year, and all non-dominated solutions complied with ANP quality standards.

In the comparison between the intensified processes (CS-1) and alternative configurations reported in the literature, the RD reached lowest normalized TIC/PBP, while HPRD presented the lowest TOC, as operated without the need for external heating utilities, unlike the configurations that required supplementary heat input. In CS-3, HPRD solutions presented biodiesel purities of 99.8 wt.%, surpassing all reported processes. Furthermore, if emissions associated with electricity consumption and glycerol purification are excluded, the CS-3B would operate with zero direct CO_2e, highlighting its potential for process decarbonization.

The results demonstrated that the HPRD configuration is a promising technology for sustainable biodiesel production at an industrial scale. Its ability to reduce external utility consumption, significantly reduce CO_2e, and maintain high economic performance under

varying process constraints and product quality requirements positions it as a viable alternative to conventional RD.

It is suggested that future works explore the implementation of alternative hyperparameter settings to improve the performance of metaheuristic algorithms in solving MOO problems. Additionally, the valorization of glycerol could be further investigated by proposing its conversion into higher value-added chemicals or its application in alternative processes, aiming to diversify the product portfolio and improve the overall process profitability. A more robust economic assessment, including the calculation of Net Present Value (NPV), Internal Rate of Return (IRR), and Minimum Attractive Rate of Return (MARR), is also recommended to provide a comprehensive evaluation of long-term investment feasibility.

6 References

Agência Nacional do Petróleo, Gás Natural e Biocombustíveis (ANP). Anuário estatístico brasileiro do petróleo, gás natural e biocombustíveis 2024. Available at: https://www.gov.br/anp/pt-br/centrais-de-conteudo/publicacoes/anuario-estatistico/anuario-estatistico-brasileiro-do-petroleo-gas-natural-e-biocombustiveis 2024#Se%C3%A7%C3%A3o%202. Accessed in: 2 dec. 2024.

Agência Nacional do Petróleo, Gás Natural e Biocombustíveis (ANP). Especificação do biodiesel. Rio de Janeiro, 2024. Available at: https://www.gov.br/anp/pt-br/assuntos/producao-e-fornecimento-de-biocombustiveis/biodiesel/especificacao-do-biodiesel. Accessed in: 19 nov. 2024.

Agência Nacional do Petróleo, Gás Natural e Biocombustíveis (ANP). Painel Dinâmico de Produtores de Biodiesel. Rio de Janeiro, 2024. Available at: https://www.gov.br/anp/pt-br/centrais-de-conteudo/paineis-dinamicos-da-anp/paineis-e-mapa-dinamicos-de-produtores-de-combustiveis-e-derivados/painel-dinamico-de-produtores-de-biodiesel#:~:text=O%20Painel%20Din%C3%A2mico%20de%20Produtores,partir%20do%20uso%20dessa%20ferramenta. Accessed in: 12 nov. 2024.

Agência Nacional do Petróleo, Gás Natural e Biocombustíveis (ANP). Preços de produtores e importadores de derivados de petróleo e biodiesel. Available at: https://www.gov.br/anp/pt-br/assuntos/precos-e-defesa-da-concorrencia/precos/precos-de-produtores-e-importadores-de-derivados-de-petroleo-e-biodiesel. Accessed in: 2 dec. 2024.

Agência Nacional do Petróleo, Gás Natural e Biocombustíveis (ANP). Resolução ANP N° 920, de 4 de abril de 2023 – DOU DE 05-04-2023. Rio de Janeiro, 2023. Available at: https://atosoficiais.com.br/anp/resolucao-n-920-2023-estabelece-a-especificacao-do-biodiesel-e-as-obrigacoes-quanto-ao-controle-da-qualidade-a-serem-atendidas-pelos-agentes-economicos-que-comercializem-o-produto-em-territorio-nacional?origin=instituicao. Access in: 19 nov. 2024.

Ahmed, Mukhtar *et al*. Process simulation and stochastic multiobjective optimisation of homogeneously acid-catalysed microalgal in-situ biodiesel production considering economic and environmental criteria. Fuel, v. 327, p. 125165, nov. 2022.

Alhijawi, Bushra; Awajan, Arafat. Genetic algorithms: theory, genetic operators, solutions, and applications. Evolutionary Intelligence, v. 17, n. 3, p. 1245–1256, 3 jun. 2024.

Ali, Zaara *et al.* Recent progress in extraction/transesterification techniques for the recovery of oil from algae biomass. Biomass Conversion and Biorefinery, v. 13, n. 4, p. 2553–2569, 8 fev. 2023.

Alptekin, Ertan; Canakci, Mustafa. Determination of the density and the viscosities of biodiesel–diesel fuel blends. Renewable Energy, v. 33, n. 12, p. 2623–2630, dez. 2008.

Antczak, Mirosława S. *et al.* Enzymatic biodiesel synthesis – Key factors affecting efficiency of the process. Renewable Energy, v. 34, n. 5, p. 1185–1194, maio 2009.

Aworanti, O. A. *et al.* Simulation and Control of Reactive Distillation of Biodiesel Production. UNIOSUN Journal of Engineering and Environmental Sciences, v. 4, n. 2, 30 set. 2022.

Babaie, Omid; Esfahany, Mohsen Nasr. Optimum process configuration for ETBE production based on TAC minimization. Separation and Purification Technology, v. 256, p. 117744, fev. 2021.

Baur, R.; Krishna, R. Distillation column with reactive pump arounds: an alternative to reactive distillation. Chemical Engineering and Processing: Process Intensification, v. 43, n. 3, p. 435–445, mar. 2004.

Benesty, Jacob *et al.* Pearson Correlation Coefficient. In: [S.l.: S.n.]. p. 1–4.

Blank, Julian; Deb, Kalyanmoy. Pymoo: Multi-Objective Optimization in Python. IEEE Access, v. 8, p. 89497–89509, 2020.

Boon-Anuwat, Natja-nan *et al.* Process design of continuous biodiesel production by reactive distillation: Comparison between homogeneous and heterogeneous catalysts. Chemical Engineering and Processing: Process Intensification, v. 92, p. 33–44, jun. 2015.

Bose, Debanik *et al.* Design and optimization of reactive distillation for enhancing supercritical transesterification process to produce biodiesel. Chemical Engineering and Processing - Process Intensification, v. 203, p. 109877, set. 2024.

Braga, Eduardo Ramos. Simulação e estudo da viabilidade técnica e econômica da produção de acrilonitrila a partir do glicerol. 2023, 204 f. Tese (Doutorado em Engenharia Química) –

Programa de Pós-Graduação em Engenharia Química, Universidade Federal da Bahia, Salvador, 2023.

Brasil. Governo oficializa ampliação da mistura de biodiesel no diesel vendido no país. Portal Gov.br, 20 mar. 2023. Available at: https://www.gov.br/pt-br/noticias/energia-minerais-e-combustiveis/2023/03/governo-oficializa-ampliacao-da-mistura-de-biodiesel-no-diesel-vendido-no-pais. Accessed in: 12 November 2024.

Brasil. Law no. 14993, from 8 de oct. 2024. Dispõe sobre a promoção da mobilidade sustentável de baixo carbono e a captura e a estocagem geológica de dióxido de carbono; institui o Programa Nacional de Combustível Sustentável de Aviação (ProBioQAV), o Programa Nacional de Diesel Verde (PNDV) e o Programa Nacional de Descarbonização do Produtor e Importador de Gás Natural e de Incentivo ao Biometano; altera as Leis nºs 9.478, de 6 de agosto de 1997, 9.847, de 26 de outubro de 1999, 8.723, de 28 de outubro de 1993, e 13.033, de 24 de setembro de 2014; e revoga dispositivo da Lei nº 10.438, de 26 de abril de 2002. Brasília, DF: Diário Oficial da União, 2024. Available at: https://www.in.gov.br/en/web/dou/-/lei-n-14.993-de-8-de-outubro-de-2024-589202404. Accessed in: 22 jan. 2025.

Brasil. Mistura de 14% de biodiesel no diesel no diesel começa a valer nesta sexta-feira. Portal Gov.br, 2024. Available at: https://www.gov.br/mme/pt-br/assuntos/noticias/mistura-de-14-de-biodiesel-no-diesel-comeca-a-valer-nesta-sexta-feira#:~:text=Em%20dezembro%20de%202023%2C%20o,1%C2%BA%20de%20mar%C3%A7o%20de%202025. Accessed in: 22 January 2025.

Camino Feltes, Maria M. *et al.* An Overview of Enzyme-Catalyzed Reactions and Alternative Feedstock for Biodiesel Production. In: Alternative Fuel. InTech, 2011.

Carranza-Abaíd, Andrés; González-García, Raúl. A Petlyuk distillation column dynamic analysis: Hysteresis and bifurcations. Chemical Engineering and Processing - Process Intensification, v. 149, p. 107843, mar. 2020.

Çengel, Yunus A.; Boles, Michael A. Thermodynamics: An Engineering Approach. 7. Ed. New York: McGraw Hill, 2011

Cerda-Flores, Sandra C.; Rojas-Punzo, Arturo A.; Nápoles-Rivera, Fabricio. Applications of Multi-Objective Optimization to Industrial Processes: A Literature Review. Processes, v. 10, n. 1, p. 133, 10 jan. 2022.

Inverter. Centrifugal Pump List, 2022. Homepage. Available at: <https://www.inverter.com/centrifugal-pump-price-list?srsltid=AfmBOopYwB_qsXztlYz7mR_85BIuRLTAwbDIkoHTvYlDDYPcIVrvZrue>. Accessed in: 29 nov. 2024.

CE Plant Cost Index Report. Plant Cost Index: September 1970 – October 2024. Chemical Engineering Online, 2024. Available at: https://www.chemengonline.com/wp-content/plugins/ce-base/views/pci-cost-download.php. Accessed in: 15 feb. 2025.

Chang, Yuqing; Bouzarkouna, Zyed; Devegowda, Deepak. Multi-objective optimization for rapid and robust optimal oilfield development under geological uncertainty. Computational Geosciences, v. 19, n. 4, p. 933–950, 25 ago. 2015.

ChemAnalyst. CALCIUM Nitrate Prices, News, Monitor, Analysis & Demand, 2025. Available at: https://www.chemanalyst.com/Pricing-data/calcium-nitrate-1555. Accessed in: 5 fev. 2025

Inverter. Centrifugal Pump List, 2022. Homepage. Available at: <https://www.inverter.com/centrifugal-pump-price-list?srsltid=AfmBOopYwB_qsXztlYz7mR_85BIuRLTAwbDIkoHTvYlDDYPcIVrvZrue>. Accessed in: 29 nov. 2024.

Chiou, Hsuan-Han *et al.* Evaluation of alternative processes of methanol production from CO2: Design, optimization, control, techno-economic, and environmental analysis. Fuel, v. 343, p. 127856, jul. 2023.

Chiu, Hsuan-Han; Yu, Bor-Yih. Synthesis of green light olefins from direct hydrogenation of CO2. Part I: Techno-economic, decarbonization, and sustainability analyses based on rigorous simulation. Journal of the Taiwan Institute of Chemical Engineers, v. 156, p. 105340, mar. 2024.

Chuah, Lai F. *et al.* A review of intensification technologies for biodiesel production. In: Biofuels and Biorefining. Elsevier, 2022. p. 87–116.

Ciriminna, Rosaria *et al.* Understanding the glycerol market. European Journal of Lipid Science and Technology, v. 116, n. 10, p. 1432–1439, 22 out. 2014.

Craide, S. Percentual de biodiesel no diesel subirá para 14% em março de 2024. Agência Brasil, 19 dec. 2023. Available at: https://agenciabrasil.ebc.com.br/economia/noticia/2023-12/percentual-de-biodiesel-no-diesel-subira-para-14-em-marco-de 2024#:~:text=O%20Conselho%20Nacional%20de%20Pol%C3%ADtica,partir%20de%20mar%C3%A7o%20de%202025. Accessed in: 22 jan. 2025.

Coker, A. Kayode. Enhanced distillation types. In: Ludwig's Applied Process Design for Chemical and Petrochemical Plants. Elsevier, 2010. p. 345–371.

De Tommaso, Jacopo *et al.* Experimental methods in chemical engineering: Process simulation. The Canadian Journal of Chemical Engineering, v. 98, n. 11, p. 2301–2320, 2 nov. 2020.

Deb, Kalyanmoy *et al.* A fast and elitist multiobjective genetic algorithm: NSGA-II. IEEE Transactions on Evolutionary Computation, v. 6, n. 2, p. 182–197, abr. 2002.

Deb, Kalyanmoy; Sindhya, Karthik; Okabe, Tatsuya. Self-adaptive simulated binary crossover for real-parameter optimization. *In*: New York, NY, USA: ACM, 7 jul. 2007.

Decarpigny, Cédric *et al.* Bioprocesses for the Biodiesel Production from Waste Oils and Valorization of Glycerol. Energies, v. 15, n. 9, p. 3381, 6 may 2022.

Deshpande, Gunavant *et al.* Multiobjective optimization of ultrasound intensified and ionic liquid catalyzed in situ algal biodiesel production considering economic, environmental and safety indicators. Chemical Engineering Research and Design, v. 180, p. 134–152, abr. 2022a.

Deshpande, Gunavant *et al.* Simultaneous optimization of economic, environmental and safety criteria for algal biodiesel process retrofitted using dividing wall column and multistage vapor recompression. Process Safety and Environmental Protection, v. 164, p. 1–14, ago. 2022b.

Douglas, James M. Conceptual Design of Chemical Processes. New York: McGraw-Hill, 1988.

Egger, Torben; FIEG, Georg. Operation, validation and model comparison for a reactive dividing wall column. Chemical Engineering Science, v. 207, p. 993–1006, nov. 2019.

Faruque, Mohammed O.; Razzak, Shaikh A.; Hossain, Mohammad M. Application of Heterogeneous Catalysts for Biodiesel Production from Microalgal Oil—A Review. Catalysts, v. 10, n. 9, p. 1025, 7 set. 2020.

Gadalla, Mamdouh A. *et al.* Reducing CO2 Emissions and Energy Consumption of Heat-Integrated Distillation Systems. Environmental Science & Technology, v. 39, n. 17, p. 6860–6870, 1 set. 2005.

Gaurav, Aashish *et al.* Transesterification of Triglyceride to Fatty Acid Alkyl Esters (Biodiesel): Comparison of Utility Requirements and Capital Costs between Reaction Separation and Catalytic Distillation Configurations. Energy & Fuels, v. 27, n. 11, p. 6847–6857, 21 nov. 2013.

Giwa, Abdulwahab; Ogunware, Michael Ayomide. Modelling, Simulation and Control of a Reactive Distillation Process for Biodiesel Production. ABUAD Journal of Engineering Research and Development (AJERD), v. 1, n. 1, p. 49–60, 31 out. 2017.

Go, Kang-Seok; Chu, Young-Hwan; Mcfarland, Eric W. Techno-economic analysis of bromine mediated propane oxidative dehydrogenation to produce propylene. Chemical Engineering Journal, v. 473, p. 145260, out. 2023.

Nascimento, Leomário G. do *et al.* Eco-efficiency analysis and intensification of the biodiesel production process through vapor recompression strategy. Energy, v. 275, p. 127479, jul. 2023.

Haigh, Kathleen F. *et al.* Kinetics of the Pre-Treatment of Used Cooking Oil Using Novozyme 435 for Biodiesel Production. Procedia Engineering, v. 42, p. 1106–1113, 2012.

Halim, A. Hanif; Ismail, I.; Das, Swagatam. Performance assessment of the metaheuristic optimization algorithms: an exhaustive review. Artificial Intelligence Review, v. 54, n. 3, p. 2323–2409, 6 mar. 2021.

Harmsen, Jan; Verkerk, Maarten. Process Intensification: Breakthrough in Design, Industrial Innovation Practices, and Education. Berlin: De Gruyter, 2020.

Hoang, Anh T.; Le, Anh T.. A review on deposit formation in the injector of diesel engines running on biodiesel. Energy Sources, Part A: Recovery, Utilization, and Environmental Effects, v. 41, n. 5, p. 584–599, 4 mar. 2019.

Holland, John H. Adaptation in Natural and Artificial Systems: An Introductory Analysis with Applications to Biology, Control, and Artificial Intelligence. Cambridge, Massachusetts; London, England: The MIT Press, 1992.

Huang, K. *et al.* Multi-Step Controlled Kinetics of the Transesterification of Crude Soybean Oil with Methanol by $Mg(OCH_3)_2$. Chemical Engineering & Technology, v. 32, n. 10, p. 1595–1604, 25 out. 2009.

Hussain, Abid *et al.* Genetic Algorithm for Traveling Salesman Problem with Modified Cycle Crossover Operator. Computational Intelligence and Neuroscience, v. 2017, p. 1–7, 2017.

Hussain, Arif *et al.* Design method for the feasibility and technical evaluation of side-reactor column configurations. Chemical Engineering and Processing - Process Intensification, v. 144, p. 107648, out. 2019.

Hwang, Ching-Lai; Yoon, Kwangsun. Methods for Multiple Attribute Decision Making. In: [S.l.: S.n.]. p. 58–191.

Imarc Group. Glycerin Price Trend, Chart, Monitor, News, Forecast & Demand. Available at: <https://www.imarcgroup.com/glycerin-pricing-report>. Accessed in: 30 nov. 2024.

Instituto Mato-Grossense de Economia Agropecuária. Indicador Soja. Available at: <https://imea.com.br/imea-site/indicador-soja>. Accessed in: 30 nov. 2024

International Energy Agency. World Energy Outlook 2023, 2023. Available at: <https://iea.blob.core.windows.net/assets/86ede39e-4436-42d7-ba2a-edf61467e070/WorldEnergyOutlook2023.pdf>. Accessed in: 10 November 2024.

Jana, Amiya K. Heat integrated distillation operation. Applied Energy, v. 87, n. 5, p. 1477–1494, maio 2010.

Jana, Amiya K. Advances in heat pump assisted distillation column: A review. Energy Conversion and Management, v. 77, p. 287–297, jan. 2014.

Jiang, Zheyu; Agrawal, Rakesh. Process intensification in multicomponent distillation: A review of recent advancements. Chemical Engineering Research and Design, v. 147, p. 122–145, jul. 2019.

Karacan, Süleyman; Karacan, Filiz. Steady-state optimization for biodiesel production in a reactive distillation column. Clean Technologies and Environmental Policy, v. 17, n. 5, p. 1207–1215, 28 jun. 2015.

Katoch, Sourabh; Chauhan, Sumit Singh; Kumar, Vijay. A review on genetic algorithm: past, present, and future. Multimedia Tools and Applications, v. 80, n. 5, p. 8091–8126, 31 fev. 2021.

Kaymak, Devrim B.; Luyben, William L. Design of Distillation Columns with External Side Reactors. Industrial & Engineering Chemistry Research, v. 43, n. 25, p. 8049–8056, 1 dez. 2004.

Kazemi, Abolghasem *et al.* Evaluation of different vapor recompression distillation configurations based on energy requirements and associated costs. Applied Thermal Engineering, v. 94, p. 305–313, fev. 2016.

Kennedy, J.; Eberhart, R. Particle swarm optimization. *In*: IEEE, 1995.

Khan, Zarmeena *et al.* Current developments in esterification reaction: A review on process and parameters. Journal of Industrial and Engineering Chemistry, v. 103, p. 80–101, nov. 2021.

Kirkpatrick, Scott; Gelatt, C. D.; Vecchi, Mario P. Optimization by Simulated Annealing. Science, v. 220, n. 4598, p. 671–680, 13 maio 1983.

Knapp, Alan K. *et al.* Characterizing differences in precipitation regimes of extreme wet and dry years: implications for climate change experiments. Global Change Biology, v. 21, n. 7, p. 2624–2633, 9 jul. 2015.

Kong, Jie *et al.* Optimization and Control of a Stabilization Column for a Propylene-Producing Fluid Catalytic Cracking Process. Industrial & Engineering Chemistry Research, v. 63, n. 49, p. 21553–21564, 11 dez. 2024.

Krishna, R. Hardware Selection and Design Aspects for Reactive Distillation Columns. In: Reactive Distillation. [S. l.]: Wiley, 2002. p. 169–189.

Kroeze, Vincent *et al.* Determination of the Minimum Catalyst Amount in the Design of Catalytic Distillation Columns. Industrial & Engineering Chemistry Research, v. 60, n. 28, p. 10254–10264, 21 jul. 2021.

Lambora, Annu; GUPTA, Kunal; CHOPRA, Kriti. Genetic Algorithm- A Literature Review. In: IEEE, fev. 2019.

Lee, Hao-Yeh; Hsiao, Tyng-Lih. Design and Simulation of Reactive Distillation Processes. In: Chemical Engineering Process Simulation. [S.l.]: Elsevier Inc., 2017.

Leung, Dennis Y. C.; Wu, Xuan; Leung, M. K. H. A review on biodiesel production using catalyzed transesterification. Applied Energy, v. 87, n. 4, p. 1083–1095, abr. 2010.

Li, Wei *et al.* Knowledge-guided multiobjective particle swarm optimization with fusion learning strategies. Complex & Intelligent Systems, v. 7, n. 3, p. 1223–1239, 18 jun. 2021.

Liu, Xuejun *et al.* Model Study on Transesterification of Soybean Oil to Biodiesel with Methanol Using Solid Base Catalyst. The Journal of Physical Chemistry A, v. 114, n. 11, p. 3750–3755, 25 mar. 2010.

Mah, R. S. H.; Nicholas, J. J.; Wodnik, R. B. Distillation with secondary reflux and vaporization: A comparative evaluation. AIChE Journal, v. 23, n. 5, p. 651–658, 17 set. 1977.

Mann, Michael E.; Emanuel, Kerry A. Atlantic hurricane trends linked to climate change. Eos, Transactions American Geophysical Union, v. 87, n. 24, p. 233–241, 13 jun. 2006.

Martinez-Morales, Jose D.; Pineda-Rico, Ulises; Stevens-Navarro, Enrique. Performance comparison between MADM algorithms for vertical handoff in 4G networks. In: IEEE, set. 2010.

Mesquita, Francisca M. R. *et al.* Liquid–liquid equilibria of systems containing cottonseed biodiesel+glycerol+ethanol at 293.15, 313.15 and 333.15K. Fluid Phase Equilibria, v. 318, p. 51–55, mar. 2012.

Mesquita, Francisca Maria R. *et al.* Liquid–Liquid Equilibrium for Ternary Mixtures of Biodiesel (Soybean or Sunflower) + Glycerol + Ethanol at Different Temperatures. Journal of Chemical & Engineering Data, v. 56, n. 11, p. 4061–4067, 10 nov. 2011.

Methanex. Pricing. Available at: <https://www.methanex.com/about-methanol/pricing/>. Accessed in: 30 nov. 2024.

Ministério do Desenvolvimento, Indústria, Comércio e Serviços. ComexStat. Available at: <https://comexstat.mdic.gov.br/pt/geral/25402>. Accessed in: 30 nov. 2024.

Mirjalili, Seyedali. Genetic Algorithm. In: [S.l.: S.n.]. p. 43–55.

Mishra, Vijay K.; Goswami, Rachna. A review of production, properties and advantages of biodiesel. Biofuels, v. 9, n. 2, p. 273–289, 4 mar. 2018.

Mittelbach, M. Advances in biodiesel catalysts and processing technologies. In: Advances in Biodiesel Production. Elsevier, 2012. p. 133–153.

Mondal, Biswarup *et al.* Nano-catalytic heterogeneous reactive distillation for algal biodiesel production: Multi-objective optimization and heat integration. Energy Conversion and Management, v. 241, p. 114298, ago. 2021.

Mondal, Biswarup; Rangaiah, Gade Pandu; Jana, Amiya K. Optimizing algal biodiesel production from a novel reactive distillation based unit: Reducing CO2 emission and cost. Chemical Engineering and Processing - Process Intensification, v. 176, p. 108948, jun. 2022.

Muthia, Rahma; Jobson, Megan; Kiss, Anton A. Determining the Design Parameters of Reactive Distillation Processes by a Quick Mapping Method. In: [S.l.: S.n.]. p. 865–870.

Myint, Lay L.; El-Halwagi, Mahmoud M. Process analysis and optimization of biodiesel production from soybean oil. Clean Technologies and Environmental Policy, v. 11, n. 3, p. 263–276, 17 set. 2009.

Noureddini, H.; Zhu, D. Kinetics of transesterification of soybean oil. Journal of the American Oil Chemists' Society, v. 74, n. 11, p. 1457–1463, nov. 1997.

Nunez, Sarahi *et al.* Assessing the impacts of climate change on biodiversity: is below 2 °C enough? Climatic Change, v. 154, n. 3–4, p. 351–365, 22 jun. 2019.

Onyia, M. I.; Mbah, G. O.; Udeh, B. C. Transesterification Kinetics of Soybean Oil. International Journal of Advanced Engineering Research and Science (IJAERS), v. 2, n. 7, jul. 2015.

Pasupulety, Nagaraju *et al.* Production of biodiesel from soybean oil on CaO/Al2O3 solid base catalysts. Applied Catalysis A: General, v. 452, p. 189–202, fev. 2013.

Patle, Dipesh S. *et al.* Multi-objective optimization of two alkali catalyzed processes for biodiesel from waste cooking oil. Energy Conversion and Management, v. 85, p. 361–372, set. 2014.

Pérez-Cisneros, Eduardo S. *et al.* An integrated reactive distillation process for biodiesel production. Computers & Chemical Engineering, v. 91, p. 233–246, ago. 2016.

Pleşu, Valentin *et al.* Simple Equation for Suitability of Heat Pump Use in Distillation. p. 1327–1332.

Puth, Marie-Therese; Neuhauser, Markus; Ruxton, Graeme D. Effective use of Spearman's and Kendall's correlation coefficients for association between two measured traits. Animal Behaviour, v. 102, p. 77–84, abr. 2015.

Qiu, Zheyan; Zhao, Lina; Weatherley, Laurence. Process intensification technologies in continuous biodiesel production. Chemical Engineering and Processing: Process Intensification, v. 49, n. 4, p. 323–330, abr. 2010.

Rodríguez-Robles, C. F. *et al.* Control analysis of batch reactive distillation column with intermittent fed. p. 1357–1362.

Sakthivel, R. *et al.* A review on the properties, performance and emission aspects of the third generation biodiesels. Renewable and Sustainable Energy Reviews, v. 82, p. 2970–2992, fev. 2018.

Saleem, Abubakar *et al.* Understanding the impact of reactive holdup on process intensification in the design of reactive distillation column. Chemical Engineering and Processing - Process Intensification, v. 191, p. 109440, set. 2023.

Saxena, Parag; Jawale, Sayali; Joshipura, Milind H. A Review on Prediction of Properties of Biodiesel and Blends of Biodiesel. Procedia Engineering, v. 51, p. 395–402, 2013.

Schober, Patrick; Boer, Christa; Schwarte, Lothar A. Correlation Coefficients: Appropriate Use and Interpretation. Anesthesia & Analgesia, v. 126, n. 5, p. 1763–1768, maio 2018.

Shahid, Ejaz M.; Jamal, Younis. Production of biodiesel: A technical review. Renewable and Sustainable Energy Reviews, v. 15, n. 9, p. 4732–4745, dez. 2011.

Shelokar, Prakash *et al.* Metaheuristics in Process Engineering: A Historical Perspective. In: Applications of Metaheuristics in Process Engineering. Cham: Springer International Publishing, 2014. p. 1–38.

Simasatitkul, Lida *et al.* Reactive distillation for biodiesel production from soybean oil. Korean Journal of Chemical Engineering, v. 28, n. 3, p. 649–655, 1 mar. 2011.

Sing, Nilam; Mahali, Kalachand; Roy, Sanjay. An Overview on Biofuels: Advantages and Disadvantages. In: Recent Developments in Chemistry and Biochemistry Research Vol. 7. BP International, 2024. p. 98–118.

Siqueira, Willian D. P., Pavão, Leandro V. Análise Econômica e Ambiental da Produção de Biodiesel via Destilação Reativa com Bomba de Calor no Contexto Brasileiro. In: Congresso Nacional de Engenharia, 1 ed., 2025, Natal. Electronic Proceedings. p. 1-15.

Soh, Lindsay *et al.* Carbon Dioxide Mediated Transesterification of Mixed Triacylglyceride Substrates. Energy & Fuels, v. 32, n. 9, p. 9624–9632, 20 set. 2018.

Souza, Thibério P. C. *et al.* Simulation and preliminary economic assessment of a biodiesel plant and comparison with reactive distillation. Fuel Processing Technology, v. 123, p. 75–81, jul. 2014.

Srinivas, N.; Deb, Kalyanmoy. Muiltiobjective Optimization Using Nondominated Sorting in Genetic Algorithms. Evolutionary Computation, v. 2, n. 3, p. 221–248, set. 1994.

Stander, Liezl; Woolway, Matthew; Van Zyl, Terence L. Surrogate-assisted evolutionary multi-objective optimisation applied to a pressure swing adsorption system. Neural Computing and Applications, v. 37, n. 2, p. 739–755, 18 jan. 2025.

Steffen, Vilmar; Oliveira, Maiquiel Schmidt de; Silva, Edson Antonio da. A Systematic Review of the Literature on Steady-State Reactive Distillation Modeling and Simulation: Challenges and Opportunities. In: Solvents - Dilute, Dissolve, and Disperse - Insights on Green Solvents and Distillation IntechOpen, 2024.

Šulgan, Branislav *et al.* Multi-Objective Assessment of Heat Pump-Assisted Ethyl Acetate Production. Processes, v. 9, n. 8, p. 1380, 6 ago. 2021.

Sun, Dayu *et al.* Mechanical vapor recompression coupling organic rankine cycle process for purification of crude biodiesel obtained by solid base-catalyzed transesterification. Energy, v. 266, p. 126499, mar. 2023.

Supranit, B. Design of internally heat-integrated distillation column (HIDiC): Uniform heat transfer area versus uniform heat distribution. Energy, v. 35, n. 3, p. 1505–1514, mar. 2010.

Talebian-Kiakalaieh, Amin; Amin, Nor A. S.; Mazaheri, Hossein. A review on novel processes of biodiesel production from waste cooking oil. Applied Energy, v. 104, p. 683–710, abr. 2013.

Tebaldi, Claudia *et al.* Extreme sea levels at different global warming levels. Nature Climate Change, v. 11, n. 9, p. 746–751, 30 set. 2021.

Tóth, László Richárd *et al.* Multiobjective optimization for efficient energy utilization in batch biodiesel production. Clean Technologies and Environmental Policy, v. 18, n. 1, p. 95–104, 1 jan. 2016.

Treeyawetchakul, C. Preliminary Modified Biodiesel Production by Coupling Reactive distillation with a Steam Reformer via Aspen Plus®. IOP Conference Series: Materials Science and Engineering, v. 778, n. 1, p. 012064, 1 abr. 2020.

Tsatse, A. *et al.* Optimal design and operation of reactive distillation systems based on a superstructure methodology. Chemical Engineering Research and Design, v. 170, p. 107–133, jun. 2021.

Turton, Richard *et al.* Analysis, Synthesis and Design of Chemical Processes. 5. ed. Boston: Prentice Hall, 2018.

Valvassore, Murielk S.; Costa, Caliane B. B.. Analysis of novel configurations of an intensified process for ethyl lactate production. Chemical Engineering and Processing - Process Intensification, v. 208, p. 110146, fev. 2025.

Van Allsburg, Kurt M. *et al.* Early-stage evaluation of catalyst manufacturing cost and environmental impact using CatCost. Nature Catalysis, v. 5, n. 4, p. 342–353, 31 mar. 2022.

Vanaki, A.; Eslamloueyan, R. Steady-state simulation of a reactive internally heat integrated distillation column (R-HIDiC) for synthesis of tertiary-amyl methyl ether (TAME). Chemical Engineering and Processing: Process Intensification, v. 52, p. 21–27, fev. 2012.

Wang, Chen *et al.* Energy-saving hybrid processes combining pressure-swing reactive distillation and pervaporation membrane for n-propyl acetate production. Separation and Purification Technology, v. 221, p. 1–11, ago. 2019.

Wang, Zhiyuan; Rangaiah, Gade Pandu. Application and Analysis of Methods for Selecting an Optimal Solution from the Pareto-Optimal Front obtained by Multiobjective Optimization. Industrial & Engineering Chemistry Research, v. 56, n. 2, p. 560–574, 18 jan. 2017.

Waskom, Michael. seaborn: statistical data visualization. Journal of Open Source Software, v. 6, n. 60, p. 3021, 6 abr. 2021.

Weinfeld, Jeffrey A.; Owens, Scott A.; Eldridge, R. Bruce. Reactive dividing wall columns: A comprehensive review. Chemical Engineering and Processing - Process Intensification, v. 123, p. 20–33, jan. 2018.

Wu, Pei-Jhen *et al.* Rigorous simulation and comprehensive analysis for the novel glycerol carbonate (GC) production process via indirect conversion of CO2. Fuel, v. 357, p. 129831, fev. 2024.

Xiao, Chengwei *et al.* Using Spearman's correlation coefficients for exploratory data analysis on big dataset. Concurrency and Computation: Practice and Experience, v. 28, n. 14, p. 3866–3878, 25 set. 2016.

Yang, Lingmei *et al.* Liquid–Liquid Equilibrium Behavior of Ternary Systems Comprising Biodiesel + Glycerol and Triglyceride + Methanol: Experimental Data and Modeling. Catalysts, v. 14, n. 5, p. 320, 12 maio 2024.

Yu, Bor-Yih. Development of two plant-wide glycerol carbonate production processes: Design, optimization and environmental analysis. Journal of the Taiwan Institute of Chemical Engineers, v. 117, p. 19–25, dez. 2020.

Zapotecas-Martínez, Saúl; García-Nájera, Abel; Menchaca-Méndez, Adriana. Engineering applications of multi-objective evolutionary algorithms: A test suite of box-constrained real-world problems. Engineering Applications of Artificial Intelligence, v. 123, p. 106192, ago. 2023.

Zhang, Zhenyu *et al.* Design and optimization of heat pump assisted reactive extractive distillation for separating benzene/n-propanol/water ternary azeotropes. Separation and Purification Technology, v. 360, p. 130994, jul. 2025.

Appendix A – Aspen Plus Flowsheet in Each Case Study

Figure A.1 – Process flowsheet for CS-1A

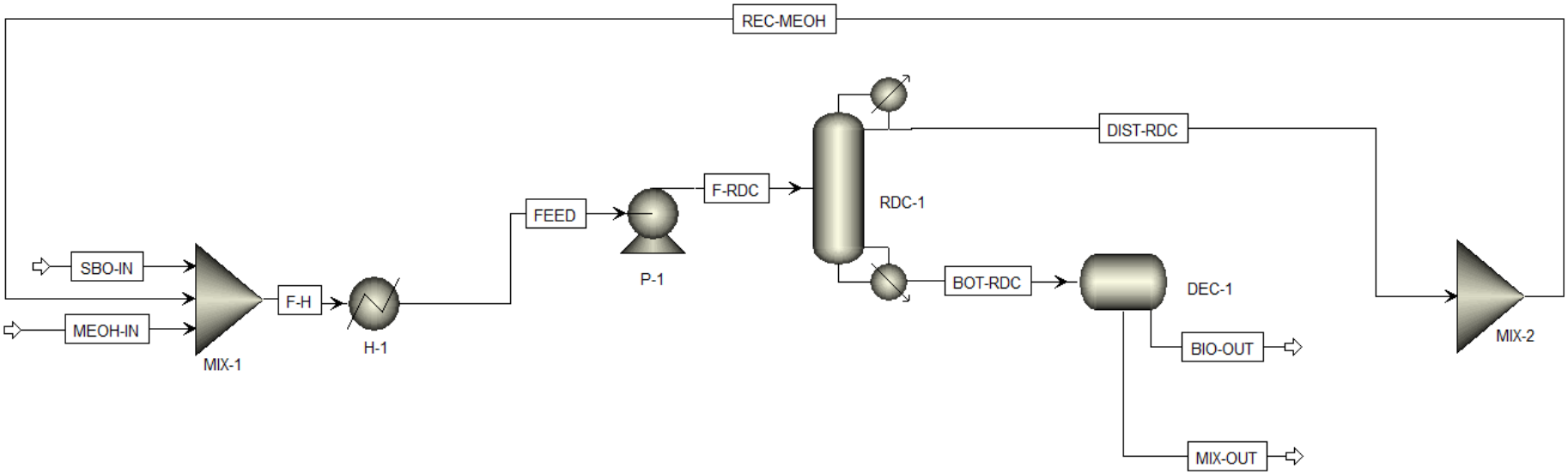

Source: Author.

Figure A.2 – Process flowsheet for CS-1B

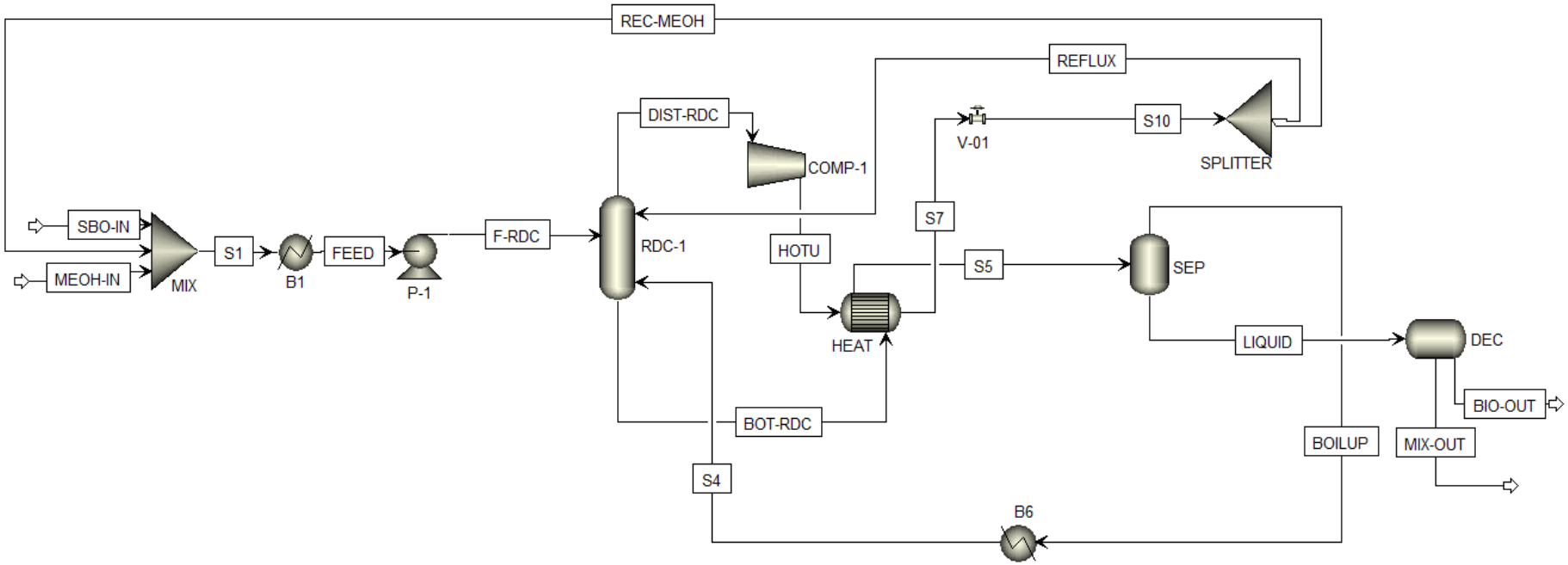

Source: Author.

Figure A.3 – Process flowsheet for CS-2A

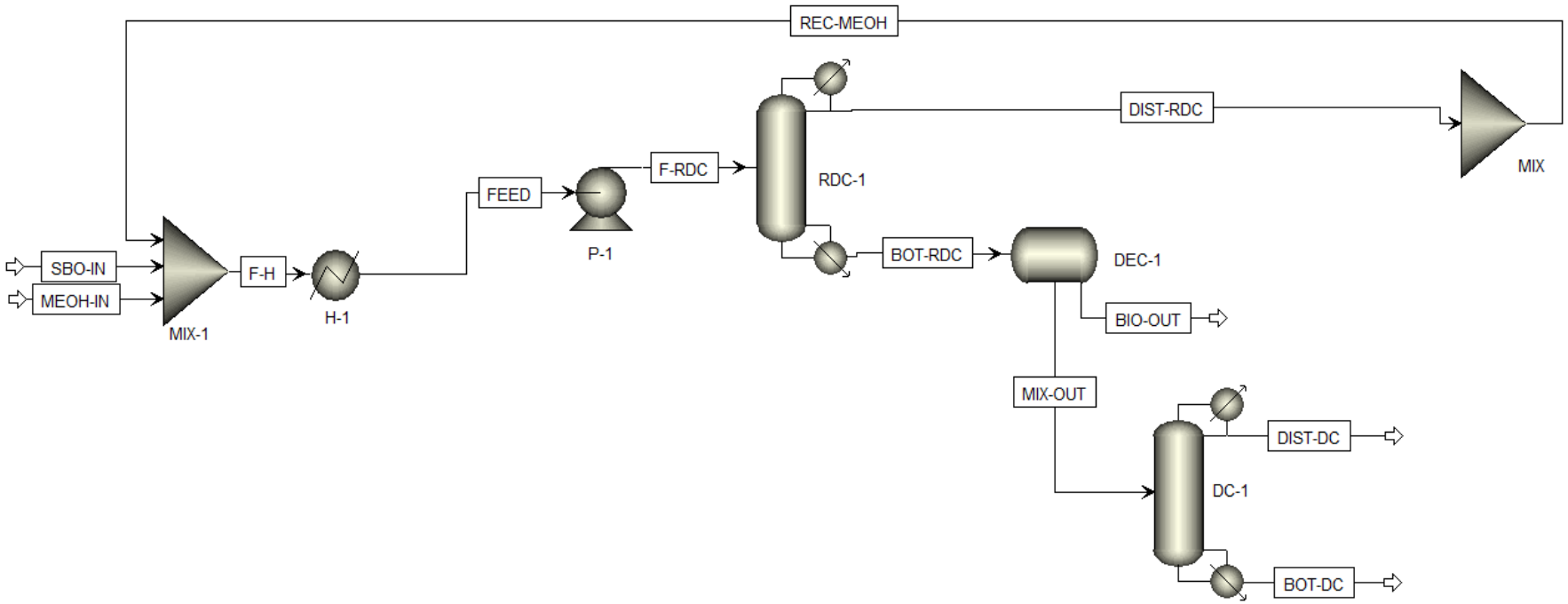

Source: Author.

Figure A.4 – Process flowsheet for CS-2B

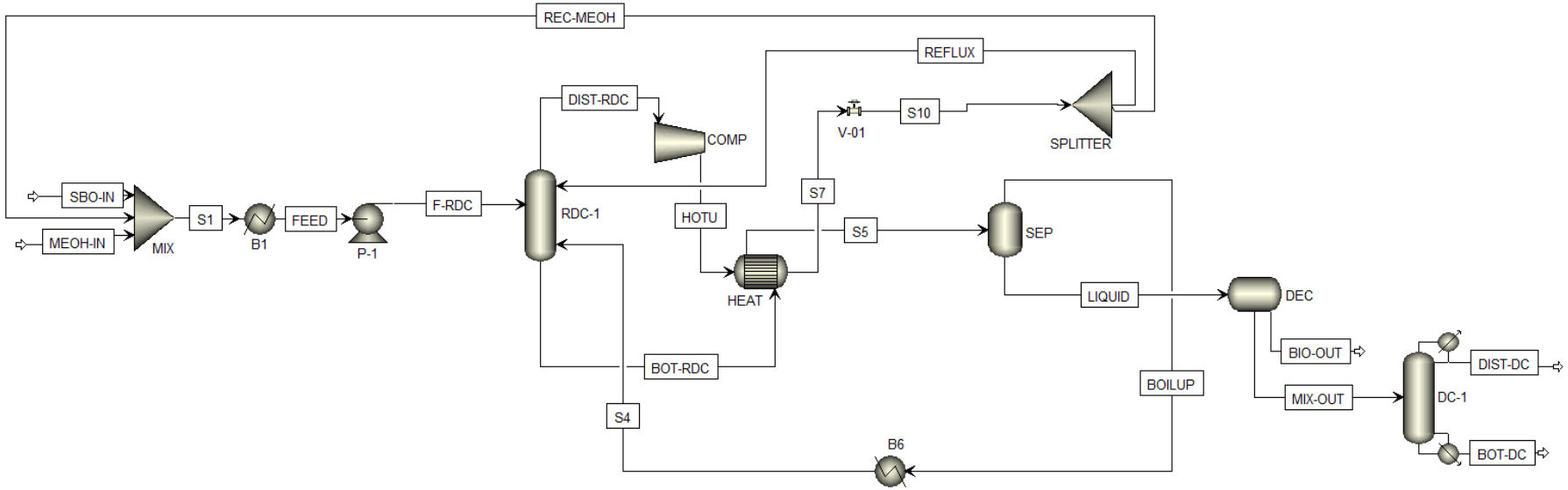

Source: Author.

Figure A.5 – Process flowsheet for CS-3A

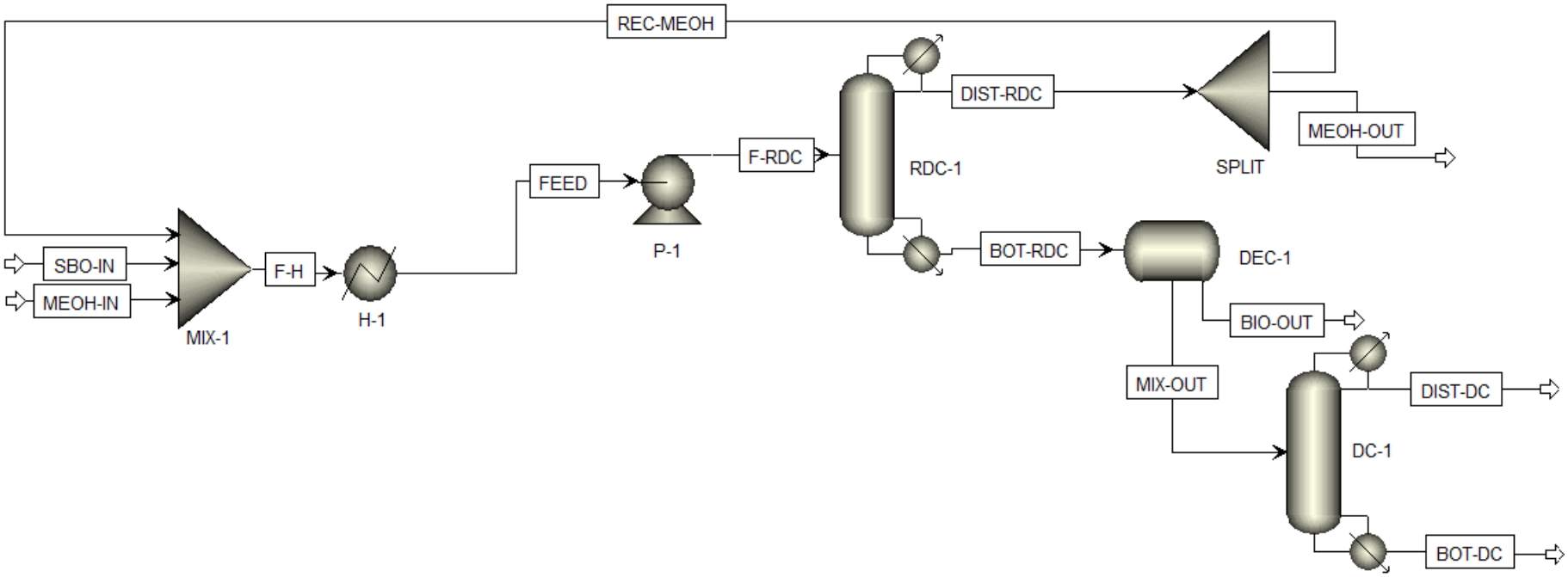

Source: Author.

Figure A.6 – Process flowsheet for CS-3B

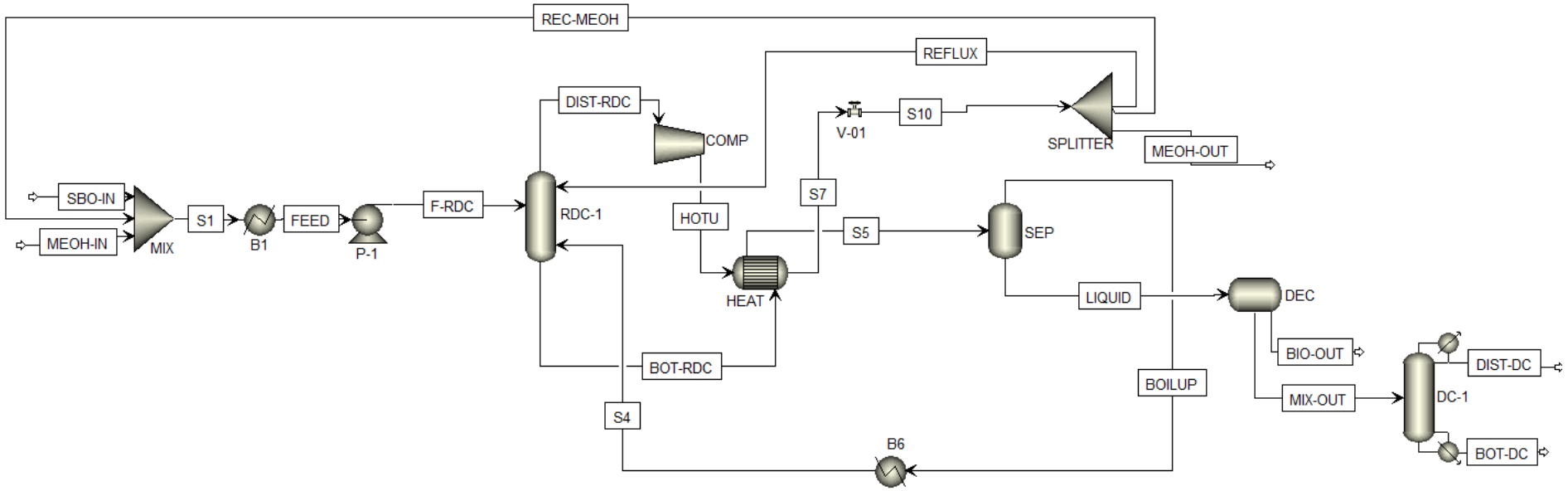

Source: Author.

Appendix B – Installed Cost Equations

B.1 – Stainless-steel distillation column vessel (Douglas, 1988):

$$IC_{Column\ Vessel} = \left(\frac{M\&S}{280}\right) 937.64\ D_{col}^{1.066}\ H_{col}^{0.802}(2.18 + 3.67\ F_p) \quad \text{(B.1)}$$

$$H = 0.6\left(\frac{N_T}{0.75} - 3\right) + 6 \quad \text{(B.2)}$$

Where:

- $IC_{Column\ Vessel}$: installed cost of stainless-steel distillation column vessel in American dollars [USD]
- D_{col}: distillation column diameter in meters [m]
- H_{col}: distillation column height in meters [m]
- F_p: pressure correction factor according to Table A.1 [dimensionless]
- N_T: number of stages [dimensionless]

Table A.1 – F_p value for each column pressure interval

Column pressure (atm)	F_p
0 - 3.40	1.00
3.40 - 6.80	1.05
6.80 - 13.60	1.15
13.60 - 20.41	1.20
20.41 - 27.21	1.35
27.21 - 34.02	1.45

B.2 – Stainless-Steel decanter (Douglas, 1988):

$$IC_{Decanter} = \left(\frac{M\&S}{280}\right) 5485.19\ D_{dec}^{1.066}\ L_{dec}^{0.802} \quad \text{(B.3)}$$

Where:

- $IC_{Decanter}$: installed cost of stainless-steel decanter in American dollars [USD]
- D_{dec}: decanter diameter in meters [m]
- H_{dec}: decanter length in meters [m]

To estimate the diameter and height of decanter, the work of Mondal, Rangaiah and Jana (2022) was used. For processing 18.11 kmol/h of biodiesel, a decanter with a diameter

of 1.1 m and a length of 3.6 m is required. Substituting these values into Equation (B.3) and using the Marshall and Swift Index for October 2024, the installed cost of the decanter is calculated as 48,038.16 USD.

For different processing capacities, the decanter cost is adjusted using the scaling relationship from Turton *et al*. (2018):

$$\frac{C_a}{C_b} = \left(\frac{A_a}{A_b}\right)^{0.3} \tag{B.4}$$

Where:

- C_a: Cost in scenario A [USD]
- C_b: Cost in scenario B [USD]
- A: Processing capacity [kmol/h]

B.3 – Distillation column plates (Douglas, 1988):

$$IC_{\,Column\ Plates} = \left(\frac{M\&S}{280}\right) 211.01\ D_{col}^{1.55} H_{col} \tag{B.5}$$

Where $IC_{Column\ Plates}$ is installed cost of sieve plates with a tray spacing of 0.6 m [USD]

B.4 – Condenser (Douglas, 1988):

$$IC_{Condenser} = \left(\frac{M\&S}{280}\right) 1466.79\ A_{cond}^{0.65} \tag{B.6}$$

Where:

- IC_{Cond}: installed cost of condenser [USD]
- A_{Cond}: condenser area [m^2]

B.5 – Reboiler (Douglas, 1988):

$$IC_{Reb} = \left(\frac{M\&S}{280}\right) 1746.07\ A_{reb}^{0.65} \tag{B.7}$$

Where:

- IC_{Reb}: installed cost of kettle-type reboiler [USD]
- A_{Reb}: reboiler area in square meters [m^2]

B.6 – Compressor (Douglas, 1988):

$$IC_{Comp} = \left(\frac{M\&S}{280}\right) 1293.72\, W_{comp}^{0.82} \quad \text{(B.8)}$$

Where:

- IC_{Comp}: installed cost of compressor using a centrifugal motor [USD]
- W_{comp}: compressor power [kW]

B.7 – Pump (Inverter, 2022):

$$IC_{Pump} = 224.09\, W_{pump} + 946.72 \quad \text{(B.9)}$$

Where:

- IC_{Pump}: installed cost of stainless-steel pump [USD]
- W_{pump}: pump work [kW]

B.8 – Heat exchanger design (Douglas, 1988):

To calculate the heat exchanger area, a counter flow design was assumed due to its higher efficiency.

$$A_{HX} = \frac{Q}{U\Delta T} \quad \text{(B.10)}$$

$$\Delta T = \frac{\Delta T_1 - \Delta T_2}{\ln\left(\frac{\Delta T_1}{\Delta T_2}\right)} \quad \text{(B.11)}$$

Where:

- A_{HX}: heat exchanger area [m^2]
- Q: heat transfer rate [kW]
- U: overall heat transfer coefficient [$kW/(m^2K)$]
- ΔT: logarithmic mean temperature difference [K]
- ΔT_1: temperature difference between the inlet hot stream and cold outlet stream in [K]
- ΔT_2: temperature difference between the outlet hot stream and cold inlet stream [K]

Appendix C – Catalyst Cost Estimation

C.1 – Cost of CaO/Al_2O_3

According to Pasupulety *et al*. (2013), the catalyst was synthesized using 3 g of CaO/Al_2O_3, 30 g of methanol, and 10 g of glycerol. The preparation method involved wet impregnation of CaO (20 wt.%) on Al_2O_3 (80 wt.%), followed by calcination. Due to the unavailability of $Ca(NO_3)_2$ in the Catcost tool, the unit price of the catalyst was estimated at 0.52 USD/kg, based on market data (ChemAnalyst, 2025). Additionally, it was assumed a medium plant capacity of 5000 kg/year of catalyst production with a selling margin of 15%, approximately.

Appendix D – Detailed Mathematic Formulation of Economic and Environmental Metrics

D.1 – TIC

$$TIC_{CS-1A} = IC_{CS-1A}^{P-1} + IC_{CS-1A}^{DEC-1} + IC_{CS-1A}^{RDC-1} \quad (D.1)$$

$$TIC_{CS-1B} = IC_{CS-1B}^{P-1} + IC_{CS-1B}^{DEC-1} + IC_{CS-1B}^{RDC-1} + IC_{CS-1B}^{COMP-1} \quad (D.2)$$

$$TIC_{CS-2A/3A} = IC_{CS-2A/3A}^{P-1} + IC_{CS-2A/3A}^{DEC-1} + IC_{CS-2A/3A}^{RDC-1} + IC_{CS-2A/3A}^{DC-1} \quad (D.3)$$

$$TIC_{CS-2B/3B} = IC_{CS-2B/3B}^{P-1} + IC_{CS-2B/3B}^{DEC-1} + IC_{CS-2B/3B}^{RDC-1} + IC_{CS-2B/3B}^{COMP-1} + IC_{CS-2B/3B}^{DC-1} \quad (D.4)$$

$$IC_{CS-A}^{RDC-1} = IC_{CS-A}^{cond,RDC-1} + IC_{CS-A}^{reb,RDC-1} + IC_{CS-A}^{ves,RDC-1} \quad (D.5)$$

$$IC_{CS-B}^{RDC-1} = IC_{CS-B}^{HX,RDC-1} + IC_{CS-B}^{ves,RDC-1} \quad (D.6)$$

D.2 – TOC

$$OC_{ele,cs}^{d} = P_{ele} W_{cs}^{d} \quad (D.7)$$

$$OC_{HU,cs}^{d} = P_{HU} Q_{reb,cs}^{d} \quad (D.8)$$

$$OC_{CU,cs}^{d} = P_{CU} Q_{cond,cs}^{d} \quad (D.9)$$

$$OC_{cat,cs}^{RDC-1} = P_{cat} m_{cat,cs}^{RDC-1} \quad (D.10)$$

$$TOC_{CS-1A} = t_{op}(OC_{ele,CS-1A}^{P-1} + OC_{HU,CS-1A}^{RDC-1} + OC_{CU,CS-1A}^{RDC-1} + OC_{cat,CS-1A}^{RDC-1}) \quad (D.11)$$

$$TOC_{CS-1B} = t_{op}(OC_{ele,CS-1B}^{P-1} + OC_{cat,CS-1B}^{RDC-1} + OC_{ele,CS-1B}^{COMP-1}) \quad (D.12)$$

$$TOC_{CS-2A/3A} = t_{op}(OC_{ele,CS-2A/3A}^{P-1} + OC_{HU,CS-2A/3A}^{RDC-1} + OC_{CU,CS-2A/3A}^{RDC-1} + OC_{cat,CS-2A/3A}^{RDC-1} + OC_{HU,CS-2A/3A}^{DC-1} + OC_{CU,CS-2A/3A}^{DC-1}) \quad (D.13)$$

$$TOC_{CS-2B/3B} = t_{op}(OC_{ele,CS-2B/3B}^{P-1} + OC_{cat,CS-2B/3B}^{RDC-1} + OC_{ele,CS-2B/3B}^{COMP-1} + OC_{HU,CS-2B/3B}^{DC-1} + OC_{CU,CS-2B/3B}^{DC-1}) \quad (D.14)$$

D.3 – Total Revenue and Reactant Cost

$$RC_{CS-A/B} = P_{SBO} \dot{m}_{SBO-IN} + P_{MeOH} \dot{m}_{MEOH-IN} \quad (D.15)$$

$$TR_{CS-1A/1B} = P_{BIO} \dot{m}_{BIO-OUT} + P_{GLY} \dot{m}_{MIX-OUT} \quad (D.16)$$

$$TR_{CS-2A/2B/3A/3B} = P_{BIO} \dot{m}_{BIO-OUT} + P_{GLY} \dot{m}_{BOT-DC} \quad (D.17)$$

D.4 – Total CO_2e from Natural Gas Steam Boilers

$$CO_2 e_{ele,cs}^{d} = \widehat{CO_2 e_{ele,cs}^{d}} W_{cs}^{d} \quad (D.18)$$

$$CO_2 e_{CS-1A} = CO_2 e_{ele,CS-1A}^{P-1} + CO_2 e_{HU,CS-1A}^{RDC-1} \quad (D.19)$$

$$CO_2e_{CS-1B} = CO_2e_{ele,CS-1B}^{P-1} + CO_2e_{ele,CS-1B}^{COMP-1} \quad \text{(D.20)}$$

$$CO_2e_{CS-2A/3A} = CO_2e_{ele,CS-2A/3A}^{P-1} + CO_2e_{HU,CS-2A/3A}^{RDC-1} + CO_2e_{HU,CS-2A/3A}^{DC-1} \quad \text{(D.21)}$$

$$CO_2e_{CS-2B/3B} = CO_2e_{ele,CS-2B/3B}^{P-1} + CO_2e_{ele,CS-2B/3B}^{COMP-1} + CO_2e_{HU,CS-2B/3B}^{DC-1} \quad \text{(D.22)}$$

Appendix E – Correlation Matrices for Each Case Study Within Search Interval

Figure E.1 – Correlation Matrix of CS-1A

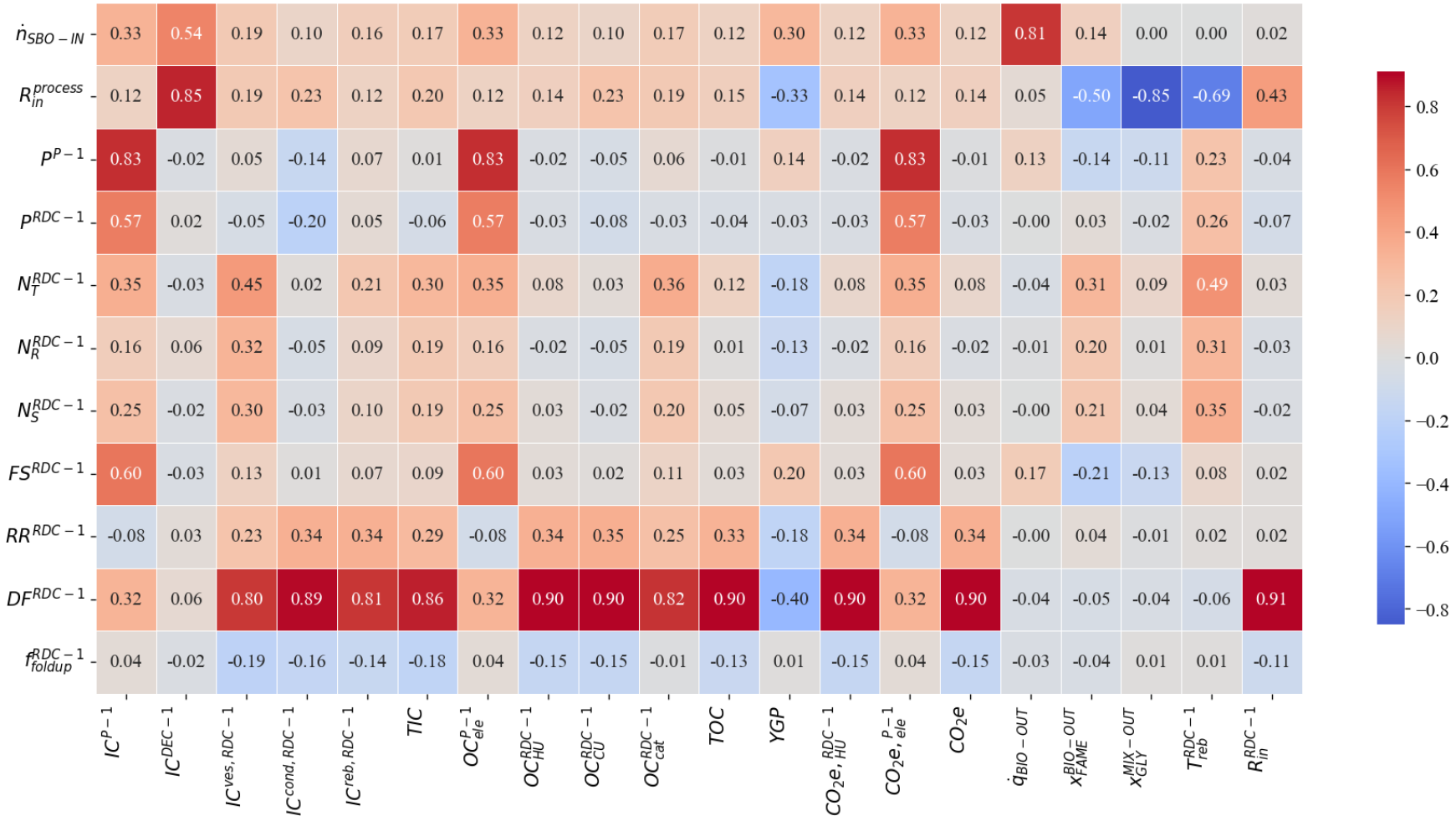

Source: Author.

Figure E.2 – Correlation Matrix of CS-1B

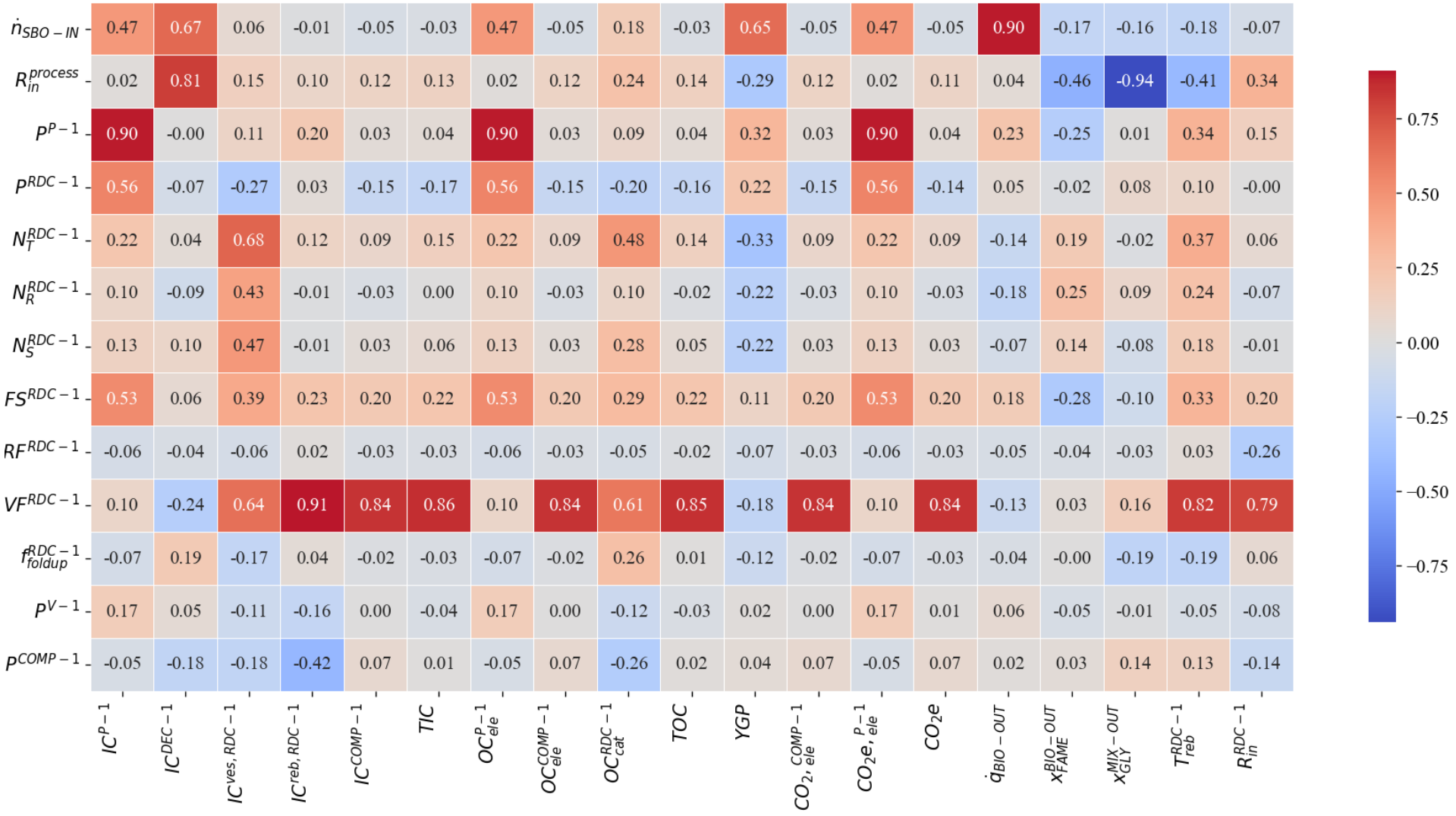

Source: Author.

Figure E.3 – Correlation Matrix of CS-2A

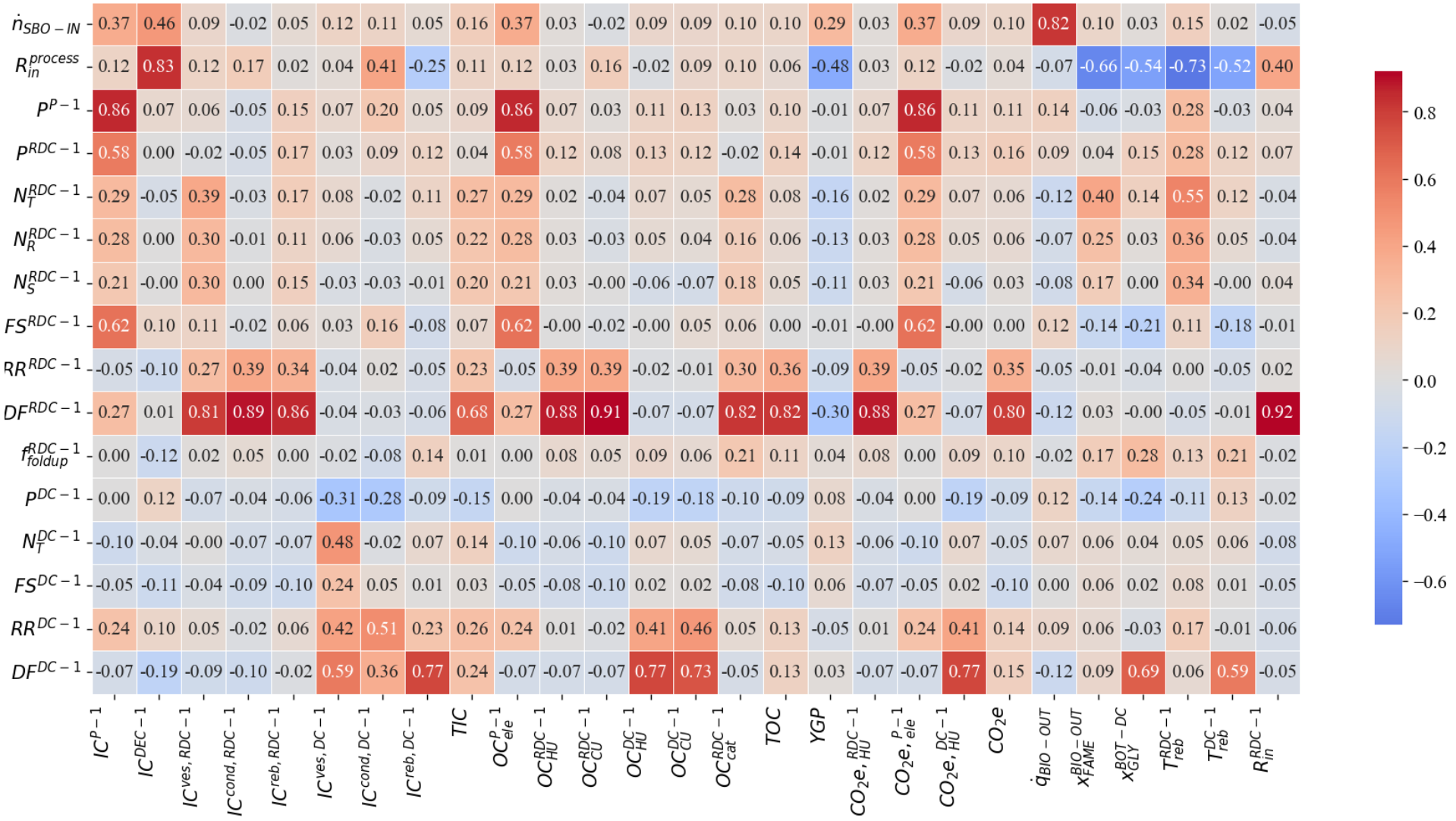

Source: Author.

Figure E.4 – Correlation Matrix of CS-2B

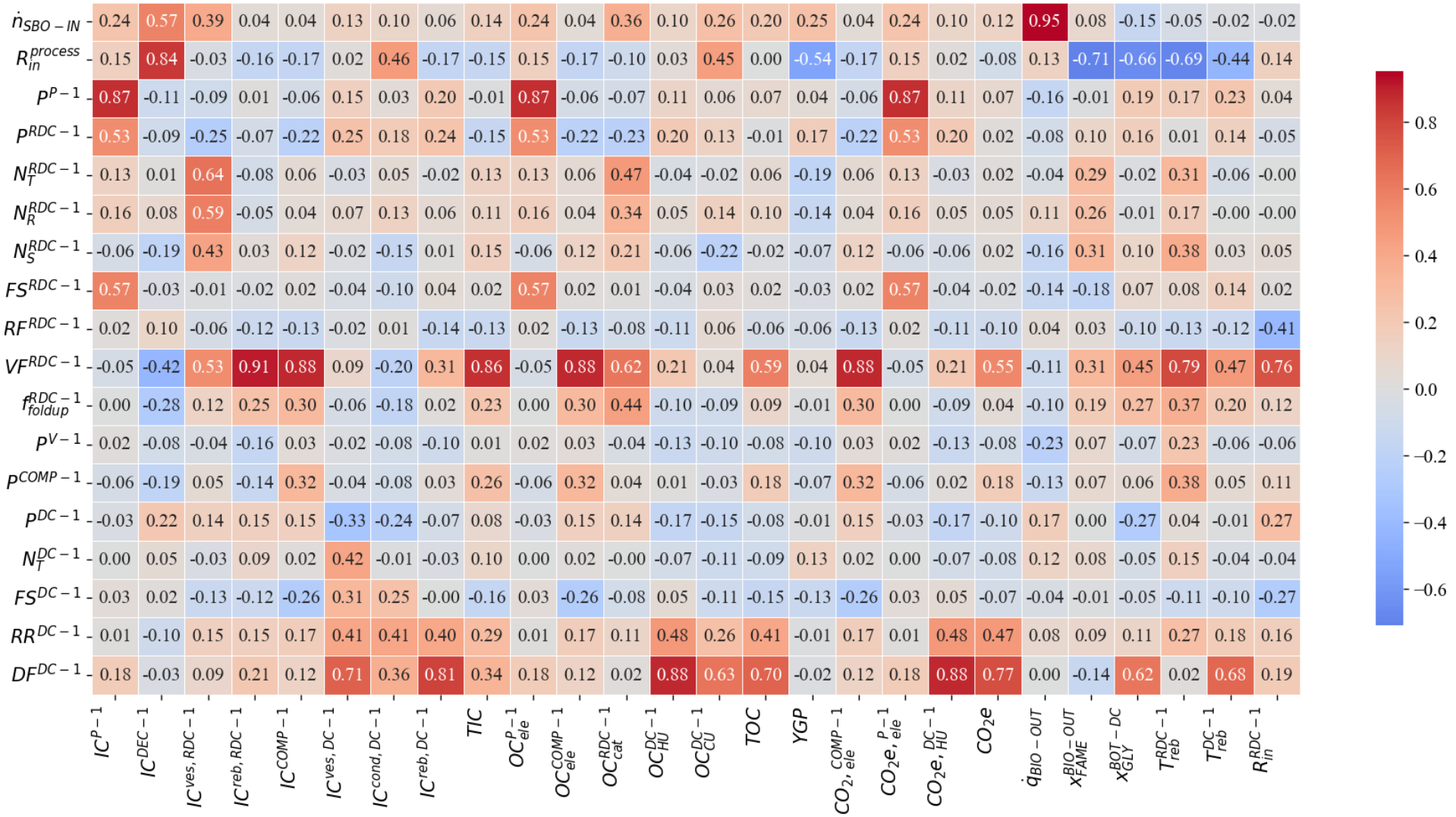

Source: Author.

Figure E.5 – Correlation Matrix of CS-3A

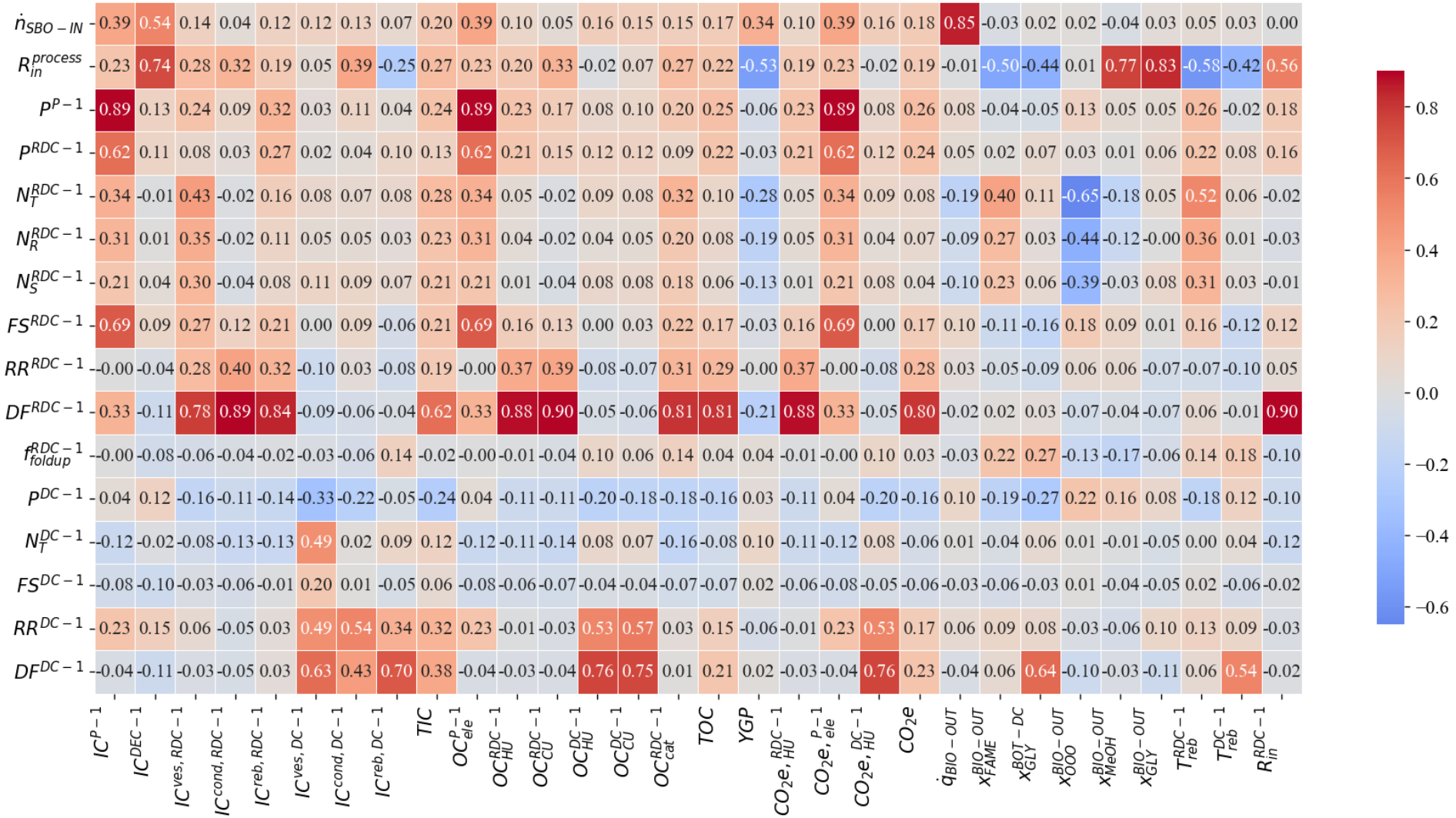

Source: Author.

Figure E.6 – Correlation Matrix of CS-3B

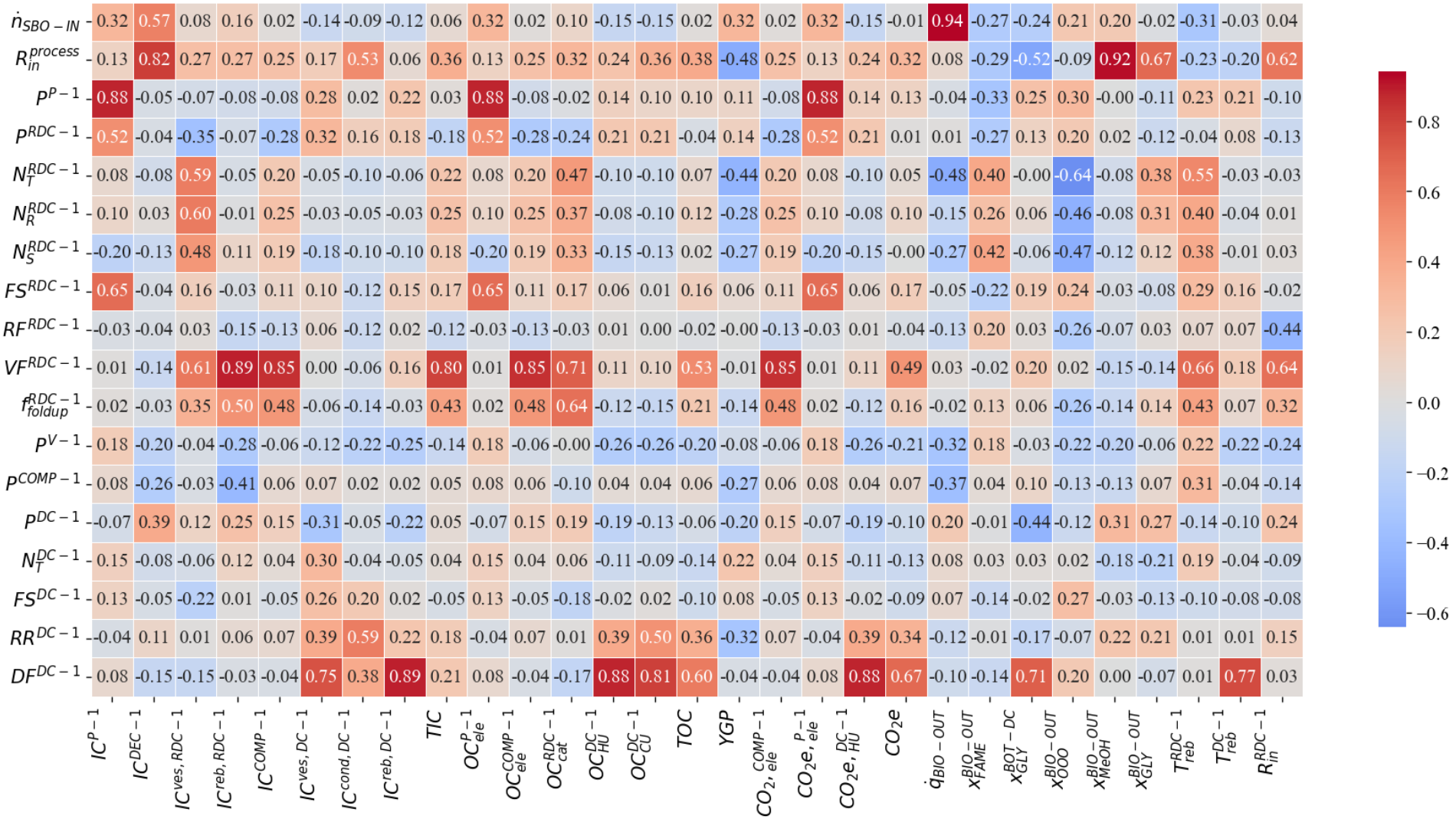

Source: Author.

Appendix F – Details of Obtained Non-Dominated Solutions

Table F.1 – Decision Variable Values of CS-1A

ID	$\dot{n}_{SBO-IN}$ (kmol/h)	$R_{in}^{process}$	P^{P-1} (atm)	P^{RDC-1} (atm)	f_{holdup}^{RDC-1}	N_T^{RDC-1}	N_R^{RDC-1}	N_S^{RDC-1}	FS^{RDC-1}	RR^{RDC-1}	DF^{RDC-1}
1	47.08	3.75	3.84	2.73	0.71	12	3	2	4	0.07	0.27
2	46.90	3.75	3.84	2.73	0.71	12	3	2	4	0.07	0.27
3	47.08	3.96	3.89	2.73	0.73	12	3	2	4	0.58	0.18
4	47.41	4.18	2.10	1.15	0.96	10	2	1	2	0.10	0.14
5	42.22	4.18	2.28	1.23	0.84	11	2	1	3	0.05	0.14
6	40.47	4.18	2.18	1.23	0.96	10	2	1	2	0.05	0.14
7	40.43	4.18	2.13	1.23	0.97	10	2	1	2	0.05	0.14
8	42.41	4.18	1.96	1.01	0.95	11	2	1	2	0.10	0.14
9	36.66	4.18	2.18	1.29	0.96	10	2	1	2	0.05	0.14
10	36.33	4.18	2.08	1.23	0.96	10	2	1	1	0.05	0.14

Source: Author.

Table F.2 – Constraint Variable Values of CS-1A

ID	$\dot{q}_{BIO-OUT}$ (L/h)	$x_{FAME}^{BIO-OUT}$	$x_{GLY}^{MIX-OUT}$	T_{reb}^{RDC-1} (°C)	R_{in}^{RDC-1}
1	53588	0.966	0.817	146	5.51
2	53382	0.966	0.817	146	5.51
3	53626	0.965	0.783	139	5.04
4	53967	0.965	0.750	110	5.03
5	47676	0.972	0.754	113	5.02
6	46027	0.966	0.750	111	5.02
7	45955	0.966	0.750	111	5.02
8	47332	0.982	0.759	110	5.03
9	41690	0.966	0.750	112	5.02
10	40773	0.977	0.756	112	5.03

Source: Author.

Table F.3 – Decision Variable Values of CS-1B

ID	$\dot{n}_{SBO-IN}$ (kmol/h)	$R_{in}^{process}$	P^{P-1} (atm)	P^{RDC-1} (atm)	P^{V-1} (atm)	P^{COMP-1} (atm)	f_{holdup}^{RDC-1}	N_T^{RDC-1}	N_R^{RDC-1}	N_S^{RDC-1}	FS^{RDC-1}	RF^{RDC-1}	VF^{RDC-1}
1	47.93	3.40	3.67	2.06	4.46	9.68	0.95	16	4	4	10	0.32	0.53
2	47.46	3.40	3.63	2.03	4.43	9.68	0.95	17	2	5	10	0.35	0.53
3	48.11	4.16	3.78	1.95	8.88	9.08	0.80	15	4	3	9	0.38	0.43
4	48.08	4.30	3.84	2.02	4.31	10.15	0.95	16	4	4	9	0.35	0.42
5	48.63	4.27	3.45	2.05	4.47	10.15	0.95	16	4	3	5	0.35	0.42
6	46.58	4.24	3.66	2.05	8.74	9.65	0.86	17	2	3	11	0.30	0.43
7	39.60	4.08	4.01	2.20	4.32	9.76	0.82	15	5	3	9	0.35	0.45
8	38.93	4.08	4.01	2.20	3.24	9.76	0.82	15	5	3	9	0.35	0.45
9	39.11	4.16	3.78	1.95	8.90	9.08	0.91	15	4	3	9	0.35	0.43
10	38.83	4.26	3.56	2.05	4.63	9.58	0.95	16	4	3	10	0.35	0.43
11	38.96	4.26	3.80	2.05	8.86	9.69	0.95	17	2	3	11	0.35	0.43
12	35.48	4.23	3.06	2.05	4.78	9.75	0.93	17	4	3	5	0.35	0.43

Source: Author.

Table F.4 – Constraint Variable Values of CS-1B

ID	$\dot{q}_{BIO-OUT}$ (L/h)	$x_{FAME}^{BIO-OUT}$	$x_{GLY}^{MIX-OUT}$	T_{reb}^{RDC-1} (°C)	R_{in}^{RDC-1}
1	54100	0.974	0.896	127	5.47
2	53122	0.981	0.901	128	5.32
3	54050	0.976	0.770	121	5.00
4	53829	0.979	0.752	122	5.08
5	53937	0.987	0.760	122	5.03
6	51855	0.984	0.762	123	5.07
7	44685	0.973	0.779	123	5.02
8	43941	0.972	0.779	123	5.01
9	43904	0.977	0.770	121	5.04
10	43423	0.980	0.757	122	5.08
11	40487	0.987	0.765	123	5.00
12	39338	0.987	0.766	123	5.03

Source: Author.

Table F.5 – Decision Variable Values of CS-2A

ID	$\dot{n}_{SBO-IN}$ (kmol/h)	$R_{in}^{process}$	P^{P-1} (atm)	P^{RDC-1} (atm)	f_{holdup}^{RDC-1}	N_T^{RDC-1}	N_R^{RDC-1}	N_S^{RDC-1}	FS^{RDC-1}	RR^{RDC-1}	DF^{RDC-1}	P^{DC-1} (atm)	N_T^{DC-1}	FS^{DC-1}	RR^{DC-1}	DF^{DC-1}
1	47.31	3.81	3.13	2.20	0.52	13	3	2	4	0.41	0.22	0.13	14	8	0.09	0.40
2	47.66	3.78	2.94	1.61	0.78	11	2	2	2	0.07	0.22	0.13	12	6	0.10	0.38
3	47.58	3.77	2.28	1.64	0.78	13	3	3	1	0.06	0.21	0.16	14	7	0.09	0.38
4	45.42	3.78	2.13	1.49	0.82	12	2	3	1	0.06	0.22	0.13	26	24	0.39	0.38
5	43.30	3.77	2.29	1.64	0.82	11	2	2	1	0.06	0.22	0.14	15	8	0.39	0.38
6	38.85	3.78	2.87	2.19	0.77	11	2	2	2	0.07	0.22	0.13	25	14	0.39	0.38
7	38.81	3.80	2.13	1.49	0.82	12	2	3	1	0.08	0.22	0.13	26	24	0.39	0.39
8	47.29	3.81	2.59	1.66	0.63	13	3	2	4	0.07	0.22	0.13	28	18	0.12	0.06
9	45.20	3.83	2.54	1.66	0.63	13	3	2	4	0.07	0.22	0.13	28	16	0.56	0.05
10	43.32	4.24	2.68	1.64	0.82	13	3	3	3	0.08	0.24	0.30	16	13	0.39	0.07
11	38.90	3.81	2.54	1.61	0.63	13	3	2	4	0.09	0.22	0.13	28	16	0.13	0.05
12	38.80	4.12	2.45	1.62	0.82	12	2	2	3	0.08	0.22	0.13	14	11	0.39	0.05

Source: Author.

Table F.6 – Constraint Variable Values of CS-2A

ID	$\dot{q}_{BIO-OUT}$ (L/h)	$x_{FAME}^{BIO-OUT}$	x_{GLY}^{BOT-DC}	T_{reb}^{RDC-1} (°C)	T_{reb}^{DC-1} (°C)	R_{in}^{RDC-1}
1	53823	0.966	0.997	139	138	5.16
2	53475	0.978	0.998	139	151	5.13
3	53281	0.980	0.998	134	155	5.07
4	51011	0.978	0.996	130	130	5.13
5	48435	0.981	0.998	131	158	5.09
6	43759	0.975	0.996	137	131	5.13
7	43606	0.977	0.995	129	124	5.17
8	53598	0.970	0.833	132	35	5.16
9	51358	0.967	0.826	130	35	5.21
10	49291	0.966	0.769	121	49	5.86
11	44283	0.966	0.829	131	35	5.16
12	43639	0.976	0.785	122	32	5.53

Source: Author.

Table F.7 – Decision Variable Values of CS-2B

ID	$\dot{n}_{SBO-IN}$ (kmol/h)	$R_{in}^{process}$	P^{P-1} (atm)	P^{RDC-1} (atm)	P^{V-1} (atm)	P^{COMP-1} (atm)	f_{holdup}^{RDC-1}	N_T^{RDC-1}	N_R^{RDC-1}	N_S^{RDC-1}	FS^{RDC-1}	RF^{RDC-1}	VF^{RDC-1}	P^{DC-1} (atm)	N_T^{DC-1}	FS^{DC-1}	RR^{DC-1}	DF^{DC-1}
1	47.06	3.74	4.12	2.09	4.34	9.88	0.76	18	4	5	11	0.56	0.53	0.17	12	9	0.14	0.36
2	46.31	3.72	4.12	2.09	2.89	9.40	0.76	18	4	5	11	0.49	0.53	0.17	11	8	0.14	0.36
3	42.40	3.74	3.94	2.02	9.30	9.89	0.76	18	3	5	11	0.49	0.53	0.21	10	7	0.13	0.36
4	37.94	3.74	3.95	2.02	4.16	10.01	0.80	18	3	5	11	0.56	0.53	0.22	38	33	0.20	0.36
5	36.55	3.74	4.05	2.02	9.00	9.55	0.80	20	4	6	12	0.55	0.55	0.26	11	8	0.15	0.36
6	35.03	3.74	3.93	2.04	2.12	10.01	0.80	18	3	5	11	0.55	0.53	0.20	11	8	0.23	0.36
7	47.24	3.74	3.91	2.01	4.27	10.13	0.77	18	4	5	11	0.55	0.53	0.20	11	8	0.23	0.11
8	46.31	3.74	4.15	2.09	2.21	9.47	0.76	18	4	5	11	0.55	0.53	0.20	11	9	0.14	0.11
9	42.48	3.74	4.21	2.30	9.00	9.83	0.76	18	3	5	11	0.55	0.53	0.22	36	29	0.14	0.11
10	38.74	3.60	3.97	2.04	3.78	9.55	0.84	18	3	5	11	0.51	0.53	0.21	11	8	0.06	0.12
11	36.53	3.59	3.94	2.02	4.29	9.89	0.78	18	3	5	11	0.47	0.52	0.17	39	36	0.15	0.10

Source: Author.

Table F.8 – Constraint Variable Values of CS-2B

ID	$\dot{q}_{BIO-OUT}$ (L/h)	$x_{FAME}^{BIO-OUT}$	x_{GLY}^{BOT-DC}	T_{reb}^{RDC-1} (°C)	T_{reb}^{DC-1} (°C)	R_{in}^{RDC-1}
1	53545	0.966	0.996	127	142	5.17
2	52738	0.965	0.996	127	143	5.21
3	48103	0.968	0.995	127	144	5.43
4	43070	0.968	0.996	127	154	5.21
5	41410	0.970	0.995	128	153	5.39
6	39838	0.966	0.996	127	150	5.11
7	53771	0.966	0.873	127	49	5.21
8	52732	0.965	0.874	127	49	5.06
9	48097	0.970	0.878	128	52	5.08
10	43801	0.972	0.907	127	55	5.00
11	41547	0.967	0.899	127	49	5.02

Source: Author.

Table F.9 – Decision Variable Values of CS-3A

ID	$\dot{n}_{SBO-IN}$ (kmol/h)	$R_{in}^{process}$	P^{P-1} (atm)	P^{RDC-1} (atm)	f_{holdup}^{RDC-1}	N_T^{RDC-1}	N_R^{RDC-1}	N_S^{RDC-1}	FS^{RDC-1}	RR^{RDC-1}	DF^{RDC-1}	P^{DC-1} (atm)	N_T^{DC-1}	FS^{DC-1}	RR^{DC-1}	DF^{DC-1}
1	49.11	3.25	1.98	1.14	0.87	13	2	1	3	0.07	0.31	0.14	22	20	0.11	0.10
2	48.11	3.24	1.84	1.02	0.87	13	2	1	3	0.08	0.32	0.14	29	19	0.62	0.10
3	45.19	3.25	2.23	1.04	0.87	13	3	1	3	0.29	0.32	0.13	23	15	0.12	0.10
4	39.98	3.24	1.99	1.14	0.86	13	3	1	3	0.42	0.32	0.15	23	14	1.59	0.10
5	38.63	3.24	2.36	1.16	0.87	13	2	1	3	0.42	0.31	0.18	23	16	0.11	0.10
6	37.92	3.24	2.23	1.04	0.87	13	2	1	3	0.32	0.32	0.18	17	12	0.11	0.10
7	37.19	3.25	1.99	1.14	0.87	13	3	1	3	0.09	0.32	0.19	23	21	0.11	0.10
8	36.82	3.25	1.86	1.02	0.90	13	3	1	3	0.08	0.31	0.15	17	15	1.57	0.09
9	36.84	3.28	1.66	1.02	0.89	13	2	1	1	0.29	0.32	0.18	23	21	0.11	0.14
10	35.55	3.28	2.22	1.03	0.87	13	2	1	3	0.85	0.31	0.13	23	14	1.59	0.12
11	36.28	3.28	2.22	1.03	0.87	13	3	1	3	0.34	0.32	0.13	23	19	0.11	0.10

Source: Author.

Table F.10 – Constraint Variable Values of CS-3A

ID	$\dot{q}_{BIO-OUT}$ (L/h)	$x_{FAME}^{BIO-OUT}$	x_{GLY}^{BOT-DC}	$x_{OOO}^{BIO-OUT}$	$x_{MEOH}^{BIO-OUT}$	$x_{GLY}^{BIO-OUT}$	T_{reb}^{RDC-1} (°C)	T_{reb}^{DC-1} (°C)	R_{in}^{RDC-1}
1	53935	0.998	0.997	0.0006	0.0014	0.0000	195	138	5.06
2	52850	0.998	0.998	0.0008	0.0013	0.0000	193	149	5.07
3	49686	0.997	0.997	0.0015	0.0014	0.0000	192	142	5.08
4	43951	0.997	0.998	0.0014	0.0014	0.0000	195	157	5.07
5	42441	0.998	0.997	0.0008	0.0014	0.0000	196	154	5.04
6	41669	0.998	0.997	0.0011	0.0013	0.0000	193	154	5.07
7	40894	0.997	0.998	0.0016	0.0014	0.0000	195	160	5.08
8	40496	0.997	0.996	0.0017	0.0014	0.0000	191	130	5.05
9	40448	0.998	1.000	0.0001	0.0016	0.0000	184	231	5.19
10	39063	0.997	0.999	0.0008	0.0017	0.0000	182	171	5.09
11	39917	0.996	0.988	0.0020	0.0017	0.0000	182	94	5.18

Source: Author.

Table F.11 – Decision Variable Values of CS-3B

ID	$\dot{n}_{SBO-IN}$ (kmol/h)	$R_{in}^{process}$	P^{P-1} (atm)	P^{RDC-1} (atm)	P^{V-1} (atm)	P^{COMP-1} (atm)	f_{holdup}^{RDC-1}	N_T^{RDC-1}	N_R^{RDC-1}	N_S^{RDC-1}	FS^{RDC-1}	RF^{RDC-1}	VF^{RDC-1}	P^{DC-1} (atm)	N_T^{DC-1}	FS^{DC-1}	RR^{DC-1}	DF^{DC-1}
1	48.01	3.29	3.01	1.21	13.42	13.61	0.75	21	3	3	12	0.35	0.52	0.22	35	21	0.40	0.19
2	46.80	3.29	4.46	2.66	20.48	20.62	0.86	22	3	3	12	0.34	0.56	0.23	37	20	0.14	0.27
3	43.24	3.29	3.65	2.57	13.51	13.57	0.76	14	2	1	5	0.41	0.56	0.23	35	8	0.26	0.28
4	39.74	3.30	3.67	2.55	19.89	20.78	0.76	20	3	2	3	0.38	0.56	0.20	39	21	0.36	0.22
5	38.95	3.30	3.67	2.55	19.87	20.78	0.76	20	3	2	3	0.40	0.56	0.20	39	21	0.40	0.21
6	38.88	3.29	4.46	2.56	20.26	20.46	0.76	21	3	2	13	0.36	0.56	0.22	39	26	0.12	0.28
7	38.61	3.29	4.33	2.53	13.83	14.01	0.73	21	3	3	12	0.36	0.56	0.23	38	26	0.35	0.27

Source: Author.

Table F.12 – Constraint Variable Values of CS-3B

ID	$\dot{q}_{BIO-OUT}$ (L/h)	$x_{FAME}^{BIO-OUT}$	x_{GLY}^{BOT-DC}	$x_{OOO}^{BIO-OUT}$	$x_{MEOH}^{BIO-OUT}$	$x_{GLY}^{BIO-OUT}$	T_{reb}^{RDC-1} (°C)	T_{reb}^{DC-1} (°C)	R_{in}^{RDC-1}
1	52717	0.998	1.000	0.0000	0.0018	0.0001	130	237	5.17
2	51384	0.998	1.000	0.0000	0.0019	0.0001	138	238	5.10
3	47465	0.998	1.000	0.0000	0.0016	0.0001	133	237	5.21
4	43637	0.998	1.000	0.0000	0.0019	0.0001	137	233	5.20
5	42763	0.998	1.000	0.0000	0.0019	0.0001	137	233	5.15
6	42689	0.998	1.000	0.0000	0.0018	0.0001	137	237	5.14
7	42396	0.998	1.000	0.0000	0.0019	0.0001	136	237	5.02

Source: Author.